Cyfoeth Naturiol Cymru
Natural Resources Wales

Sources, Pathways and Fate of Suspended Sediments in the Milford Haven Estuary: Observations, Modelling and Future Change

Report No: 1019

Authors: Peter E. Robins, Thomas W. Clough, Soizic Garnier, Iain Fairley, Frances Ratcliffe, Lily Pauls

Author Affiliation: Bangor University

About Natural Resources Wales

Natural Resources Wales' purpose is to pursue sustainable management of natural resources. This means looking after air, land, water, wildlife, plants and soil to improve Wales' well-being, and provide a better future for everyone.

Evidence at Natural Resources Wales

Natural Resources Wales is an evidence-based organisation. We seek to ensure that our strategy, decisions, operations and advice to Welsh Government and others are underpinned by sound and quality-assured evidence. We recognise that it is critically important to have a good understanding of our changing environment. We will realise this vision by:

- Maintaining and developing the technical specialist skills of our staff;
- Securing our data and information;
- Having a well resourced proactive programme of evidence work;
- Continuing to review and add to our evidence to ensure it is fit for the challenges facing us; and
- Communicating our evidence in an open and transparent way.

This Evidence Report series serves as a record of work carried out or commissioned by Natural Resources Wales. It also helps us to share and promote use of our evidence by others and develop future collaborations. However, the views and recommendations presented in this report are not necessarily those of NRW and should, therefore, not be attributed to NRW.

Report series: Marine and Coastal Evidence Reports
Report number: 1019
Publication date: October 2026
Contractor: Bangor University
Contract Manager: P.E. Robins
Title: **Sources, Pathways and Fate of Suspended Sediments in the Milford Haven Estuary: Observations, Modelling and Future Change**
Author(s): **P.E. Robins, T.W. Clough, S. Garnier, I. Fairley, F. Ratcliffe, L. Pauls**
Peer Reviewer(s): Nicola Rimington, Mike Camplin, Liz Hopley
Approved By: Andrea Winterton
Restrictions: None

Distribution list

Core distribution list managed by the Library: National Library of Wales, British Library, Welsh Government, NatureScot, Natural England

Recommended citation for this volume:

P.E. Robins, T.W. Clough, S. Garnier, I. Fairley, F. Ratcliffe, L. Pauls. 2026. Sources, Pathways and Fate of Suspended Sediments in the Milford Haven Estuary: Observations, Modelling and Future Change. NRW Marine and Coastal Evidence Reports, Report No: 1019, 119pp.

Contents

About Natural Resources Wales 2
Evidence at Natural Resources Wales 2
Distribution list 3
Recommended citation for this volume: 3
Crynodeb Gweithredol 8
Executive summary 12
1 Introduction 16
2 Methodology 22
2.1 Observations of turbidity in the Milford Haven 22
2.1.1 Observational data in the Milford Haven 23
2.2 Model development 28
2.2.1 Model setup and parameterisation 28
2.2.3 Model scenarios 36
3 Results 42
3.1 Observations of turbidity in the Milford Haven 42
3.1.1 Equivalence between turbidity datasets 49
3.1.2 Drivers of maerl bed turbidity 52
3.2 Simulations of turbidity in the Milford Haven 69
3.2.1 Scenario-1a: December 2023 - January 2024 69
3.2.2 Scenario-1b: November 2025 - January 2026 74
3.2.3 Scenario-3: Maintenance dredging 80
3.2.4 Scenario-4: Sediment mobilisation at South Hook jetty 82
3.2.5 Scenario-5: Maerl bed erosion 85
3.2.6 Scenario-6: Sea-level rise dredging 87
3.2.7 Sensitivity tests: Sediment density 93
4 Discussion and conclusion 96
4.1 Summary 96
4.2 Synopsis of likely factors affecting sedimentation at the maerl bed 100
4.3 Comparative studies 101
4.4 Management implications 102
4.5 Limitations and future recommendations 104
5 Appendices 113

5.1 Appendix A1 - Turbidity calibration 113
5.2 Appendix A2 – Estuary residence time 114
5.3 Appendix A3 – Sediment evolution 116
5.4 Appendix A4 – Sea-level rise scenarios 119
5.5 Appendix A5 – Model sensitivity testing 120

List of Figures

Figure 2.1.1. *Map of the Milford Haven estuary.*

Figure 2.12.1. *Model validation of sea surface height at Milford Haven, Mumbles and Ilfracombe.*

Figure 2.2.2. *Model validation of water level and velocity, at the maerl bed site, Milford Haven.*

Figure 2.2.3. *Model validation of sea surface salinity across eleven stations within the Milford Haven.*

Figure 2.2.4. *Simulated velocity in Milford Haven during dominant flood and ebb conditions.*

Figure 3.1.1. *Observations of water level, river discharge, river turbidity, and maerl bed turbidity.*

Figure 3.1.2. *Distribution plots and seasonal boxplots of observations (2023–2024).*

Figure 3.1.3. *Distribution plots and seasonal boxplots of observations (2025–2026).*

Figure 3.1.4. *Scatter plots comparing maerl bed turbidity between the two observation campaigns.*

Figure 3.1.5. *Conversion of maerl bed turbidity measurements from mV to FNU units.*

Figure 3.1.6. *Power spectral density estimate of maerl bed turbidity observations (2023–2024).*

Figure 3.1.7. *Twenty-four-hour time series of maerl bed turbidity and horizontal velocity.*

Figure 3.1.8. *Scatter plot of maerl bed turbidity versus water level.*

Figure 3.1.9. *Cross-correlation between maerl bed turbidity and water level.*

Figure 3.1.10. *Scatter plot of de-tided maerl bed turbidity versus RMS water level.*

Figure 3.1.11. *Scatter plots of log-transformed river turbidity versus river discharge.*

Figure 3.1.12. *River discharge time series for the Eastern and Western Cleddau.*

Figure 3.1.13. *Scatter plots of log-transformed river turbidity versus river discharge.*

Figure 3.1.14. *Scatter plots of log-transformed river turbidity versus river discharge.*

Figure 3.1.15. *Cross-correlation between river turbidity and de-tided maerl bed turbidity.*

Figure 3.1.16. *Total river discharge from the Eastern and Western Cleddau rivers.*

Figure 3.1.17. *Scatter plots of log-transformed, de-tided maerl bed turbidity vs total river discharge.*

Figure 3.1.18. *Scatter plots and cross-correlations between maerl bed turbidity and river turbidity.*

Figure 3.1.19. *Scatter plots and cross-correlations between maerl bed turbidity and river discharge.*

Figure 3.2.1. *Scenario-1a: Median turbidity time series.*

Figure 3.2.2. *Scenario-1a: Sediment travel time from the river input through the estuary.*

Figure 3.2.3. *Scenario-1a: Spatial distribution of maximum turbidity for the fine silt/clay fraction.*

Figure 3.2.4. *Scenario-2: Spatial distribution of maximum turbidity for the fine silt/clay fraction.*

Figure 3.2.5. *Scenario-2: Maximum turbidity along the estuary for coarse silt and fine silt/clay.*

Figure 3.2.6. *Scenario-1b: Spatial distribution of maximum turbidity for the fine silt/clay fraction.*

Figure 3.2.7. *Scenario-1b: Median turbidity time series for the fine silt/clay fraction (maerl bed area).*

Figure 3.2.8. *Scenario-1b: Spatial distribution of maximum fine silt/clay bed mass accumulation.*

Figure 3.2.9. *Scenario-1b: Depth–time plots of turbidity, salinity and velocity the maerl bed.*
Figure 3.2.110. *Scenario-1b: Turbidity, salinity, velocity, and bed shear stress at the maerl bed.*
Figure 3.2.111. *Scenario-3: Maximum turbidity along the longitudinal estuary transect.*
Figure 3.2.112. *Scenario-4: Maximum turbidity along the longitudinal estuary transect.*
Figure 3.2.113. *Scenario-4: Spatial distribution of total sediment thickness at weekly intervals.*
Figure 3.2.114. *Scenario-5: Turbidity at the maerl bed and cumulative bed mass change.*
Figure 3.2.115. *Scenario-5: Maximum turbidity for fine silt/clay and fine sand.*
Figure 3.2.116. *Scenario-6: Max. turbidity along the estuary under sea-level rise dredging scenarios.*
Figure 3.2.117. *Scenario-6: Maximum turbidity >10^{-4} FNU for fine silt/clay under sea-level rise.*
Figure 3.2.118. *Scenario-6: Maximum sediment thickness exceeding 0.001 mm under sea-level rise.*
Figure 3.2.119. *Scenario-6: Modelled hydrodynamic response to projected sea-level rise.*
Figure 3.2.1201. *Sensitivity of modelled turbidity to parameterisation* of the *fine silt/clay fraction.*

List of Tables

Table 2.1.1. *Model parameterisation of mud and sand fractions.*
Table 2.1.2. *Summary of model scenarios.*
Table 2.1.3. *Sediment transport parameter sensitivity tests.*

Crynodeb Gweithredol

Gall dyfroedd cymylog mewn afonydd sy'n cynnwys crynodiadau uchel o waddod sy'n arnofio effeithio'n negyddol ar gynefinoedd, rhywogaethau a physgodfeydd mewn aberoedd. Er enghraifft, gall llai o olau gan fod y dŵr yn gymylog gyfyngu ar ffotosynthesis a lleihau'r ocsigen toddedig sydd ar gael ar gyfer resbiradaeth a thwf pysgod. Gall mygu oherwydd dyddodiad gwaddod effeithio'n negyddol ar amrywiaeth o gynefinoedd ar wely'r môr.

Fodd bynnag, yn aml nid oes gennym ddealltwriaeth dda o ffynonellau ac ymddygiad gwaddodion sy'n arnofio mewn aberoedd. Mae hyn yn atal rhanddeiliaid rhag gwneud penderfyniadau gwybodus am y gwaith rheoli sydd ei angen i gefnogi ecosystemau aberoedd. Mae'r bwlch hwn yn ein gwybodaeth yn deillio o'r ffaith mai cyfyngedig yw'r data sydd ar gael a bod diffyg modelu eglur ar gyfer aberoedd. Felly, ymchwiliodd yr astudiaeth hon i ddeinameg cymylogrwydd aberoedd drwy ddadansoddiad newydd o ddata arsylwi eglur a modelau efelychu.

Ymchwiliodd y prosiect hwn i ddeinameg cymylogrwydd yn astudiaeth achos Aberdaugleddau – gan ystyried ffynonellau gwaddod o'r ddwy brif afon (Cleddau Ddu a Chleddau Wen). Canolbwyntiodd yr astudiaeth ar wely maerl yn yr aber allanol; cynefin sy'n dueddol o gael ei fygu gan waddod. Nod y prosiect hefyd oedd deall beth sy'n digwydd i waddod a gaiff ei symud yn sgil carthu, gweithgarwch diwydiannol arall, a ffactorau naturiol sy'n achosi gwaddod i arnofio yn yr aber. Yn olaf, ymchwiliodd y prosiect i sut gallai cynnydd yn lefel y môr newid hydrodynameg aberoedd a dynameg gwaddod sy'n arnofio.

Casglwyd arsylwadau o gymylogrwydd, amodau llanw a llif afonydd rhwng Gorffennaf 2023 a Ionawr 2024, a rhwng Rhagfyr 2025 a Ionawr 2026. Dadansoddwyd y rhain i nodweddu cymylogrwydd ar y gwely maerl, ac i ddeall ffactorau'r llanw a'r afon sy'n achosi cymylogrwydd. Roedd cymylogrwydd wrth y gwely maerl yn gyffredinol yn amrywio o 1 i ~30 FNU, ond yn codi hyd at ~200 FNU o bryd i'w gilydd (h.y. cymylog iawn gyda golau'n gyfyngedig iawn) gan barhau ychydig oriau. Roedd cymylogrwydd yn amrywio'n bennaf oherwydd llif y llanw. Credir bod y cymylogrwydd yn ymestyn ar hyd yr aber, ac yn cynnwys gwaddodion wedi'u codi o wely'r aber yn ystod llifau llanw brig yn ogystal â gwaddodion o'r afon sy'n mynd i mewn i'r aber o bryd i'w gilydd. Mae'r gwaddodion hyn wedi'u cymysgu ledled yr aber; gall gronynnau llai (clai a siltiau) barhau i arnofio am sawl diwrnod, tra bod gwaddodion mwy yn setlo pan fo'r dŵr yn tawelu.

Mae'r cwmwl yn symud yn ôl ac ymlaen drwy'r aber gyda cheryntau'r llanw, gan fynd i ffwrdd o'r lan pan fydd y llanw'n mynd allan a chael ei wthio yn ôl i fyny'r aber pan fydd y llanw'n dod i mewn. Mae'r llanw sy'n mynd allan yn gwthio'r cwmwl i ffwrdd o'r lan, a gall ledaenu gan fynd yn llai dwys. Yna, bydd mwyafrif y gwaddodion sy'n arnofio yn dod yn ôl i'r aber ar

y llanw canlynol sy'n dod i mewn, a bydd gwaddodion sydd wedi setlo yn arnofio eto. Caiff y rhain yna'u cludo dros y gwely maerl, gan gynhyrchu cymylogrwydd cyson am sawl awr cyn lleihau yn ystod dŵr tawel y penllanw. Mae'r cwmwl yn teithio i fyny'r afon ac yn crynhoi yn y sianeli sy'n culhau yn yr aber uchaf – dyma gymylogrwydd aberol ar ei fwyaf. Yna mae'r llanw canlynol sy'n mynd allan yn symud hyn tua'r môr ac yn ôl dros y gwely maerl gan gynhyrchu'r lefel uchaf o gymylogrwydd yn ystod y llanw trai hwyr, cyn i'r cwmwl mwyaf symud oddi ar y lan – ar ôl hynny mae'r cylch hwn yn ailadrodd dros y llanw nesaf (hynny yw, dau gylch llanw y dydd). Yn nodedig, roedd y cylch llanw bob pythefnos rhwng y gorllanw a'r llanw bach yn newid y cymylogrwydd yn sylweddol: gwelwyd mwy o gymylogrwydd am ychydig ddyddiau yn ystod y gorllanw. Mae'r llanwau mwy yn achosi ceryntau penllanw cryfach a straen croeswasgu ar y gwely – hynny yw, gan achosi i waddodion yr aber arnofio eto. Maent hefyd yn golygu bod ardal fwy yn dod yn ddigon bas fel y gall tonnau oherwydd gwynt yn lleol symud gwaddod, gan gyfrannu at gynyddu cymylogrwydd.

Yn ystod cyfnodau o lif uchel yn yr afon, roedd cymylogrwydd yn sgil y llanw yn llai amlwg oherwydd bod gwaddod o'r afon yn dominyddu o ran creu cymylogrwydd ar y gwely maerl. Roedd y cymylogrwydd a welwyd yn y ddwy afon Cleddau yn uwch nag ar y gwely maerl; roedd cymylogrwydd yr afon yn 1–10 FNU yn ystod amodau llif isel (h.y. glawiad isel) ond yn cynyddu i 10^4–10^5 FNU yn ystod achlysuron o lif uchel. Cynyddodd cymylogrwydd yn yr afonydd wrth i arllwysiad gynyddu cyn tueddu i arafu wedyn yn ystod arllwysiad uwch; fodd bynnag, roedd y berthynas yn gymhleth ac yn debygol o ddibynnu ar y glawiad diweddar a'r amser ers y tro diwethaf i'r afon fod ar ei lefel uchaf. Datgelodd dadansoddiadau traws-cydberthynas berthynas gadarnhaol ystadegol-arwyddocaol rhwng cymylogrwydd afonydd a chymylogrwydd ar y gwely maerl, gydag oedi o sawl diwrnod rhwng y ddau. Mae hyn yn awgrymu y gall cymylogrwydd uwch yn yr afonydd gynyddu cymylogrwydd ar y gwely maerl. Fodd bynnag, mae'n debyg bod yr amser oedi penodol yn cael ei bennu gan ddwyster a hyd digwyddiadau llifogydd yr afon, yn ogystal ag amrywioldeb prosesau hydrodynamig. Dylid nodi bod amryw o afonydd yn llifo i'r aber a dim ond dwy sydd â mesuryddion llif a chymylogrwydd – felly gallai'r cymylogrwydd wrth y gwely maerl gael ei achosi gan fewnbynnau o afonydd eraill, gyda data'r afonydd yn brocsi ar gyfer y mewnbynnau hyn.

Datblygwyd model cludo gwaddod sy'n arnofio a hydrodynamig tri dimensiwn eglur ar gyfer Aberdaugleddau. Cafodd y model ei raddnodi a'i ddilysu yn erbyn data hydrodynamig arsylwadol ac yna ei baramedreiddio i efelychu cyfres o senarios sy'n berthnasol i waddodiad ar y gwely maerl.

Atgynhyrchodd y senarios model cychwynnol hydrodynameg ymgyrchoedd arsylwi 2023–24 a 2025–26, ond dim ond mewnbwn gwaddod sy'n arnofio o'r afon (Cleddau) a efelychwyd (hynny yw, dim gwaddod sy'n arnofio a ddaeth oddi mewn i'r aber). Parhaodd y ffracsiynau clai a silt mân a efelychwyd (<83 µm) i arnofio am sawl diwrnod a chyrhaeddon nhw ardal y gwely maerl, ond setlodd ffracsiynau silt a thywod mwy bras yn gyflym ymhellach i fyny'r afon. Ar y gwely maerl, cyrhaeddodd cyflymderau llanw uchafbwynt o ~0.7 m/e yn haen yr

arwyneb yn ystod llifogydd y gorllanw (cyflymderau uchaf llanw'r trai oedd ~0.6 m/e), gyda phroffil cyflymder fertigol nodweddiadol, h.y. cyflymder yn lleihau gyda dyfnder a chyflymder, croeswasgu a chymylogrwydd yn cynyddu gyda dyfnder. Roedd y golofn ddŵr wedi'i chymysgu'n dda i raddau helaeth. Roedd cymylogrwydd a efelychwyd yn cydberthyn â'r llanw a'r croeswasgiad cyflymder fertigol, gyda chymylogrwydd yn uwch yn ystod y gorllanw nag yn ystod y llanw bach ac yn uwch yn agosach at wely'r môr nag at yr wyneb. Roedd y cymylogrwydd a efelychwyd wedi'i ddominyddu gan y trai (hynny yw, allforiad net o waddod tuag at geg yr aber) ac yn sylweddol is na'r lefelau cymylogrwydd a arsylwyd. Mae'r gwahaniaeth hwn oherwydd mai dim ond gwaddodion afon Cleddau a fewnbynnwyd i'r model; mewn gwirionedd, mae gwaddodion sy'n arnofio a ddaw oddi fewn i'r aber a ffynonellau gwaddod afonol eraill yn cyfrannu at gymylogrwydd yr aber. At hynny, roedd y cymylogrwydd a efelychwyd yn sensitif iawn i'r math o waddod a dwysedd y gronynnau a fewnbynnwyd i'r model, gan awgrymu bod arsylwadau cywir o ddosraniadau a chategorïau maint gwaddod sy'n arnofio yn bwysig ar gyfer astudiaethau modelu pellach. Rhagwelodd yr efelychiadau cychwynnol hyn setliad bach o siltiau a chlai ar y gwely maerl.

Efelychodd senarios modelu dilynol waddodion yn symud ac yn arnofio o leoliadau o fewn yr aber. Roedd un senario yn efelychu ail-symud gwaddodion yn safle gwaredu Neyland Yacht Haven (~17 km i fyny'r afon o'r gwely maerl), lle mae carthu cynnal a chadw trwyddedig yn digwydd yn rheolaidd. Dangosodd yr efelychiadau hyn y gall siltiau a chlai a ail-symudwyd o Neyland gyrraedd y gwely maerl mewn ychydig ddyddiau. Fodd bynnag, mae'r lefelau'n dal i fod yn llawer is na'r cymylogrwydd a welwyd ar y gwely maerl. Roedd yr efelychiadau hyn hefyd yn rhagweld setliad bach o waddodion ar y gwely maerl.

Roedd senario arall yn efelychu ail-symud gwaddod wrth lanfa South Hook, sydd ychydig gannoedd o fetrau i'r dwyrain o'r gwely maerl. Cadarnhaodd yr efelychiadau hyn y gall clai, siltiau a thywod mân wedi'u hail-symud o'r cyffiniau hyn barhau i arnofio dros y gwely maerl, gan gynhyrchu cymylogrwydd o hyd at ~0.6 FNU. Setlodd y gwaddodion trymach a garthwyd (tywod mân) yn gyflym yn agos at y ffynhonnell – gan gynnwys dros y gwely maerl gan gynhyrchu haen hyd at 0.5 mm o drwch – tra setlodd y siltiau a'r clai mân yn y baeau arfordirol cyfagos ychydig gilometrau i ffwrdd dros y chwe wythnos dilynol. Efelychodd senario pellach erydiad gwaddodion naturiol gwely'r môr yn uniongyrchol ar y gwely maerl a dangosodd, o ystyried haen ddigon mawr o siltiau a chlai y gellir eu herydu, y gallai'r straen croeswasgu ar y gwely oherwydd y llanw lleol godi'r ffracsiynau hyn i gynhyrchu gwerthoedd cymylogrwydd a oedd yn cyfateb i'r lefelau a arsylwyd. Fodd bynnag, ni chafodd tywod mân ei erydu i raddau helaeth yn ystod yr efelychiad, a oedd yn cwmpasu nifer o gylchoedd llanw rhwng y gorllanw a'r llanw bach. Byddai mesur y gwaddodion sy'n ffurfio gwely'r aber yn well yn gwella modelu yn y dyfodol.

Yn olaf, perfformiwyd senarios model gan ystyried cynnydd rhagamcanol yn lefel y môr o hyd at +0.78 m yn yr 21ain ganrif. Mae'r efelychiadau hyn yn dangos sut y disgwylir i hydrodynameg yr aber newid mewn ymateb i gynnydd yn lefel y môr. Roedd y senarios yn

efelychu carthu o Neyland yn rhan uchaf yr aber ac yn rhagweld y byddai'r cymylogrwydd ar y gwely maerl yn fwy na dwbl o'i gymharu â'r achos presennol. Mae hyn oherwydd bod cynnydd yn lefel y môr wedi cynyddu fflwcs cyfaint y llanw a chyflymderau'r llanw o fewn yr aber. Cynyddodd ehangder gofodol y cwmwl hefyd i fyny'r afon ac i lawr yr afon.

I grynhoi, dangosodd yr arsylwadau berthynas gadarnhaol rhwng cymylogrwydd a'r cylch llanw, ar amserlenni lled-ddyddiol a phob pythefnos. Nododd yr arsylwadau hefyd berthynas gadarnhaol ond cymhleth rhwng mewnbynnau afonol a chymylogrwydd ar y gwely maerl. Ychwanegodd yr efelychiadau model feintioli at y berthynas hon, gan awgrymu mai dim ond cyfrannau bach o siltiau a chlai o afonydd Cleddau Ddu a Chleddau Wen a gyrhaeddodd y gwely maerl yn uniongyrchol o dan yr amodau llanw/afon a arsylwyd. Archwiliodd y model hefyd effaith gweithgarwch anthropogenig ar gymylogrwydd aberoedd: mae canlyniadau'n dangos nad yw'n debygol y bydd y carthu presennol yn Neyland yn cael effaith fawr ar ddyddodiad ar y gwely maerl; mae efelychiadau'n dangos bod symudiad hanesyddol gwaddod yn ystod adnewyddu'r cei yn debygol o fod wedi arwain at ddyddodiad ar y gwely maerl.

Executive summary

Turbid river waters containing high concentrations of suspended sediment can negatively impact estuarine habitats, species, and fisheries. For example, reduced light penetration caused by turbidity can limit photosynthesis and reduce dissolved oxygen available for fish respiration and growth. Smothering due to sediment deposition can negatively affect a range of seabed habitats. However, the sources and behaviour of suspended sediments in estuaries are often poorly understood. This prevents stakeholders from making informed decisions about the management needed to support estuary ecosystems. This knowledge gap stems from limited data availability and lack of high-resolution modelling of estuarine regions. This study, therefore, investigated estuarine turbidity dynamics through new analysis of high-resolution observational data and model simulations.

This project investigated turbidity dynamics for the case study of the Milford Haven estuary, considering sediment sources from the two main rivers (the Eastern Cleddau and Western Cleddau). The study focused on a maerl bed in the outer estuary; a habitat that is vulnerable to smothering by sediment. The project also aimed to understand the fate of sediment mobilised by dredging, other industrial activity, and natural sediment resuspension within the estuary. Finally, the project investigated how sea-level rise might change the estuarine hydrodynamics and suspended sediment dynamics.

Observations of turbidity, tidal conditions and river flows were collected during July 2023 – January 2024 and December 2025 – January 2026. These were analysed to characterise turbidity at the maerl bed, and to understand the tidal and riverine drivers of turbidity. Turbidity at the maerl bed generally ranged from 1 to ~30 FNU, but with episodic spikes up to ~200 FNU (i.e., highly turbid with limited light penetration) that lasted a few hours. Variability in turbidity was predominantly driven by tidal flows. It is believed the turbidity plume extends throughout the estuary, consisting of sediments resuspended from the estuary bed during peak tidal flows as well as riverine sediments which enter the estuary during episodic events. These sediments are mixed throughout the estuary; smaller particles (clays and silts) can remain in suspension for several days, while coarser sediments settle during slack water. The plume moves back and forth through the estuary with the tidal

currents, spreading out offshore during the outgoing tide and being pushed back up-estuary during the incoming tide. The outgoing tide advects the turbid plume offshore, which can spread laterally and reduce in concentration. The majority of suspended sediments then re-enter the estuary on the following incoming tide and settled sediments are resuspended. These are transported over the maerl bed, producing a broadly consistent turbidity signal for several hours before reducing during slack high water. The turbid plume travels upstream and concentrates in the narrowing channels in the upper estuary to form an estuarine turbidity maximum. The following outgoing tide then moves the turbidity maximum seawards and back over the maerl bed producing a peak turbidity signal during the late ebbing tide, before the maximum moves offshore – after which the cycle repeats over the next tide (i.e., two tidal cycles per day). Notably, the fortnightly spring-neap tidal cycle substantially modulated turbidity: increased turbidity was observed for a few days during spring tides. The larger tidal ranges drive stronger peak tidal currents and bed shear stress (i.e., promoting resuspension of estuarine sediments). They also mean that a greater area becomes shallow enough that local wind waves can mobilise sediment, contributing to the increased turbidity.

During periods of high river flow, the tidal modulation of turbidity became less obvious because river-derived sediment inputs temporarily dominate turbidity at the maerl bed. Observed turbidity within the two Cleddau rivers were higher than at the maerl bed; typically, riverine turbidity were 1–10 FNU during low flow conditions (i.e., low rainfall) but increasing to 10^4–10^5 FNU during episodic high flow events. Turbidity in the rivers increased with increasing river discharge before tending to plateau during higher discharge values; however, the relationship was complex and likely dependant on the recent rainfall and time since the last peak in river level. Cross-correlation analyses revealed a statistically significant positive relationship between riverine turbidity and turbidity at the maerl bed, with a lag of several days. This suggests that elevated turbidity in the rivers can increase turbidity at the maerl bed, however the specific lag time is likely determined by the intensity and duration of the river flood events, as well as variability hydrodynamic processes. It should be noted that there are various rivers that flow into the estuary and only two have flow and turbidity gauges, so the turbidity at the maerl bed might be caused by other fluvial inputs, with the river data being proxies for these inputs.

A high-resolution three-dimensional hydrodynamic and suspended sediment transport model was developed for the Milford Haven estuary. The model was calibrated and validated against observational hydrodynamic data and then parameterised to simulate a series of scenarios pertinent to sedimentation at the maerl bed.

The initial model scenarios reproduced the hydrodynamics of the 2023–24 and 2025–26 observation campaigns, but simulated only riverine (Cleddau) suspended sediment inputs (i.e., no resuspension of sediments from within the estuary). The simulated clay and fine silt fractions (<83 µm) remained in suspension for several days and reached the maerl bed area, but coarser silt and sand fractions quickly settled further upstream. At the maerl bed, tidal velocities peaked at ~0.7 m/s in the surface layer during spring flood tides (peak ebb tidal velocities were ~0.6 m/s), with a characteristic vertical velocity profile, i.e., decreasing velocity with depth and increasing velocity shear and turbulence with depth. The water column was largely well-mixed. Simulated turbidity correlated with the tide and vertical velocity shear, with turbidity being higher during spring than neap tides and higher closer to the seabed than at the surface. Simulated turbidity was ebb-dominant (i.e., a net export of sediment towards the estuary mouth) and substantially lower than observed turbidity levels. This difference is because only Cleddau riverine suspended sediments were inputted to the model; in reality, resuspended sediments from within the estuary and other riverine sediment sources contribute to the estuarine turbidity plume. Further, the simulated turbidity was highly sensitive to the sediment type and particle density inputted into the model, suggesting that accurate observations of suspended sediment size class distributions are important for further modelling studies. These initial simulations predicted negligible settlement of riverine silts and clays at the maerl bed.

Subsequent modelling scenarios simulated resuspension and remobilisation of sediments from locations within the estuary. One scenario simulated the remobilisation of sediments at the Neyland Yacht Haven disposal site (~17 km upstream of the maerl bed), where licensed maintenance dredging routinely occurs. These simulations indicated that silts and clays remobilised from Neyland can reach the maerl bed in a few days, however, the levels are still much less than observed turbidity at the maerl bed. These simulations also predicted negligible settlement of sediments at the maerl bed. Another scenario simulated sediment remobilisation at the South Hook jetty, which is a few hundred metres east of the maerl bed.

These simulations confirmed that remobilised clays, silts, and fine sands, from this vicinity can remain in suspension over the maerl bed, producing turbidity of up to ~0.6 FNU. The heavier dredged sediments (fine sands) quickly settled close to the source site – including over the maerl bed producing a bed layer up to 0.5 mm thick – whilst the finer silts and clays settled in the adjacent coastal bays a few kilometres away over the subsequent six weeks. A further scenario simulated erosion of the natural seabed sediments directly at the maerl bed and demonstrated that, given a large enough erodible layer of silts and clays, the local tidally driven bed shear stress could resuspend these fractions to produce turbidity values that matched observed levels. Fine sands, however, were largely not eroded during the simulation, which covered multiple spring-neap tidal cycles. Better quantification of the sediments that make up the estuary bed would improve future modelling.

Finally, model scenarios were performed considering 21st century projected sea-level rise of up to +0.78 m. These simulations demonstrate how the hydrodynamics of the estuary are expected to change in response to sea-level rise. The scenarios simulated dredging from Neyland in the upper-estuary and predicted the turbidity at the maerl bed to more than double compared to the present-day case. This is because sea-level rise increased the tidal volume flux and tidal velocities within the estuary. The spatial extent of the turbidity plume also increased in both upstream and downstream directions.

In summary, the observations showed a positive relationship between turbidity and the tidal cycle, at both semi-diurnal and fortnightly timescales. The observations also identified a positive but complex relationship between fluvial inputs and turbidity at the maerl bed. The model simulations added quantification to this relationship, suggesting that only small proportions of riverine silts and clays from the East and West Cleddau directly reached the maerl bed under the observed tidal/riverine conditions. The model also explored the impact of anthropogenic activity on estuarine turbidity: results show that current dredging at Neyland is unlikely to have a major effect on deposition at the maerl bed; simulations indicate that historic mobilisation of sediment during jetty refurbishment is likely to have led to deposition on the maerl bed.

1 Introduction

Estuaries in the UK are highly dynamic and turbid coastal systems, exposed to the interactions of both terrestrial and marine suspended sediment regimes. Highly turbid waters can negatively impact sensitive estuarine habitats, species dynamics, and fisheries (Lunt and Smee 2020). Light penetration, for example, can be substantially reduced in highly turbid waters, which can limit the ability of plants and phytoplankton to photosynthesise (Gameiro et al. 2011), as well as hinder the ability of juvenile fish to locate prey leading to shifts in distributions (Lowe et al. 2015). Fine suspended sediments can impede fish respiration and growth, while the settlement of fine sediments can smother breeding grounds and habitats leading to reduced oxygen and hatching success (Lunt and Smee 2020). Turbid waters are often polluted with metals, pesticides, pathogens, microplastics, and nutrients which can lead to further negative impacts such as eutrophication, algal bloom development, and hypoxia events (Schmidt et al. 2019; Wurtsbaugh et al. 2019). Interactions and aggregations of suspended sediments and microplastics with pathogens and nutrients may enhance these negative effects in turbid estuaries (Malham et al. 2014).

Estuarine hydrodynamics and suspended sediment processes are highly variable and changeable and differ considerably between estuary types and geographies, and over episodic, seasonal, interannual, and climatic time scales (Lyddon et al. 2023). There are critical knowledge gaps in how rainfall, catchment runoff, and river flow dynamics drive riverine suspended sediment loads and their transport through and settlement within estuaries (Biguino et al. 2023; Wolanski and Elliott 2024). These knowledge gaps stem from limited understanding of the sediment sources, catchment and riverine transmission, estuarine hydrodynamics, sediment aggregations and transformations, and deposition / resuspension processes of different sediment types and different catchment-estuary systems, often because of a lack of good quality monitoring and simulation data. Without this knowledge, it is difficult for statutory advisers and regulators to implement evidence-based management of estuaries.

Investigating climate change impacts for UK estuaries up to now has been limited by coarse (e.g., daily, $\mathcal{O}$10 km scales) coastal climate projections (Robins et al. 2016; Holt et al. 2025). However, recent downscaling of the latest climate projections from the Met Office (UKCP18) have provided hourly and sub-km scale resolution data for future river flows and sea levels (e.g., Lyddon et al. 2025), which can be used to improve our understanding of estuary vulnerability to climate change. Given this and that there is a UK government policy-gap in how UK estuaries should be managed in response to projected climate change (Robins and Lyddon 2026), it is timely and crucial that transferable methods are developed to improve understanding of estuarine suspended sediment dynamics for sustainable and effective management of the marine environment.

An area where this evidence gap has been noted is the Milford Haven estuary, South Wales, part of the Pembrokeshire Marine / Sir Benfro Forol Special Area of Conservation (SAC). The Milford Haven estuary habitats have been assessed as being in unfavourable and declining condition and requiring further research to understand the pressures affecting its status, how these pressures are expected to change in the future, and what can be done to improve their condition (Bohn 2014; Jackson-Bué et al. 2025). An understanding of suspended sediment dynamics in the Milford Haven estuary was identified as a NRW marine evidence priority historically (Marine and Coastal collaborative research ideas). More recently, the lack of knowledge regarding the source, dynamics and fate of sediments in the estuary was emphasised during work on the condition of Marine Protected Areas (MPAs) for Welsh Government's Nature Networks Programme (Ratcliffe 2026). The project investigated the causes of declines in marine species and habitats, with one component focused on the Milford Haven maerl bed. There is Wales' only known bed of maerl (coralline red algae) in the lower estuary region and monitoring showed a decline of live maerl of over 90% in recent years. The report investigated each factor which could impact the maerl bed, including sedimentation, and the project highlighted how poorly sedimentation was understood within this estuary. Maerl is an extremely sensitive species to multiple environmental factors; without knowing the causes of the decline, including potential changes in turbidity, it is not possible to implement management measures to improve the condition of the maerl bed.

The industrialisation of the Milford Haven harbour has meant that there have been major anthropogenic impacts to accommodate the needs of the port, including within-estuary construction, capital and maintenance dredging. The impact from sedimentation from these activities against background suspended sediment movements presents a complex picture when advising on planning and site management.

Located within the Pembrokeshire Marine Special Area of Conservation, the Milford Haven has been designated for a range of Annex I habitat features: Estuaries, Large shallow inlets and bays, Mudflats and sandflats, and Reefs. Within this estuary, there are several rare and protected habitats such as Wales' only maerl bed, intertidal and subtidal seagrass beds, and oyster beds. Further, the Haven once supported important fisheries. Herring used to be a prominent fishery in the area and has been in decline in recent years; spawning grounds can be found in the upper reaches of the estuary. Oysters were also abundant in the Haven and supported a fishery which is now non-existent. The natural harbour provided by the Haven has led to the area becoming one of the most significant ports in the UK; it is the UK's largest energy port and the biggest port in Wales. Land use has also changed in the catchments feeding into the Haven, with increases in intensive grazing and arable farming over the last few decades, which are likely to increase river turbidity by accelerating soil erosion and nutrient runoff (Clermont et al. 2023). Together, against a background of changeable extreme weather events, these activities create a complex picture of sediment sources and sediment-dynamics within the Milford Haven estuary. The specifics, and relative importance, of how extreme weather events, dredging, and agricultural activities contribute to sedimentation in the estuary are not known. More information on the behaviour and movement of sediment from the various sources under different conditions is required to understand whether they are likely to pose a smothering risk to the maerl bed. This study will help assess the risk the different sediment sources pose to the maerl bed, primarily through smothering.

1.1 Aims and objectives

The central aim of this project was to improve understanding of suspended sediments within the Milford Haven estuary, sourced from the East and West Cleddau rivers. The project also aimed to understand the fate of point-source sediment loads from permitted dredged sites within the estuary. Finally, the project investigated how sea-level rise projections would likely change the river-sourced suspended sediment dynamics within the estuary. Specifically, the project addressed the following questions:

Q1) What are the hydrological and riverine turbidity dynamics of the Milford Haven catchment? I.e., How do suspended sediment loads from the East and West Cleddau rivers vary under different antecedent hydrological conditions?

Q2) Focussing on the maerl bed in the lower Milford Haven estuary, how do river flows and associated suspended sediments influence the maerl bed? How do tidal and estuarine hydrodynamics affect riverine suspended sediments? What is the sedimentation and resuspension behaviour of riverine suspended sediments at the maerl bed?

Q3) How does permitted dredging and sediment remobilisation in the Milford Haven affect the suspended sediment dynamics of the estuary, and specifically at the maerl bed?

Q4) How might projected 21st century sea-level rise influence the riverine suspended sediment dynamics within the Milford Haven?

To achieve the project's aims and address Q1-Q4, firstly observational data collected in the Milford Haven was presented and analysed. Specifically, data was available from 2023-2025 and comprised measurements of turbidity and hydrodynamics at the maerl bed and in the East and West Cleddau rivers. Temporal variability was assessed, and statistical relationships between the river flows, riverine turbidity, and estuarine turbidity were investigated (Q1 and Q2). Secondly, a high-resolution three-dimensional hydrodynamic and suspended sediment transport model of the estuary and wider offshore region was developed. The model simulated the 2023-2025 observation period, allowing for spatio-temporal understanding of the hydrodynamics and turbidity dynamics beyond the

observational sites (Q1 and Q2). Finally, the model was used to simulate the point source dredging scenarios (Q3) and the projected sea-level rise scenarios (Q4).

This project supports the development of science and technology to improve fundamental understanding of coastal dynamics, water quality, hazard risk, and climate change impacts. It will allow NRW and other stakeholders to have an improved understanding of the vulnerability of estuarine systems and their habitats and ecosystems to extreme events and climate change, hence will contribute to Wales having a marine environment which is resilient and sustainable against the effects of climate change. Changes to estuarine hydrodynamics and sediment dynamics caused by a changing climate are a global issue. The way the Milford Haven model has been co-developed by stakeholders (NRW) and modellers can act as a pilot to inform similar initiatives in other estuaries. The project is therefore relevant to other Welsh, UK and global estuarine regions. Further, the study showcases the development of a model that is foundational – i.e., developed for hydrodynamics and suspended sediment dynamics, but the modelling software can be built upon for other applications, such as morphological change, water quality indicators, and biochemical processes in estuaries, e.g., to investigate erosion, pollution, or eutrophication.

From a coastal management perspective, the project will provide:

- More confidence from NRW in relevant casework responses and the ability to advise on specific activities in the Haven to ensure that they are not having a detrimental impact to designated species and habitats.
- More confidence in delivering the right restoration projects. For example, Project Seagrass, Oyster restoration projects such as Natur am Byth, and other initiatives will benefit from the study because the species that they are restoring are sensitive to sedimentation.
- Increased confidence in assessment of the condition of designated features, such as the maerl bed, and stronger support for management which will bring features into favourable condition: e.g., by improved management of sediment remobilisation activities.
- More resilience to climate change: Sedimentation is likely to become a bigger problem in the future due to increased rainfall which can affect both riverine sediment load and

the amount (and timing/duration) that reaches specific habitats. The monitoring and modelling presented here will better prepare NRW for these events in the future.

- Better management of fisheries that ensures fisheries activities and regulation are coordinated with robust understanding of suspended sediment dynamics.
- Improved monitoring and reporting: NRW's duties around monitoring and reporting on the status of marine species and habitats will be strengthened with by this project. The modelling can be used to target monitoring of specific locations to understand how predicted sediment impacts are affecting the marine environment.

In terms of marine and coastal policy, this project builds on several UK estuary climate impact studies (e.g., Robins and Lyddon 2026), that contribute towards the scientific evidence needed to future-proof UK estuaries over the coming century.

2 Methodology

In this section we describe the methodology for the two work streams: (2.1) Observations of turbidity in the Milford Haven, where we describe and analyse existing and new hydrodynamic and suspended sediment data from within the estuary to address Q1-Q2; and (2.2) Model simulations of turbidity in the Milford Haven, where we describe the development and application of a 3D hydrodynamic and suspended sediment transport model, used to simulate a range of suspended sediment scenarios to address Q1-Q4.

2.1 Observations of turbidity in the Milford Haven

Since 2023, NRW have conducted hydrodynamic and turbidity surveillance of the Milford Haven, to improve understanding of suspended sediment dynamics surrounding the maerl bed in the lower estuary (Fig. 2.1.1). These deployments and data are described in section 2.1.1. An initial analysis of the data has suggested links between fluvial inputs and turbidity at the maerl bed and provides a foundational resource to address the core questions (Q1-Q2). During December 2025 and January 2026, NRW contracted CMAR to deploy further equipment (acoustic doppler velocimeter (ADV), pressure transducer and two optical backscatter sensors (OBSs)) to measure the hydrodynamics and suspended sediment concentrations at the maerl bed (Poate et al. 2026). Turbidity data from NRW deployed sondes in the East and West Cleddau rivers, just upstream of the tidal limits in these rivers are also available for these times (Fig. 2.1.1).

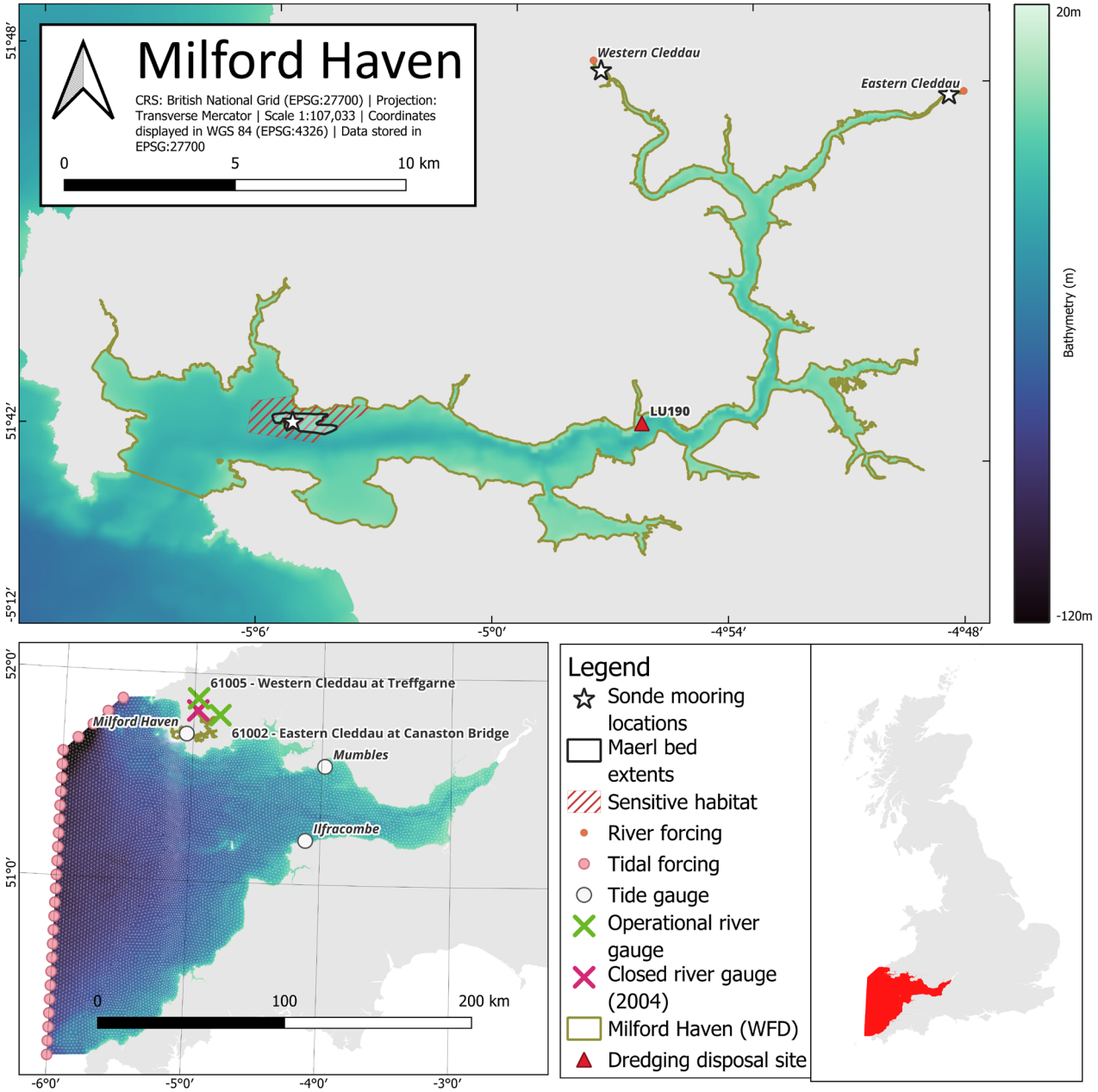


Figure 2.1.1. *Map of the Milford Haven estuary, showing the estuary size and shape, bathymetry, as well as the mooring locations and maerl bed. The model domain and discretisation covering the wider Severn estuary is also shown along with a UK map.*

2.1.1 Observational data in the Milford Haven

Previous data measured within the Milford Haven since 2023 was collated, processed, and analysed to characterise the present-day hydrodynamics and suspended sediment dynamics within the estuary. This data was also used to parameterise, calibrate, and validate

the modelling described in section 2.2. From this work, key data gaps were identified and recommendations made for further monitoring efforts.

Water levels within the lower estuary were recorded by a CTD deployed at the maerl bed (51.703°N, 5.088°W), providing local tidal elevation data at high temporal resolution. This was supplemented by records from the Milford Haven (51.706°N, 5.052°W), Mumbles (51.570°N, 3.975°W) and Ilfracombe (51.211°N, 4.111°W) tide gauges operated by the National Tide and Sea Level Facility (https://ntslf.org/tides; NTSLF 2025), providing tidal elevations and residual surge data across the broader Bristol Channel region. This hydrodynamic data was used for model validation.

Salinity data were obtained from NRW Water Framework Directive (WFD) surveys (available on request), comprising salinity samples collected approximately 5 times over a 1-hour window at eleven stations distributed across the upper Milford Haven during 18-19 September 2024. These data were used for model validation. Sampling locations were concentrated in the upper estuarine creeks and tributaries, making them well suited for validating the modelled extent of saline intrusion over time.

River discharge data at 15-minute temporal resolution were obtained from gauging stations closest to the tidal limits of each river, operated by Natural Resources Wales. For the Western Cleddau, discharge records were sourced from the Treffgarne gauge (61005; NRFA 2025a). Eastern Cleddau discharge was obtained from the Canaston Bridge gauge (61002; NRFA 2025b). This hydrological data was used for the observational analysis and for boundary forcing of the model.

Measurements of suspended sediment concentration were recorded by NRW at the Milford Haven maerl bed during two monitoring campaigns: from July 2023 to March 2024 and from early December 2025 to mid-January 2026 (approximately five weeks of observations). During the 2023-2024 deployment, a YSI EXO2 multiparameter sonde was deployed at the maerl bed (51.702466°N, 5.075235°W), recording water depth and turbidity at 10-minute intervals. Additional parameters, including pressure, salinity, dissolved oxygen, specific conductivity, total dissolved solids, total suspended solids, and temperature, were also

measured by the instrument but were not used in the present study. The sonde was mounted on a bed frame approximately 30 cm from the seabed, although the exact sensor height above the seabed was not recorded during the deployment. Turbidity measurements, expressed in Formazin Nephelometric Units (FNU), were calibrated against suspended sediment concentration (g/L) under laboratory conditions using seawater mixed with varying quantities of seabed sediment collected adjacent to the deployment site using a Niskin bottle and grab sampling.

During the 2025–2026 deployment, near-bed current velocity and direction were measured using an Acoustic Doppler Velocimeter (ADV) mounted on a seabed frame positioned on the maerl bed (51.70345°N, 5.0771°W). In addition, a pressure sensor was deployed to derive water depth throughout the monitoring period. These data were used for the observational analysis and for model validation. Two optical backscatter sensors (OBS1 and OBS2), mounted on the same frame, were used to monitor suspended sediment variability within the water column. OBS1 and OBS2 were positioned approximately 20 cm and 34.5 cm above the seabed, respectively, and recorded turbidity in mV units. Measurements were collected in burst mode every 30 min, with each burst consisting of 2400 samples acquired at 4 Hz over a 10 min period. As for the 2023–2024 deployment, in situ water samples were collected using a Niskin bottle to estimate suspended sediment concentrations at the site. However, the limited number of calibration samples restricted the quantitative interpretation of the OBS measurements, and turbidity values could not be robustly converted into the FNU or suspended sediment concentration units used during the 2023–2024 deployment.

In parallel with both monitoring campaigns, NRW conducted sonde deployments in the Eastern and Western Cleddau rivers to measure suspended sediment concentration (g/L) and turbidity (FNU) at 15 min intervals. This riverine suspended sediment data was used for the observational analysis and for boundary forcing of the model.

2.1.2 Data analysis

Following inspection of the turbidity time series, several periods affected by sensor malfunction were removed from the analysis. During the 2023–2024 deployment, maerl bed

turbidity measurements became unrealistically high from late October 2023 to early December 2023, and again after 21 February 2024; these periods were therefore discarded (Fig. 3.1.1). The first period was likely caused either by sonde malfunction or burial of the instrument within the sediment. The second period resulted from the mooring rope attached to the surface buoy becoming incorrectly re-secured during servicing and subsequently becoming entangled with the sensor. Additional issues were identified in the river turbidity datasets. Between late November 2023 and mid-January 2024, the Eastern Cleddau turbidity record was incorrectly saved and duplicated the Western Cleddau time series. To reconstruct the missing Eastern Cleddau data, a proportional relationship between Eastern and Western Cleddau turbidity was derived using the remainder of the 2023–2024 deployment, and this relationship was used to estimate the missing values. During the first few days of the 2025–2026 deployment, unrealistically high turbidity values were recorded in the Eastern Cleddau, most likely due to partial burial of the turbidity sensor. This section of the record was replaced using observations from the Western Cleddau for the corresponding period.

To facilitate comparison between datasets collected at different sampling frequencies, time series were resampled to hourly resolution prior to analysis. Hourly mean values were calculated for water level, river discharge, river turbidity, and maerl bed turbidity. For analyses involving combined river forcing, a total river discharge variable was calculated as the sum of discharge from the Eastern and Western Cleddau rivers. Similarly, total river turbidity was calculated as the sum of turbidity observations from both rivers.

To isolate the influence of river-derived suspended sediment inputs from semi-diurnal and diurnal tidal variability, a de-tided turbidity signal was derived from the maerl bed turbidity observations using a Godin low-pass filter (Thomson & Emery 2024). The resulting de-tided turbidity signal was subsequently used in river-forcing analyses and cross-correlation calculations. Root mean square (RMS) water level (z_{RMS}) was additionally calculated to represent variations in tidal energy at spring–neap timescales:

$$z_{RMS} = Godin\{\sqrt{(z - \overline{z})^2}\} + \overline{z}$$

where $\overline{z} = \frac{1}{N}\sum_{i=1}^{N} z_i$ represents the mean water level over the deployment period, and $Godin\{\}$ denotes application of the Godin low-pass filter.

For both campaigns, seasonal analyses were undertaken by grouping observations into summer, autumn, and winter periods. Distribution plots and seasonal boxplots were used to characterise variability between seasons and deployments. Power spectral density (PSD) estimates were calculated using hourly turbidity observations from the 2023–2024 deployment to identify dominant temporal frequencies within the maerl bed turbidity record and assess the influence of tidal forcing. Pearson correlation and cross-correlation analyses, using hourly lag increments, were undertaken to quantify the influence of tidal and riverine processes on maerl bed turbidity. For tidal analyses, lags of up to 12 h were investigated to capture semi-diurnal tidal variability. For river-forcing analyses, lags of up to 6 days were considered to assess delayed transport and persistence of river-derived suspended sediments within the estuary. The two monitoring campaigns were analysed separately because maerl bed turbidity was measured using different units during each deployment (FNU during 2023–2024 and mV during 2025–2026).

To investigate the influence of individual river discharge events on turbidity dynamics, discharge peaks were identified from the river discharge time series for both the Eastern and Western Cleddau rivers. Each discharge peak was characterised according to three attributes: (i) peak prominence, (ii) the time elapsed since the previous discharge peak maximum, and (iii) the prominence of the preceding discharge peak. Equivalent analyses were also undertaken using the combined total river discharge time series. Discharge events were classified using threshold values of 38 h for event separation and 9 $m^3\ s^{-1}$ for the prominence of both current and antecedent discharge peaks. These thresholds were selected to produce comparable numbers of events above and below each threshold. The resulting classifications were subsequently used in scatter plot and cross-correlation analyses to investigate the influence of discharge-event magnitude, timing, and antecedent hydrological conditions on 2023-2024 maerl bed turbidity dynamics, including the distinction between clustered and isolated (‘first flush’) river events.

2.2 Model development

The modelling methodology has been designed to resolve key features and processes within the Milford Haven, including estuarine habitat features (e.g., mudflats, sandflats, fast-flowing channels, mobile sand features) and complex hydrodynamic and water quality processes (e.g., tidal propagation, recirculating eddies, salinity gradients, turbidity maxima, suspended sediment plumes, sedimentation and resuspension). These hydrodynamic and water quality processes act with high spatial and temporal variability, and are sensitive to changes in the tidal regime, sea level, river flow, and riverine suspended sediment loading. The modelling describes a transferable method for investigating estuarine turbidity and fine sediment settlement and resuspension dynamics driven by both marine and riverine interactions.

2.2.1 Model setup and parameterisation

A 3D hydrodynamic and sediment transport model of the Milford Haven was developed using Delft3D Flexible Mesh Suite (Delft3D-FM; Deltares 2025), where the D-Flow hydrodynamic module was coupled with the D-Morphology sediment transport module. The model domain extends from the tidal limits of the East and West Cleddau rivers, through the full extent of the Milford Haven estuary, to an open boundary in the Irish Sea (Fig. 2.1.1). The unstructured flexible mesh grid comprises 81,783 nodes with a minimum spatial resolution of 3.5 m in narrow channels and around key estuarine habitat features, increasing to 3.3 km at the offshore tidal boundary. Grid orthogonality is 0.387. The vertical dimension was resolved using 10 equally-segmented sigma layers, enabling representation of stratification and depth varying velocity and suspended sediment fluxes.

Bathymetry was compiled from multiple sources (see Barada et al., 2026b). Intertidal and shallow subtidal areas were resolved using Lidar Composite Digital Terrain Model Wales (NRW, 2025; 2 m resolution), integrating LiDAR and nearshore multibeam sonar. Estuarine channel bathymetry was sourced from Admiralty Seabed Mapping Service data (UKHO 2024), corrected from Chart Datum to local mean sea level (MSL) using spatially varying tidal amplitudes derived from the FES2022 global tidal model. Offshore regions were filled

using EMODnet (2022) digital bathymetry (~115m resolution, referenced to MSL). All datasets were merged as point clouds and interpolated onto the model grid using ArcGIS TopoToRaster to produce a hydrologically consistent bathymetric surface.

Open sea boundary conditions were prescribed as time-varying sea surface height, depth-averaged velocity components (U, V), and salinities, extracted from the Copernicus Marine Service NEMO ocean model (CMEMS 2026). River discharge boundaries at East and West Cleddau rivers were forced using 15-minute flow records provided by NRW.

The sediment transport configuration includes cohesive (mud) fractions representing fine sediments supplied from fluvial inputs, and a non-cohesive sand fraction representing the seabed at the maerl bed. Mud and sand fractions (Table 2.2.1) were assigned specific densities, dry bed densities, and grain size D50 following Lepesqueur et al. (2019), with critical stress for erosion at the maerl bed parameterised at 0.17 N/m2 (Poate et al. 2026).

Table 2.2.1. *Model parameterisation of mud and sand fractions according to specific densities, dry bed densities, and grain size D50 following Lepesqueur et al. (2019).*

Grain Size Class	Specific density (kg m^{-3})	Dry bed density (kg m^{-3})	Grain size (m)
500 µm (Medium Sand)	2,480	1600	0.0005
200 µm (Fine Sand)	2,420	1325	0.0002
100 µm (Very Fine Sand)	2,850	1050	0.0001
83 µm (Coarse Mud)	1,810	775	0.000083
63 µm (Fine Mud)	2,170	500	0.000063

Riverine suspended sediment concentrations were prescribed as time-varying boundary conditions at the East and West Cleddau tidal limits, derived from the sonde observations described in section 2.1. Observed turbidity (FNU) was converted to suspended sediment concentrations (SSC) using a site-specific linear calibration (SSC mg/L = 1.520 × FNU − 1.40), derived from calibration water samples collected during the 2023 NRW field campaign (Appendix A1).

Sand transport was computed using the van Rijn (1993) suspended load formulations, whereas mud transport was governed by the Partheniades-Krone formulations

(Partheniades 1965). Initial bed composition was set to zero in baseline simulations, isolating the contribution of fluvially-supplied suspended sediment to estuarine turbidity. For maerl bed erosion simulations, a sand layer of 0.5 m thickness was specified exclusively over the maerl bed extents, with a D50 of 231 µm and specific density of 2420 kg/m^3, estimated from NRW grab samples. These simulations were used to assess whether modelled near-bed velocities and bed shear stresses are sufficient to mobilise and resuspend maerl bed material.

2.2.2 Model calibration and validation

The model was calibrated and validated against independent observational datasets spanning hydrodynamic, salinity, and suspended sediment variables. Tidal validation, across the wider model domain, was performed by comparing modelled water levels against records from the Milford Haven, Mumbles and Ilfracombe tide gauges (BODC 2025) for the period 01-31 January 2000, following a 2-month spin-up. At Milford Haven, the model reproduced observed water levels with an RMSE of 0.176 m and a correlation coefficient of 0.995 (Fig. 2.2.1a). Harmonic analysis of the M2 tidal constituent yielded an amplitude error of -0.036 m and a phase error of -5.0°, with corresponding S2 errors of +0.020 m and -3.8°. At Mumbles, RMSE was 0.199 m (r = 0.998), with M2 amplitude and phase errors of -0.153 m and +2.0°, respectively (Fig. 2.2.1b). Performance was reduced at Ilfracombe, where RMSE increased to 0.394 m (r = 0.990) and the M2 amplitude error was -0.304 m with a phase error of +7.1° (Fig. 2.2.1c).

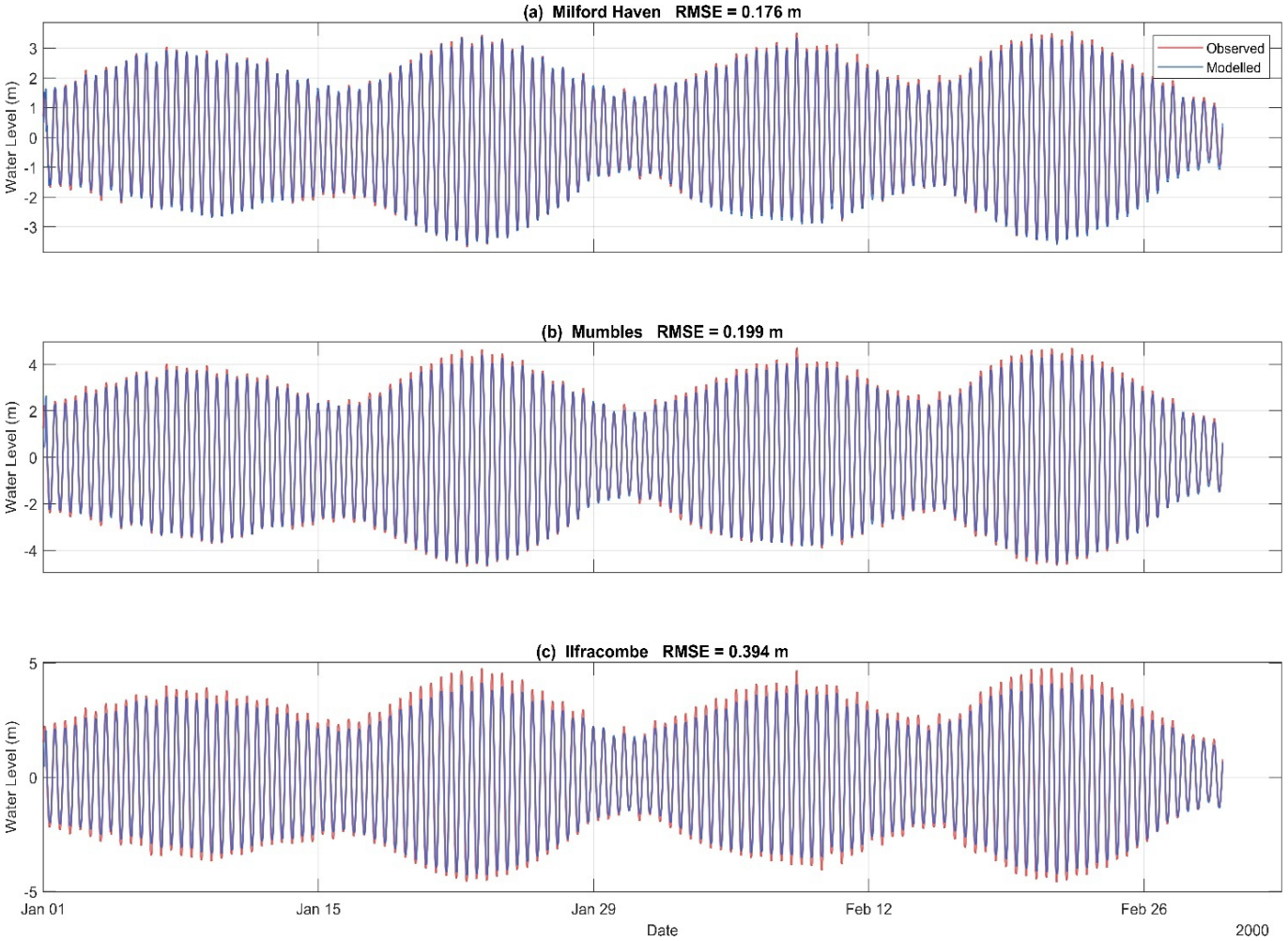


Figure 2.2.1. *Model validation of tidal elevations against records from the (a) Milford Haven, (b) Mumbles and (c) Ilfracombe tide gauges for the period 01-31 January 2000.*

Water level and velocity validation, within the Milford Haven estuary, was conducted at the maerl bed site in the lower estuary (lat: 51.703, lon: -5.077), over the period 04 December 2025 to 13 January 2026. Water level was reproduced with an RMSE of 0.269 m and a correlation coefficient of 0.987, indicating accurate reproduction of tidal phasing and amplitude at the deployment location (Fig. 2.2.2). Velocity magnitude yielded an RMSE of 0.067 m/s and a correlation of 0.645, reflecting reasonable reproduction of the tidal velocity signal with some underestimation of peak flows.

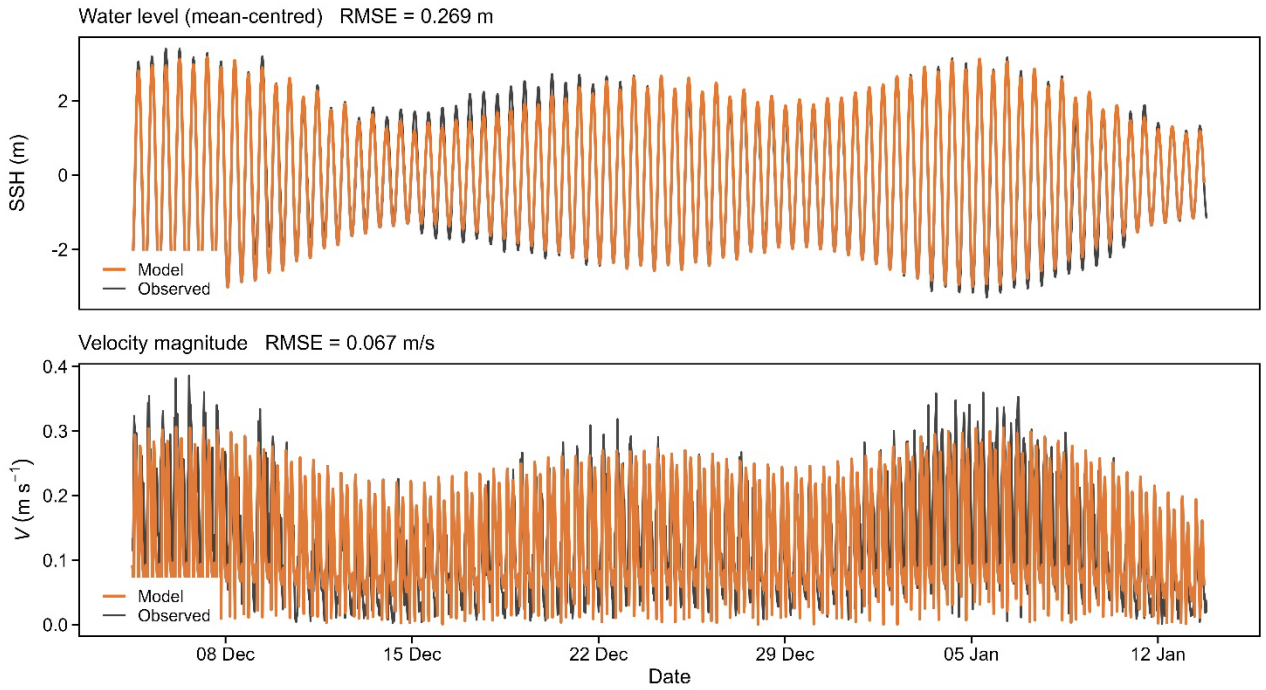


Figure 2.2.2. *Model validation of water level and velocity, at the maerl bed site within the Milford Haven estuary, during 04 December 2025 to 13 January 2026.*

Salinity validation was conducted using discrete water quality samples collected across eleven stations within the Milford Haven estuary during 18 - 19 September 2024. Modelled surface salinity was extracted at the grid cell nearest to each observation station and the closest model output timestep to each sample time. The overall RMSE across all stations was 1.72 ppt, with a correlation of r = 0.959 between modelled and observed values pooled across all stations (Fig. 2.2.3). Per-station RMSE ranged from 0.34 ppt at E Cleddau Site 16 to 2.74 ppt at E Cleddau Site 15, with the largest errors concentrated at upper-estuary and tributary sites where freshwater influence and salinity gradients are strongest.

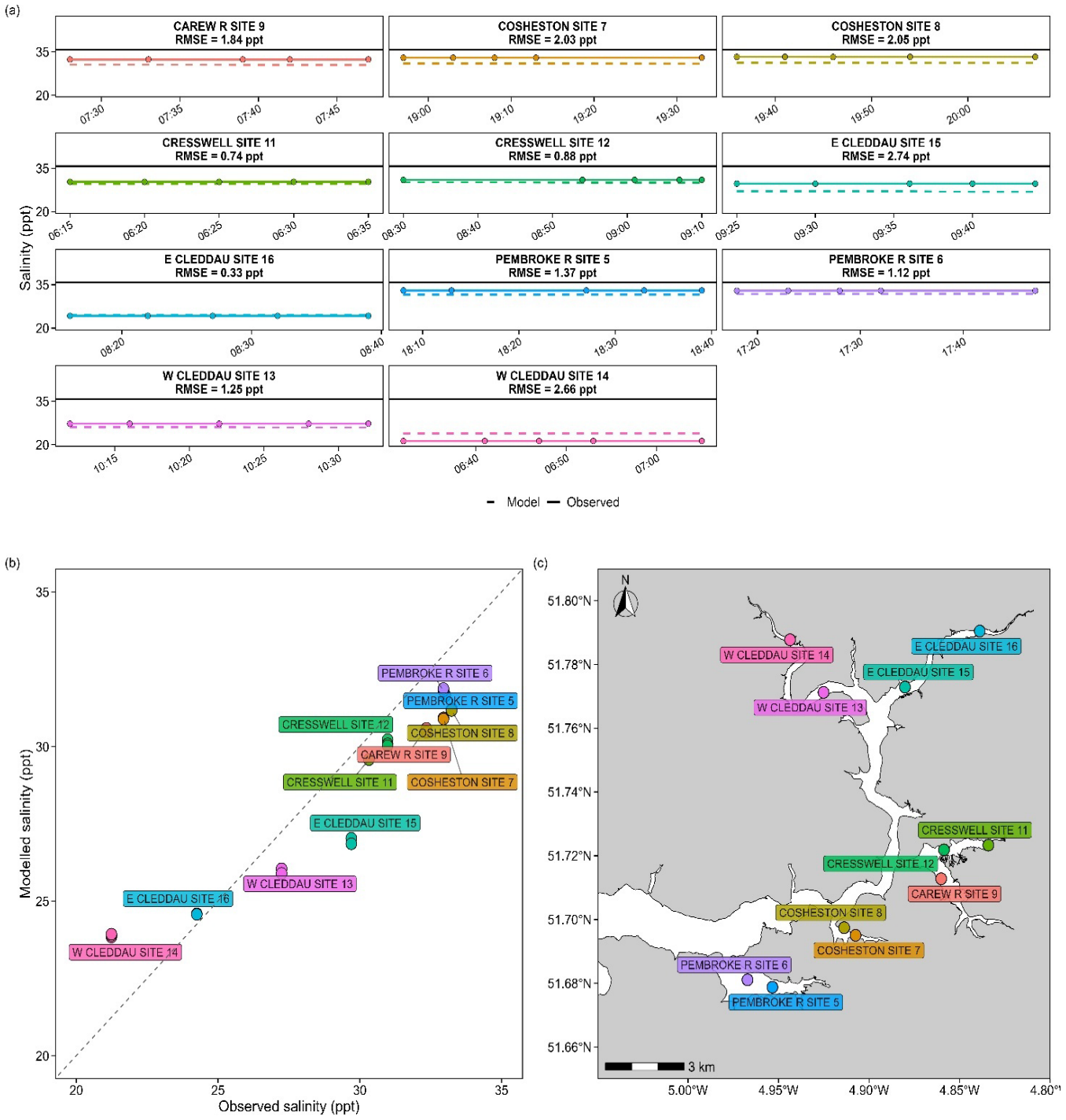


Figure 2.2.3. *Model validation of sea surface salinity against water samples collected across eleven stations within the Milford Haven estuary during 18 - 19 September 2024. Panel (a) shows time series comparisons, panel (b) shows time-averaged comparisons, and panel (c) shows the observation site locations.*

Based on the Dec 2023 – Jan 2024 simulation (Scenario-1a described in section 2.2.3), the depth-averaged tidal currents within the Milford Haven estuary exhibited a clear bidirectional pattern aligned with the estuary shape and main channel orientation (Fig. 2.2.4). During the flood tide, flow was directed northwards and then eastwards into the estuary, accelerating through the main channel (seaward of the maerl bed) with peak spring tide flows up to ~1.0 m/s. During the ebb tide, the flow reverses westward and then southwards (seawards) with peak spring tide flows up to ~0.7 m/s and concentrated in the southern part of the channel. At the maerl bed, spring tidal currents peaked at 0.72 m/s (flood) and 0.61 m/s (ebb). The flood tidal phase lasted approximately 4.3 hours, while the ebb phase lasted 7.5 hours consistent with the flood dominant asymmetry characteristics of a macrotidal funnel-shaped estuary (Friedrichs & Aubrey, 1988).

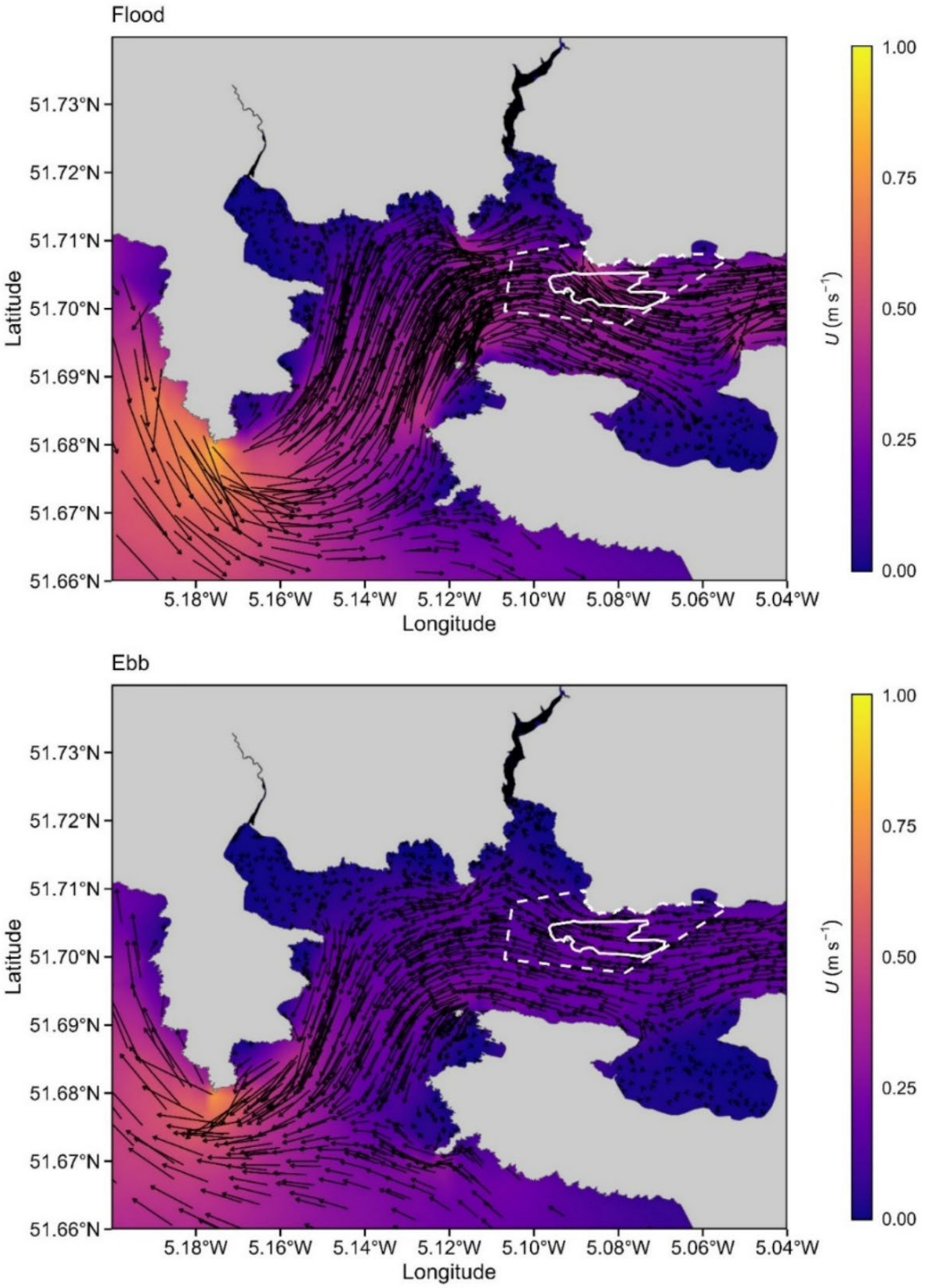


Figure 2.2.4. *Depth-averaged tidal current speed and direction at Milford Haven during dominant flood (upper) and ebb (lower) conditions, derived from composite mean velocity fields across all flood and ebb timesteps respectively (December 2025 – January 2026). Background colour shows mean current speed (m/s). Arrows indicate flow direction and are scaled to speed.*

2.2.3 Model scenarios

Six model scenarios were designed to address Q1-Q4, building upon the validated hydrodynamic configuration. These scenarios are described below and summarised in Table 2.2.2. Additionally, six simulations were designed to assess the sensitivity of the modelled suspended sediment dynamics to uncertainties in key sediment transport parameters, also described below and summarised in Table 2.2.3.

Scenario-1: Real-world scenarios (Q1)

Two simulation periods were run corresponding to the NRW sonde deployments at the maerl bed: Scenario-1a covered 01 December 2023 – 14 January 2024; and Scenario-1b covered 01 December 2025 – 14 January 2026. Both simulations were forced with observed boundary conditions comprising (1) sea level, velocity and salinity data at the open sea boundary (reanalysis data derived from the Copernicus marine data portal); (2) river discharge data at the Eastern and Western Cleddau tidal limits (river gauge data); and (3) suspended sediment concentration data at the Eastern and Western Cleddau tidal limits (NRW Sonde data). Five sediment fractions were considered (D50 = 1 mm – 63 µm) as detailed in Table 2.2.1. These simulations determine the extent to which riverine (Cleddau) suspended sediment contributed to turbidity at the maerl bed under observed conditions.

Scenario-2: High river flow scenario (Q1)

A semi-idealised simulation was designed using constant high river discharges in the Cleddau rivers representative of the 95th percentile flows (Eastern Cleddau: 35.532 m^3/s; Western Cleddau: 51.342 m^3/s). All other boundary conditions were consistent with Sceanio-1a (i.e., the Dec 2023 – Jan 2024 observed tidal and riverine suspended sediment concentrations). This semi-idealised scenario assessed riverine suspended sediment transport under an extreme high river flow event.

Scenario-3: Maintenance dredging scenarios (Q2/Q3)

Three simulations were performed to represent licenced trickle dredging efforts at Neyland Yacht Haven (Marine Licence DML1743v3). The simulations applied a point source suspended sediment concentration at disposal site LU190, for three hours during the licensed spring ebb tidal state on 06 December 2025. Sediment fractions followed the licensed material composition (fine silt 60%, coarse silt 30% and sand 10%) for three sediment load events: (Scenario-3a) low (100 kg/m^3); (Scenario-3b) mid (150 kg/m^3); and (Scenario-3c) high (300 kg/m^3). All three runs used observed sea level and river flow boundary conditions consistent with Scenario-1b (i.e., the Dec 2025 – Jan 2026 observation period). No suspended sediment was inputted at the river boundaries (i.e., only suspended sediment from Neyland Yacht Haven was simulated).

Scenario-4: **Sediment mobilisation at the jetty** ***(Q2)***

A further simulation was conducted to investigate the potential impact of sediment mobilisation activities at the South Hook jetty within the inner estuary (51.699°N, 5.080°W) – close to the maerl bed location (Fig. 2.1.1). Sediment fractions followed the same licensed material composition as the Neyland Yacht Haven scenarios (Scenario-3), with suspended sediment discharges applied as a point source over a full spring tidal cycle (12.5 hours) commencing 06 December 2025 11:00 using the mid-range discharge concentration of 150 kg/m^3. Tidal boundary conditions and river discharges were consistent with Scenario-1b (i.e., the Dec 2025 – Jan 2026 observation period). No suspended sediment was inputted at the river boundaries (i.e., only suspended sediment from the jetty was simulated).

Scenario-5: Maerl bed erosion scenario (Q2)

Two simulations were deployed covering the Dec 2025 – Jan 2026 observation period (described for Scenario-1b). The simulations applied a bed composition of: (Scenario-5a) a sand sediment fraction representative of sediment grab samples at the maerl bed site (231 µm; Bunker et al. 2026); and separately (Scenario-5b) a mud sediment fraction representative of dredged material. These single sediment fractions were applied exclusively

over the maerl bed extents (0.5 m thickness) with zero sediment prescribed elsewhere. No suspended sediment was inputted at the river boundaries. These simulations assessed whether modelled bed shear stresses are sufficient to mobilise different grain classes under real tidal and fluvial forcing.

Scenario-6: Sea-level rise dredging scenario (Q4)

To investigate how future sea-level rise may alter the dispersal and impact of dredge-derived sediment, the high dredging scenario (300 kg/m^3) was repeated under (Scenario-6a) 2050 and (Scenario-6b) 2100 sea-level rise projections of +0.29 m and +0.78 m, respectively, consistent with UKCP18 RCP8.5 anomaly predictions (Met Office 2018). The elevated sea level modifies the tidal prism, current velocities, and sediment transport pathways throughout the estuary, providing an assessment of how the turbidity footprint of routine dredging operations may change under future sea-level rise conditions.

Table 2.2.2. *Summary of model scenarios, detailing sea level and river boundary forcing, suspended sediment source, bed structure, and simulation period. Shading indicates the conditions being changed for each partitioned scenario.*

Scenario	Sea level boundary	River discharge	SSC source	Bed structure	Scenario duration
1a) *Real-world 2023*	Observed (NEMO) SSH, V, SSS	15-minute observed	Rivers - NRW sonde	Zero	01 Dec 23 – 14 Jan 24
1b) *Real-world 2025*	Observed (NEMO) SSH, V, SSS	15-minute observed	Rivers - NRW sonde	Zero	01 Dec 25 – 14 Jan 26
2) *High river flow*	Observed (NEMO) SSH, V, SSS	Constant discharge	Rivers - NRW sonde	Zero	01 Dec 23 – 14 Jan 24
3a) *Dredge low SSC*	Observed (NEMO) SSH, V, SSS	15-minute observed	Point source @ LU190: 0.93 kg/s	Zero	01 Dec 25 – 14 Jan 26
3b) *Dredge mid SSC*	Observed (NEMO) SSH, V, SSS	15-minute observed	Point source @ LU190: 1.39 kg/s	Zero	01 Dec 25 – 14 Jan 26
3c) *Dredge high SSC*	Observed (NEMO) SSH, V, SSS	15-minute observed	Point source @ LU190: 2.78 kg/s	Zero	01 Dec 25 – 14 Jan 26
4) *Sediment mobilisation*	Observed (NEMO) SSH, V, SSS	15-minute observed	Point source @ 51.699°N, 5.080°W: 1.39 kg s^{-1}	Zero	01 Dec 25 – 14 Jan 26

***5a)** Maerl bed erosion (sand)*	Observed (NEMO) SSH, V, SSS	15-minute observed	0.5 m sand, D50 231 µm, ρ 2,420 kg/m³ (maerl bed only)	Zero (except maerl bed)	01 Dec 25 – 14 Jan 26
***5b)** Maerl bed erosion (mud)*	Observed (NEMO) SSH, V, SSS	15-minute observed	0.5 m mud, D50 63 µm, ρ 2,170 kg/m³ (maerl bed only)	Zero (except maerl bed)	01 Dec 25 – 14 Jan 26
***6a)** 2050 dredge*	Observed (NEMO) 2025 SSH +0.29 m SLR, V, SSS	Baseline 2025 flows	Point source @ LU190: 2.78 kg/s	Zero	Dec 2050
***6b)** 2100 dredge*	Observed (NEMO) 2025 SSH +0.78 m SLR, V, SSS	Baseline 2025 flows	Point source @ LU190: 2.78 kg/s	Zero	Dec 2100

Sensitivity testing

A series of six simulations were designed to assess the sensitivity of the modelled suspended sediment dynamics to uncertainties in key sediment transport parameters (Table 2.2.3). Run S1 represents the baseline configuration used throughout this study, retaining the parameter set applied across all scenario simulations, based on Lepesqueur et al. (2019). Run S2 addresses known parameter inconsistencies identified during model setup, providing a corrected baseline against which subsequent runs can be compared. Run S3 introduces physically defensible grain densities (2,650 kg/m^3 across all fractions), representing a conservative baseline with internally consistent parameters. Run S4 further modifies dry bed density for the silt and sand fractions, reducing coarse silt dry bed density to 500 kg/m^3 and fine silt to 300 kg/m^3, reflecting reduced compaction. Run S5 applies lower specific densities representative of organic-rich or flocculated material and reduces settling velocities for both silt fractions to 1.0×10^{-4} m/s in freshwater and saline conditions. Run S6 represents a minimum plausible density scenario with maximum bed penetration, applying the lowest specific densities across all fractions (2,400–1,100 kg/m^3), the lowest dry bed densities, and increased critical stresses for both deposition (0.20–0.25 N/m^2) and erosion (0.20–0.25 N/m^2). Critical stress for deposition in the baseline configuration (Run S1) was set to 1,000 N/m^2, effectively suppressing deposition limitation, whereas all subsequent runs apply physically realistic deposition thresholds of 0.1–0.2 N/m^2.

Table 2.2.3. *Sediment transport parameter sensitivity tests. Green shading indicates values that differ from the Run 1 baseline. τ_t = critical shear stress; sV = settling velocity.*

Fraction	Parameter	Run S1 (Baseline)	Run S2 (Issues repaired)	Run S3 (Physical baseline)	Run S4 (Reduced dry bed)	Run S5 (Organic-rich)	Run S6 (Min. density)
Medium sand (500 µm)	*Specific density (kg m^{-3})*	2480	2480	2650	2650	2500	2400
Medium sand (500 µm)	*Dry bed density (kg m^{-3})*	1600	1600	1600	1400	1400	1200
Fine sand (200 µm)	*Specific density (kg m^{-3})*	2420	2420	2650	2650	2500	2400
Fine sand (200 µm)	*Dry bed density (kg m^{-3})*	1325	1325	1325	1100	1100	900
Very fine sand (100 µm)	*Specific density (kg m^{-3})*	2850	2850	2650	2650	2500	2400
Very fine sand (100 µm)	*Dry bed density (kg m^{-3})*	1050	1050	1050	800	800	700
Coarse silt (83 µm)	*Specific density (kg m^{-3})*	1810	1810	2650	2650	1400	1200
Coarse silt (83 µm)	*Dry bed density (kg m^{-3})*	775	775	775	500	500	400
Coarse silt (83 µm)	*sV freshwater (m s^{-1})*	2.5×10^{-4}	2.5×10^{-4}	2.5×10^{-4}	2.5×10^{-4}	1.0×10^{-4}	5.0×10^{-5}
Coarse silt (83 µm)	*sV saline (m s^{-1})*	2.5×10^{-4}	2.5×10^{-4}	2.5×10^{-4}	2.5×10^{-4}	1.0×10^{-4}	5.0×10^{-5}
Coarse silt (83 µm)	*τ_t deposition (N m^{-2})*	1000	0.15	0.15	0.15	0.15	0.20
Coarse silt (83 µm)	*τ_t erosion (N m^{-2})*	0.17	0.17	0.17	0.17	0.17	0.20

Fraction	Parameter	Run S1 (Baseline)	Run S2 (Issues repaired)	Run S3 (Physical baseline)	Run S4 (Reduced dry bed)	Run S5 (Organic-rich)	Run S6 (Min. density)
Fine silt (63 µm)	*Specific density (kg m^{-3})*	2170	2170	2650	2650	1200	1100
Fine silt (63 µm)	*Dry bed density (kg m^{-3})*	500	500	500	300	300	200
Fine silt (63 µm)	*sV freshwater (m s^{-1})*	2.5×10^{-4}	2.5×10^{-4}	2.5×10^{-4}	2.5×10^{-4}	5.0×10^{-5}	5.0×10^{-5}
Fine silt (63 µm)	*sV saline (m s^{-1})*	2.5×10^{-4}	2.5×10^{-4}	2.5×10^{-4}	2.5×10^{-4}	5.0×10^{-5}	5.0×10^{-5}
Fine silt (63 µm)	*τ_t deposition (N m^{-2})*	1000	0.10	0.15	0.15	0.15	0.20
Fine silt (63 µm)	*τ_t erosion (N m^{-2})*	0.17	0.17	0.17	0.17	0.17	0.25

3 Results

In this section we describe the results from the two work streams: (3.1) Observations of turbidity in the Milford Haven, where we have analysed hydrodynamic and suspended sediment data from within the estuary, used to address Q1-Q2; and (3.2) Model simulations of turbidity in the Milford Haven, where we describe outputs from the Delft3D hydrodynamic and suspended sediment transport modelling, used to address Q1-Q4.

3.1 Observations of turbidity in the Milford Haven

3.1.1 Seasonality and data distribution

Observations of water level and turbidity at the maerl bed were analysed alongside observations of river discharge and turbidity from the Western and Eastern Cleddau rivers to investigate the relative influence of riverine and tidal processes on maerl bed turbidity (Fig. 3.1.1.). Two monitoring campaigns were undertaken: an approximately eight-month period from July 2023 to March 2024 (with a one-month interruption due to sensor malfunction), and a second campaign spanning approximately six weeks from December 2025 to January 2026. These records clearly captured tidal variability over both semi-diurnal and fortnightly spring-neap tidal cycles (Fig. 3.1.1; first panel), as well as capturing multiple high and low river flow events (Fig. 3.1.1; second panel).

Water depth at the maerl bed fluctuated between approximately 5–12 m during the 2023-2024 deployment and between 3-11 m during the 2025-2026 deployment, driven by the macro-tidal, semi-diurnal, tidal regime of the southern Irish Sea. The differences in absolute water depth between the two monitoring periods is attributed to differences in tidal phasing (long-period tidal modulation) causing differences in tidal amplitude, and slight variations in site location and sensor positioning on the seabed. These observations indicate that variability in oscillatory tidal currents, at both semi-diurnal and fortnightly (spring-neap) time scales, represents a persistent mechanism capable of periodically resuspending bed sediments.

Discharge in both the Eastern and Western Cleddau rivers was highly episodic and event-driven (Fig. 3.1.1; second panel). River flow remained low for extended periods but was interrupted by short-duration peaks exceeding 80 m^3/s, particularly during autumn and winter storm events. The Eastern Cleddau generally exhibited higher peak flow and greater baseline discharges than the Western Cleddau. Considering the two deployments combined together, the Eastern Cleddau experienced a 5^{th}, 50^{th} and 95^{th} percentile of 2.1 m^3/s, 9.4 m^3/s and 37.4 m^3/s compared with 0.7 m^3/s, 5.8 m^3/s and 17.3 m^3/s for the Western Cleddau.

Riverine turbidity showed similar episodic behaviour but with substantially greater variability than discharge (Fig. 3.1.1; third panel). Turbidity in both rivers frequently increased during high-flow events, with extreme peaks exceeding 10^4–10^5 FNU during autumn and winter. These turbidity spikes indicate substantial mobilisation of suspended sediments during storm-driven runoff events. However, not all discharge peaks corresponded directly with equivalent turbidity responses, suggesting variability in sediment availability or antecedent catchment conditions.

Turbidity at the maerl bed was recorded using different units across the two monitoring campaigns: FNU during the 2023-2024 deployment and mV during the 2025-2026 deployment (Fig. 3.1.1; fourth panel). Although short-term fluctuations occurred at tidal frequencies, longer periods of elevated turbidity frequently followed major river discharge and river turbidity events and were superimposed on a ~15-day oscillation characteristic of the spring–neap tidal cycle. Baseline turbidity at the maerl bed generally remained low (typically <10 FNU or <400 mV), but several prolonged increases occurred during autumn and winter, with peaks exceeding 100 FNU or 2000 mV. These elevated periods often lagged major river events, suggesting the transport of river sediments into the estuarine system, followed by their deposition and subsequent tidal resuspension.

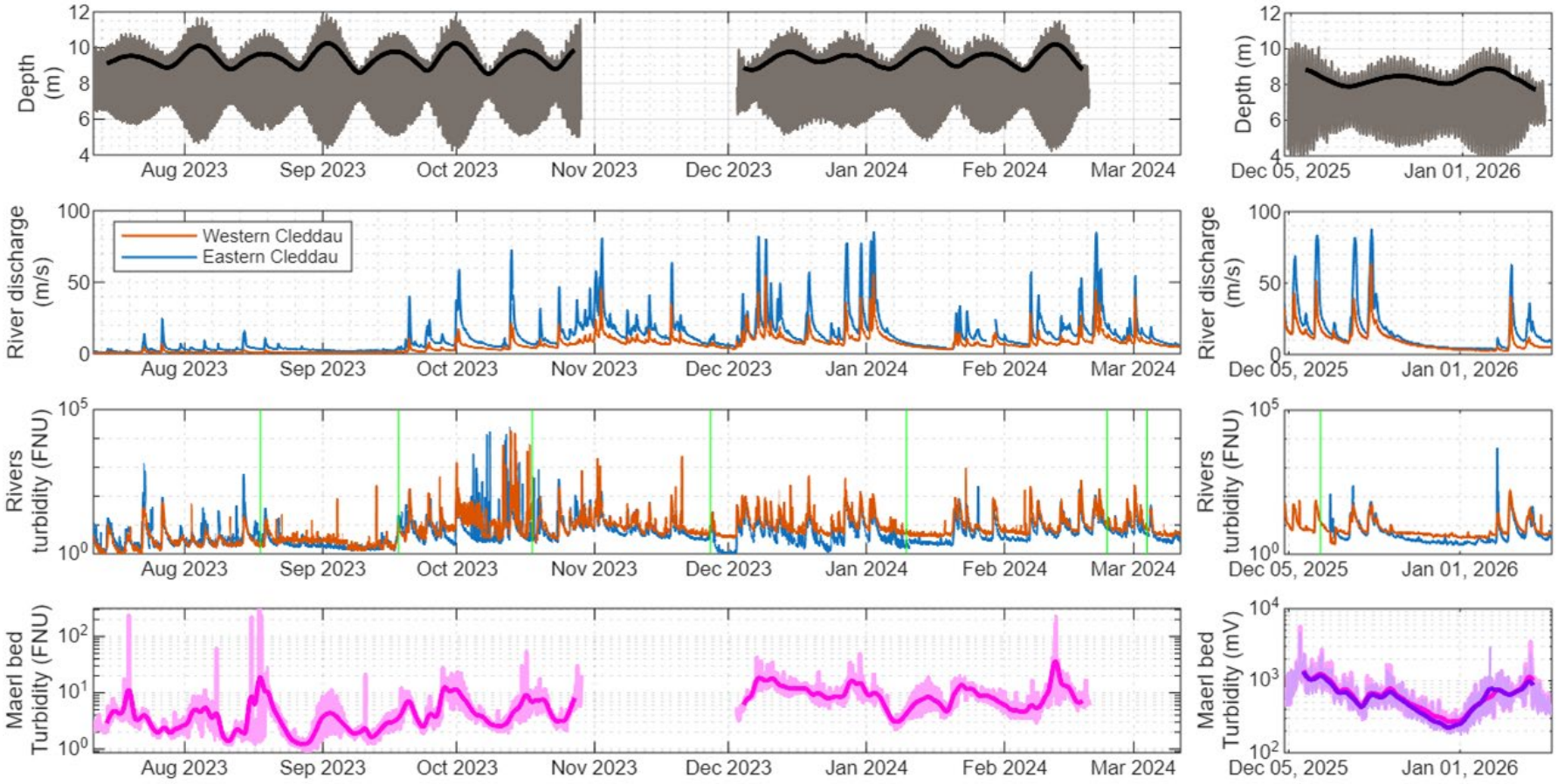


***Figure 3.1.1**: Observational datasets: The plots on the left show the 2023–2024 dataset, while those on the right present the 2025–2026 observations. From top to bottom: (i) water level, with the grey line showing the tides and the black line showing the RMS water level; (ii) river discharge for both the Western and Eastern Cleddau; (iii) river turbidity for both the Western and*

Eastern Cleddau with green lines showing when data were retrieved from the instrument; and (iv) maerl bed turbidity data, with thin lines showing raw measurements and thicker lines showing de-tided turbidity. For the 2025–2026 dataset, maerl bed turbidity was recorded at two heights above the bed: 20 cm (pink) and 34.5 cm (purple).

Seasonal analysis further highlighted the relative importance of riverine and tidal controls (Figs. 3.1.2 and 3.1.3). The histogram of water depth also showed a near-normal distribution centred around mid-tidal elevations and the boxplots showed that water level distributions remained similar across seasons, with median depths consistently around ~8 m for the 2023-2024 deployment and ~7 m for the 2025-2026 deployment (Figs. 3.1.2.a and 3.1.3.a) with the difference due to differences in depth at the deployment locations.

River discharge exhibited strong seasonal differences (Figs. 3.1.2.b and 3.1.3.b). Summer was characterised by consistently low flows with median discharge of 2.9 m^3 s^{-1} for the Eastern Cleddau and 0.9 m^3 s^{-1} for the Western Cleddau. In contrast, autumn and winter displayed higher median discharges and greater variability, with numerous extreme events. Median discharges in the Eastern Cleddau reached 13.6 m^3/s during autumn 2023 and 11.6 m^3/s during winter 2023-2024, while corresponding values for the Western Cleddau were 7.9 m^3/s and 7.2 m^3/s, respectively. This pattern was particularly pronounced in the Eastern Cleddau, where peak flows regularly exceeded 60–80 m^3/s. In comparison, the Western Cleddau exhibited lower extreme flows, with the highest outliers occurring during autumn 2025 and reaching 62 m^3/s.

Similarly, river turbidity increased substantially during autumn and winter compared to summer (Figs. 3.1.2.c and 3.1.3.c), indicating greater sediment export from both catchments during wetter months. In the Easter Cleddau, median turbidity increased from 2.5 FNU during summer 2023 to 5.3 FNU during autumn 2023 and 4.5 FNU during winter 2023-2024. Slightly higher values were observed during the 2025-2026 deployment, with median turbidity reaching 5.3 FNU during autumn and 3.5 during winter. The Western Cleddau exhibited a similar seasonal pattern with overall higher turbidity values. Median turbidity increased from 2.7 FNU during summer 2023 to 9.4 FNU during autumn 2025 and 7 FNU during winter 2025-2026. Notably, although river discharge was consistently higher in the Eastern Cleddau, turbidity levels were generally higher in the Western Cleddau. This difference likely reflects contrasting catchment characteristics, including differences in land use (e.g., urban versus agricultural environments), as well as the differing locations of turbidity and discharge measurements within each river system.

Turbidity at the maerl bed also showed clear seasonal variation (Figs. 3.1.2.d and 3.1.3.d). Median turbidity was lowest during summer 2023 with a value of 2.6 FNU, before increasing to 7.7 FNU during autumn 2023 and remaining elevated throughout winter 2023-2024 at 6.9 FNU. During the 2025-2026 deployment, autumn and winter exhibited similar median turbidity values, although autumn was characterised by slightly higher extreme values, likely reflecting the stronger discharge events observed during autumn 2025 relative to winter 2025-2026. The two sensors deployed during the 2025-2026 campaign also revealed small vertical differences in turbidity near the seabed. OSB1, positioned closest to the seabed at 20 cm above the bed, recorded slightly higher turbidity values, with median turbidity of 579 mV in autumn and 553 mV in winter, compared with 551 mV and 538 mV, respectively, for OSB2 located 34.5 cm above the sea bed. This suggests enhanced suspended sediment concentrations closer to the bed, likely associated with near-bed resuspension processes. Autumn and winter autumn distributions also exhibited broader ranges and more frequent high-turbidity events, including extreme outliers exceeding 100 FNU for the 2023-2024 deployment and 1000 mV for the 2025-2026 deployment. The seasonal increase in maerl bed turbidity mirrored seasonal increases in river discharge and river turbidity, suggesting that river-derived sediment supply strongly influences background turbidity conditions at the maerl bed.

Together, these results indicate that tidal processes and riverine inputs fluctuate over different time scales and interact within the estuary. Tides appear to drive short-term periodic fluctuations in turbidity through repeated sediment resuspension and advection back and forth along the estuary with the flood and ebb phases of the tidal cycle. The turbidity also fluctuates over a fortnightly time scale due the spring-neap tidal cycle. Additionally, river flows and associated suspended sediment loads act as episodic sediment delivery mechanisms that can elevate overall turbidity at the maerl bed. The highest recorded turbidity at the maerl bed occurred when strong tidal and riverine processes interacted: during periods (e.g., mid-February 2024 and early December 2025) of increased fluvial sediment delivery followed by enhanced resuspension of deposited material during peak spring tidal currents. This demonstrates that maerl bed turbidity is governed by both tidal mixing and advection, and catchment-derived sediment inputs, with river influence becoming particularly important during autumn and winter storm events.

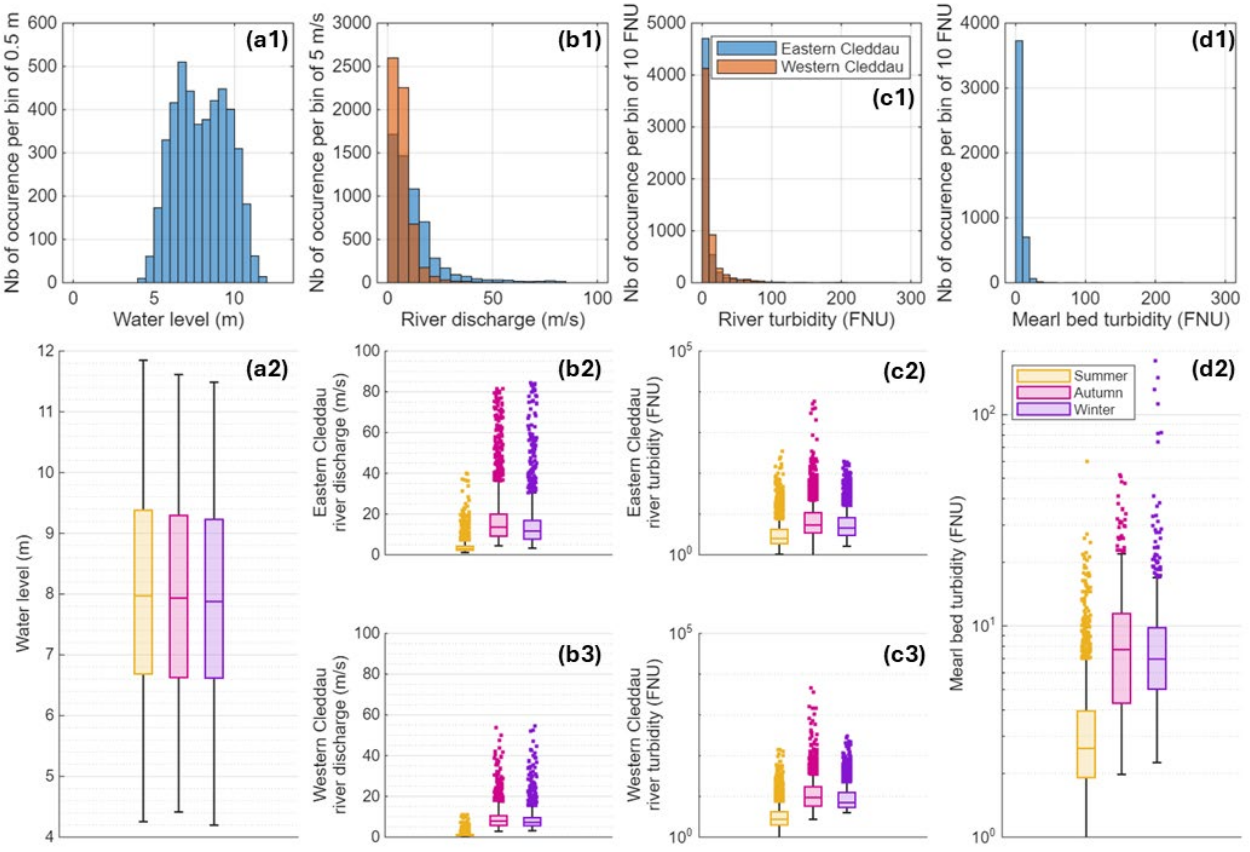


Figure 3.1.2. *Distribution plots (panels 1) and seasonal boxplots (panels 2) of observations collected during 2023–2024. Each column represents a different variable: (a) water level, (b) river discharge for both rivers, (c) river turbidity for both rivers, and (d) maerl bed turbidity.*

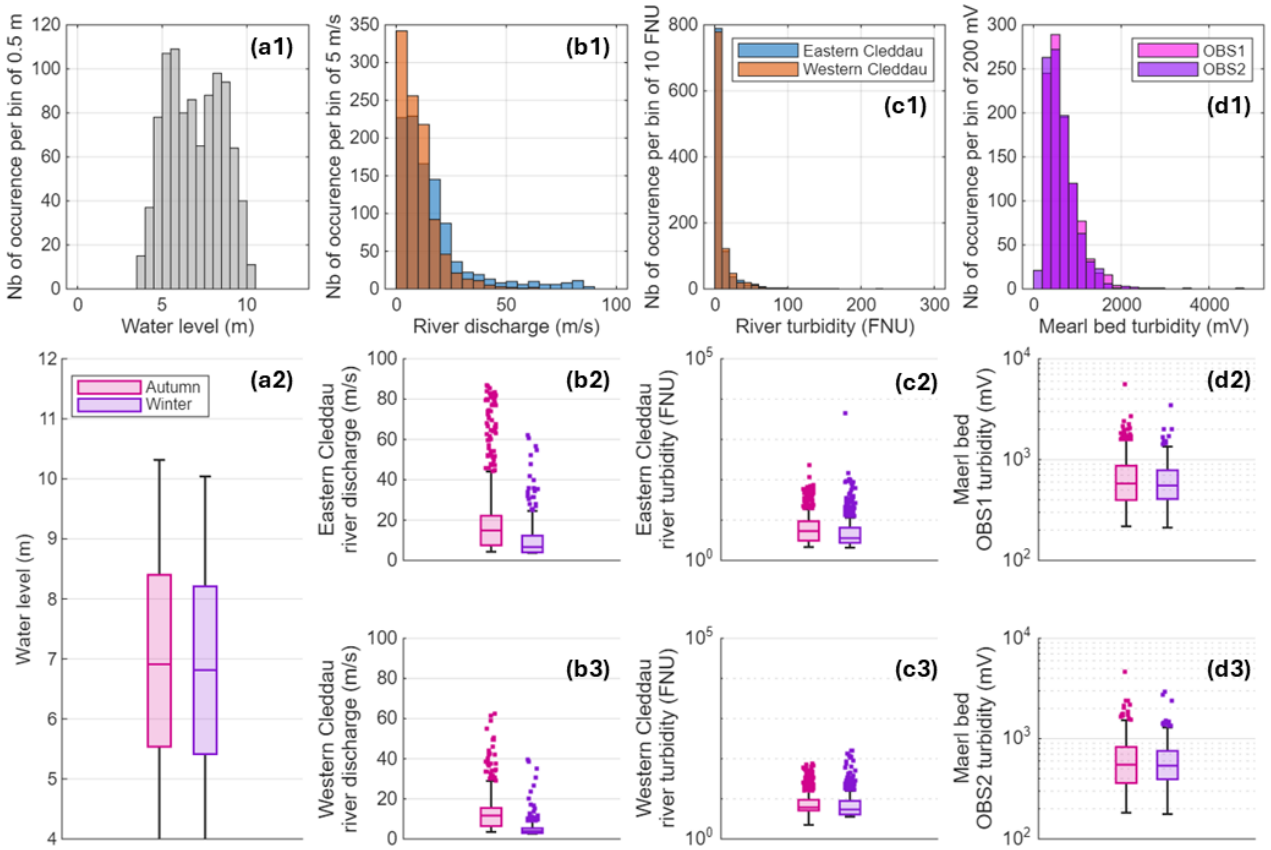


Figure 3.1.3. *Distribution plots (panels 1) and seasonal boxplots (panels 2) of observations collected during 2025–2026. Each column represents a different variable: (a) water level, (b) river discharge for both rivers, (c) river turbidity for both rivers, and (d) maerl bed turbidity measured at two depths: OSB1 (20 cm) and OSB2 (34.5 cm).*

3.1.1 Equivalence between turbidity datasets

The two observation campaigns measured turbidity at the maerl bed using different units: FNU during the 2023–2024 deployment and mV during the 2025–2026 deployment, which complicates direct comparison and combined analyses of the two datasets. Previous calibration work indicates that the relationship between these two units is approximately linear at low turbidity values but becomes exponential at higher concentrations. To establish a conversion between the two datasets, percentile increments from both maerl bed turbidity distributions were plotted against one another (Fig. 3.1.4; left panel). This approach was used to identify a relationship between the two distributions and to express FNU turbidity as a function of mV turbidity.

Both deployments exhibited highly skewed turbidity distributions. During the 2023–2024 deployment, maerl bed turbidity ranged from approximately 1 to 1200 FNU, with 90% of hourly observations below 12 FNU. During the 2025–2026 deployment, turbidity ranged from approximately 200 to 6000 mV, with 90% of hourly observations below 1110 mV. Based on the percentile comparison, the relationship between mV and FNU turbidity was best described using three functions (Fig. 3.1.4; right panel):

- For values below **2000 mV**, turbidity followed a linear relationship with FNU.
- Between **2000 and 4800 mV**, the relationship remained linear but with a slope approximately twice as steep.
- Above **4800 mV** (representing approximately the upper 1% of observations), the relationship followed an exponential trend.

Using these relationships, the 2025–2026 turbidity record was converted into FNU units, enabling comparison with the 2023–2024 dataset (Figs. 3.1.4b and c). The 2023–2024 deployment recorded turbidity values ranging from 2 to 1200 FNU, with mean values of approximately 6.6 FNU for the OBS1 instrument and 6.0 FNU for OBS2. In comparison, the converted 2025–2026 dataset ranged from approximately 0.1 to 60 FNU, while exhibiting a similar mean turbidity of approximately 6.6 FNU. These results indicate that average turbidity conditions were comparable between deployments, whereas extreme turbidity events differed substantially.

This conversion should be considered a first-order approximation. River inputs were the primary driver of extreme maerl bed turbidity events, and the two deployments captured different river discharge regimes. Although both observation periods exhibited similar mean discharge values, the longer 2023–2024 deployment captured a greater number of extreme discharge events than the shorter 2025–2026 deployment (Figs. 3.1.2b and 3.1.3b). Consequently, it is likely that the 2023–2024 dataset includes a broader range of high-turbidity events than the 2025–2026 record. This may result in an underestimation of high FNU values when converting the 2025–2026 mV dataset, particularly for observations within the exponential portion of the calibration curve.

An additional source of uncertainty is the unknown deployment height of the 2023–2024 turbidity sensor above the seabed. Differences in sensor elevation may have influenced the magnitude of recorded turbidity values and should be considered when interpreting comparisons between the two deployments.

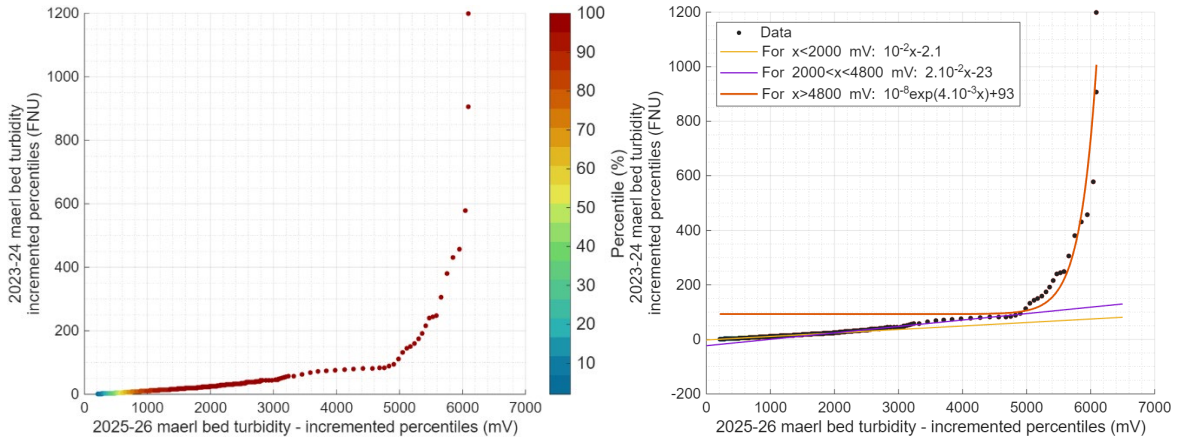


Figure 3.1.4. *Scatter plots comparing percentile increments in maerl bed turbidity between the two observation campaigns. The y-axis represents turbidity measurements from the 2023–2024 campaign (FNU), while the x-axis shows turbidity measurements from the OSB1 sensor during the 2025–2026 campaign (mV). The left panel displays percentile levels, indicated by the colour bar. The right panel shows the relationship between FNU and mV turbidity values, fitted using three different functions.*

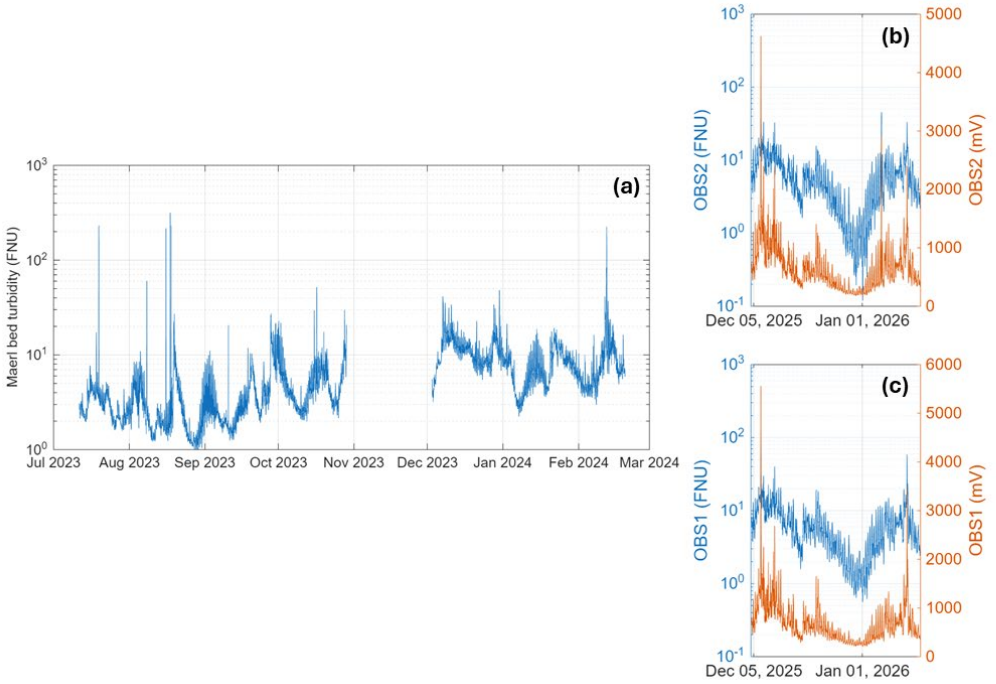


Figure 3.1.5. *Conversion of maerl bed turbidity measurements from mV to FNU units. Panel (a) shows maerl bed turbidity values from the 2023–2024 campaign, originally recorded in FNU. Panels (b) and (c) show maerl bed turbidity measurements from the 2025–2026 campaign, originally recorded in mV (right y-axis), at two heights above the bed: OSB1 (20 cm) and OSB2 (34.5 cm).These measurements were converted to FNU units (left y-axis) using the fitted relationship presented in Figure 3.1.4.*

3.1.2 Drivers of maerl bed turbidity

Tidal control on turbidity

The spectral analysis indicates that tidal forcing exerts a clear control on turbidity variability over the maerl bed. The power spectral density of the 2023–2024 maerl bed turbidity record (Fig. 3.1.6) was characterised by distinct peaks at specific tidal frequencies. The highest spectral energy occurred at the spring–neap modulation period (~14.7 days), while secondary notable peaks were evident at the semi-diurnal M2 tidal frequency (~12.4 h period) and at a quarter-diurnal frequency (~6.2 h period).

The dominance of the fortnightly tidal signal suggests that spring–neap tidal variability exerts a stronger control on maerl bed turbidity than individual semi-diurnal tidal cycles. This can

also be seen qualitatively in Fig. 3.1.1. This likely reflects the cumulative effect of the stronger peak currents during spring tides than neaps, which increases bed shear stress and enhances sediment resuspension within the estuary over several tidal cycles during the spring tidal phase. The spectral energy peak at quarter-diurnal frequency represents the semi-diurnal tidal propagation in/out of the estuary, which produces four high-flow events per day – i.e., two flood tides and two ebb tides per day. The slightly higher spectral energy peak at semi-diurnal than quarter-diurnal frequency likely reflects the asymmetry in the turbidity signal over a tidal cycle, i.e., that observed turbidity was enhanced during the ebb tidal phase compared with the flood phase, as explained in more detail below. Additionally, the influence of episodic river-driven turbidity events may to some extent mask the spectral energy signal at the semi-diurnal and quarter-diurnal frequencies. This is because river-driven turbidity events typically develop over timescales of hours to a few days (i.e., are not periodic) and overlap with quarter- and semi-diurnal tidal variability. This interaction likely reduces the relative contribution of the quarter- and semi-diurnal tidal signals in the turbidity record.

A closer examination of maerl bed turbidity and horizontal velocity over two days is shown in Fig. 3.1.7 (upper panel) during a period of low river discharge towards the end of December 2025. Our interpretation of these observations is as follows. During the flooding tide (positive x-velocity), turbidity at the maerl bed remained broadly constant at around 500 mV and then decreased to a minimum shortly after slack high water. This represents the upstream advection of the estuarine turbidity plume into the estuary and over the maerl bed. The broadly constant turbidity signal indicates that the turbid plume, which was washed offshore during the previous ebb tidal phase, was able to spread out in the offshore area, unrestricted, and so when advancing back over the maerl bed during the flood had not (yet) concentrated into a turbidity maximum. The turbid plume advanced upstream, resuspending any available estuarine sediments as it advanced, and the suspended sediments concentrated in the upper estuary due to the narrowing and shoaling of the channels and interaction with riverine suspended sediments at the tidal limit – and so formed an estuarine turbidity maximum (ETM). Then, on the following ebbing tide, the ETM was advected seawards and back over the maerl bed producing a peak turbidity signal (reaching 700-900 mV) during the late ebb tide, shortly before slack low water. In contrast, this pattern

became less distinct during periods characterised by intense river discharge events (e.g., 06-08 December 2025; Fig. 3.1.7, lower panel), indicating that river flow and river-derived sediment inputs can temporarily dominate turbidity with values at the maerl bed exceeding 1000 mV and with the tidal periodicity largely masked.

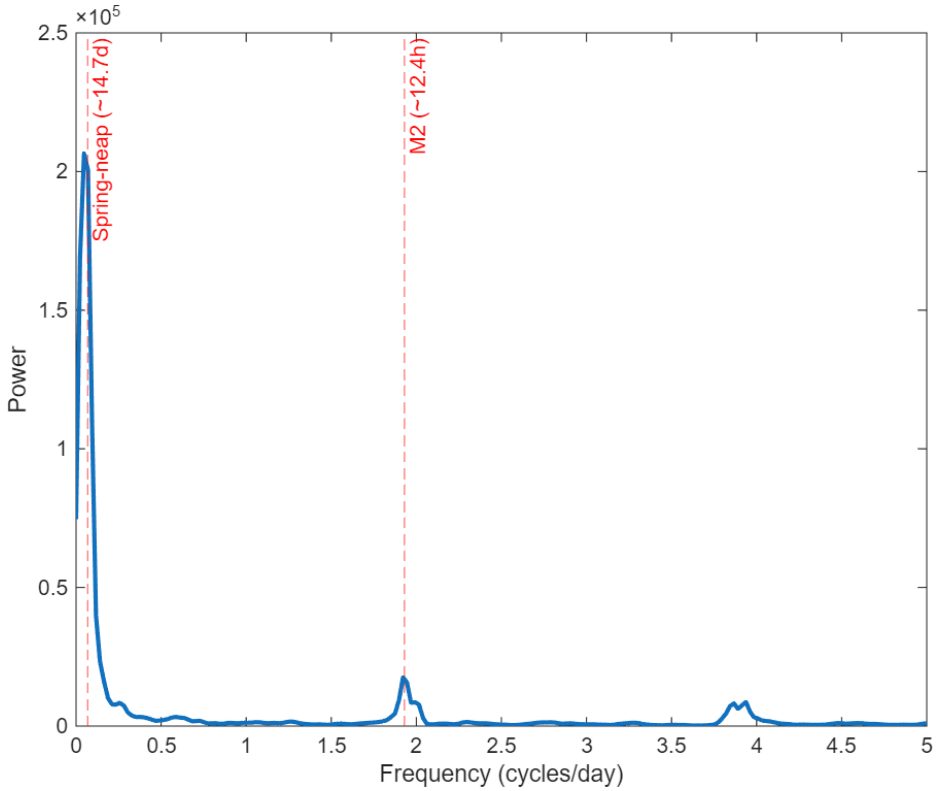
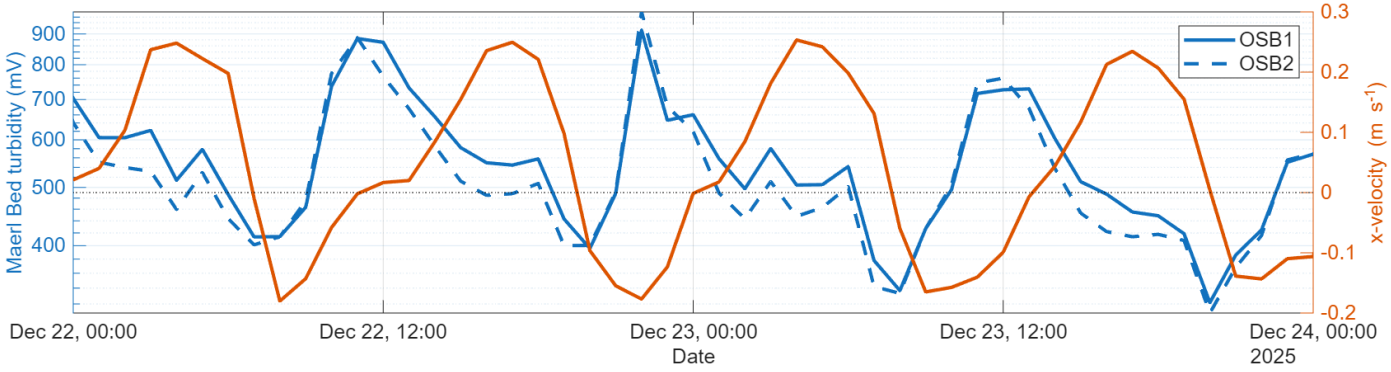


Figure 3.1.6. *Power spectral density estimate of hourly maerl bed turbidity observations from the 2023–2024 campaign. The two vertical red dashed lines indicate the dominant tidal harmonics present in the signal.*



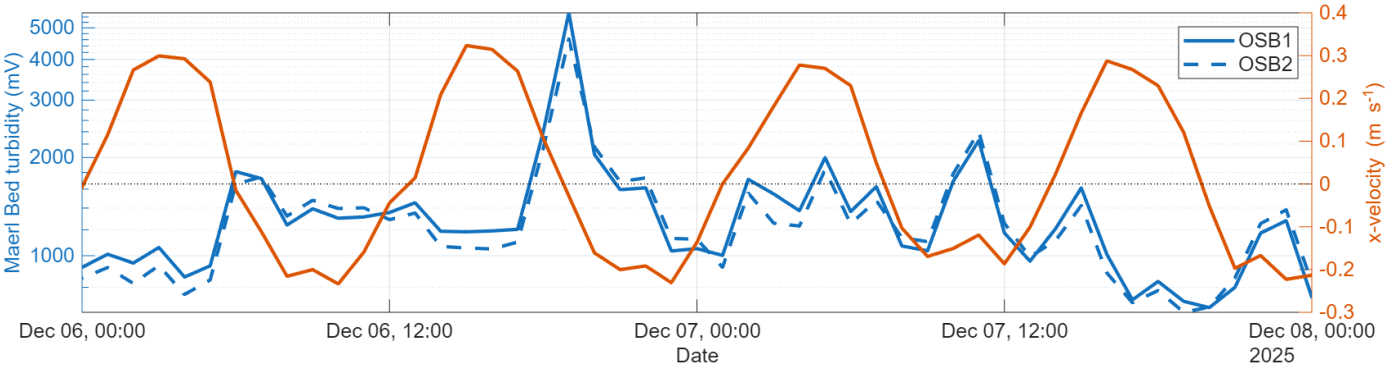


Figure 3.1.7. *Twenty-four-hour time series of maerl bed turbidity and horizontal velocity selected to illustrate turbidity variability during a period of low river discharge (upper panel) and during intense river discharge events (lower panel).*

The two sensors deployed during the 2025–2026 campaign also highlight the presence of a vertical gradient in maerl bed turbidity (Figs 3.1.8 and 3.1.9). The 1 h earlier and slightly stronger correlations observed at OSB2 suggest that turbidity fluctuations closer to the seabed remain more tightly coupled to tidal water-level variations. It is also notable that correlations between maerl bed turbidity and water level were stronger during the 2025–2026 campaign than during the 2023–2024 campaign. This difference may partly reflect the different units used to quantify turbidity, with the 2025-2026 campaign measured in mV and the 2023-2024 campaign measured in FNU. As discussed in section 3.1.2 (Figs. 3.1.2d and 3.1.3d), turbidity values expressed in mV exhibited a less skewed distribution than those expressed in FNU, resulting in a distribution that more closely resemble the near-normal distribution of the water level observations (Figs 3.1.2a and 3.1.3a). This may partially explain the stronger correlation coefficients observed during the 2025–2026 deployment.

Correlation and cross-correlation analyses further support the influence of tidal forcing on maerl bed turbidity (Figs. 3.1.8 and 3.1.9). During the 2023–2024 campaign, turbidity was positively correlated with water level, with the strongest significant correlations (r = 0,09) occurring with lags of approximately 3 h (and again after 9 h), i.e., during peak tidal flow. A similar pattern was observed during the 2025–2026 campaign, where both sensors (OSB1 and OSB2) exhibited coherent tidal-scale variability. Maximum positive correlations (r = 0.2) occurred with lags of approximately 4–5 h, followed by negative correlations with lags of 8–9 h, reflecting the transition between flood and ebb tidal phases.

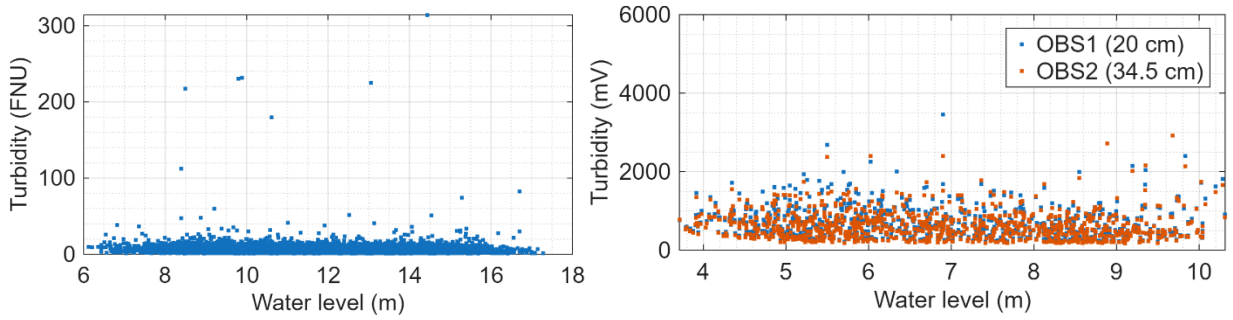


Figure 3.1.8. *Scatter plot of maerl bed turbidity versus water level. The left panel shows observations from the 2023–2024 campaign, while the right panel shows observations from the 2025–2026 campaign at two heights above the bed: OSB1 (20 cm) and OSB2 (34.5 cm).*

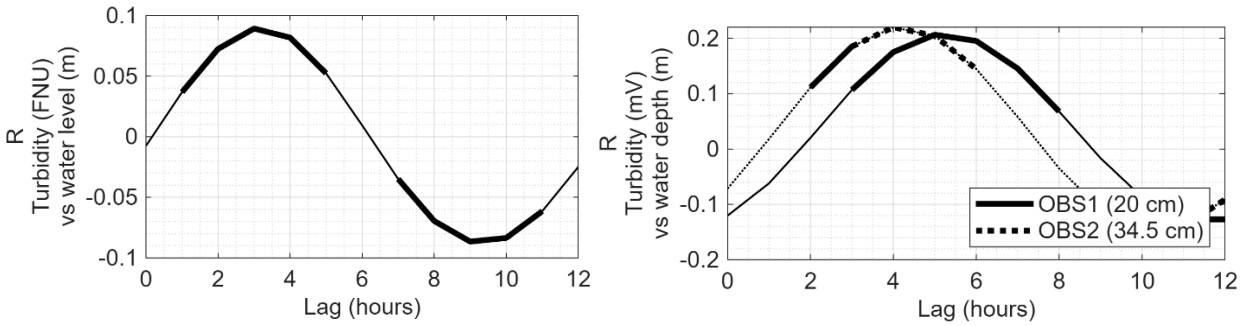


Figure 3.1.9. *Cross-correlation between maerl bed turbidity and water level for hourly lags up to 12 hours. The left panel shows correlations for the 2023–2024 observations, while the right panel shows results from the 2025–2026 campaign at two heights above the bed: OSB1 (20 cm, dotted line) and OSB2 (34.5 cm, solid line). Correlations that are significant at the 95% confidence level are shown with thicker line widths, while non-significant correlations are shown with thinner lines.*

Using a similar method, correlation and cross-correlation analyses between the de-tided maerl bed turbidity and RMS water level data further highlight the importance of the spring-neap tidal cycle in driving turbidity at the maerl bed (Figs. 3.1.10 and 3.1.11). During the 2023–2024 deployment, correlation coefficients reached up to r = 0.4, with maximum correlation occurring at near-zero lag, indicating that variations in maerl bed turbidity responded almost instantaneously to changes in tidal energy associated with the spring–neap cycle. The 2025-2026 deployment only captured two complete spring-neap cycles, which was considered insufficient to perform a robust cross-correlation analysis at a fortnightly timescale. These results are consistent with the spectral analysis, which identified higher spectral energy at the spring–neap timescale compared with the semi-diurnal tidal

component, indicating that fortnightly tidal variability exerts a stronger control on maerl bed turbidity than individual tidal cycles.

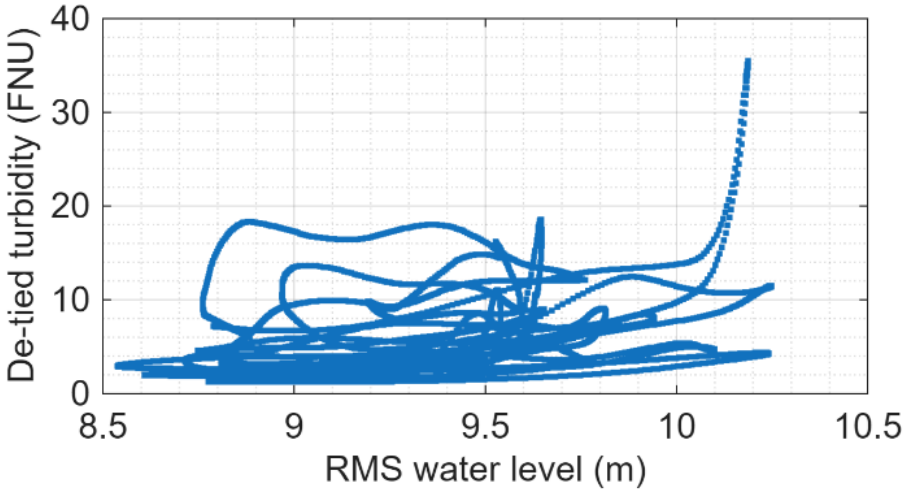


Figure 3.1.10. *Scatter plot of de-tided maerl bed turbidity versus RMS water level for the 2023–2024 campaign.*

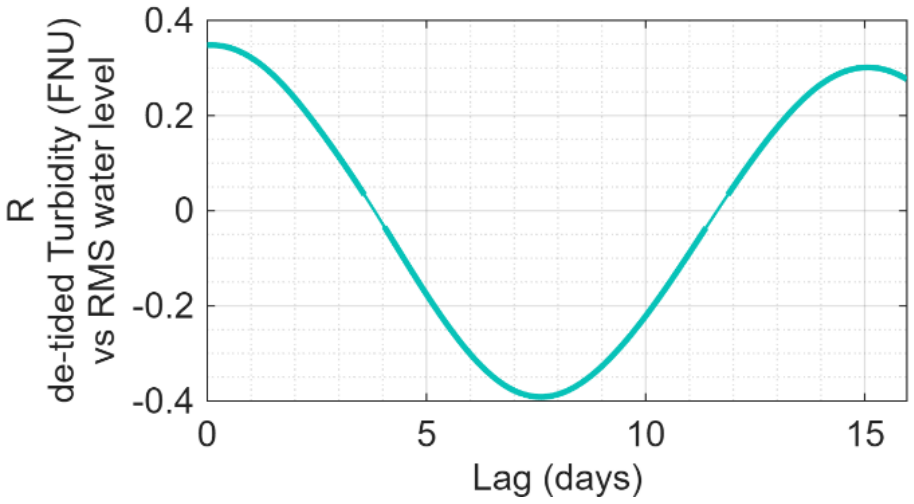


Figure 3.1.11. *Cross-correlation between de-tided maerl bed turbidity and RMS water level for hourly lags up to 12 hours for the 2023–2024 observations. Correlations that are significant at the 95% confidence level are shown with thicker line widths, while non-significant correlations are shown with thinner lines.*

Riverine control on turbidity

To investigate the influence of river discharge, individual discharge peaks were identified for both the Eastern and Western Cleddau rivers (Fig. 3.1.12). Each peak was then characterised according to three attributes: (i) peak prominence, (ii) the time elapsed since the previous discharge peak maximum, and (iii) the prominence of the preceding discharge peak. Using this classification, we examined how different types of river discharge events influenced sediment dynamics by analysing scatter plots and cross-correlations between river discharge, river turbidity, and maerl bed turbidity.

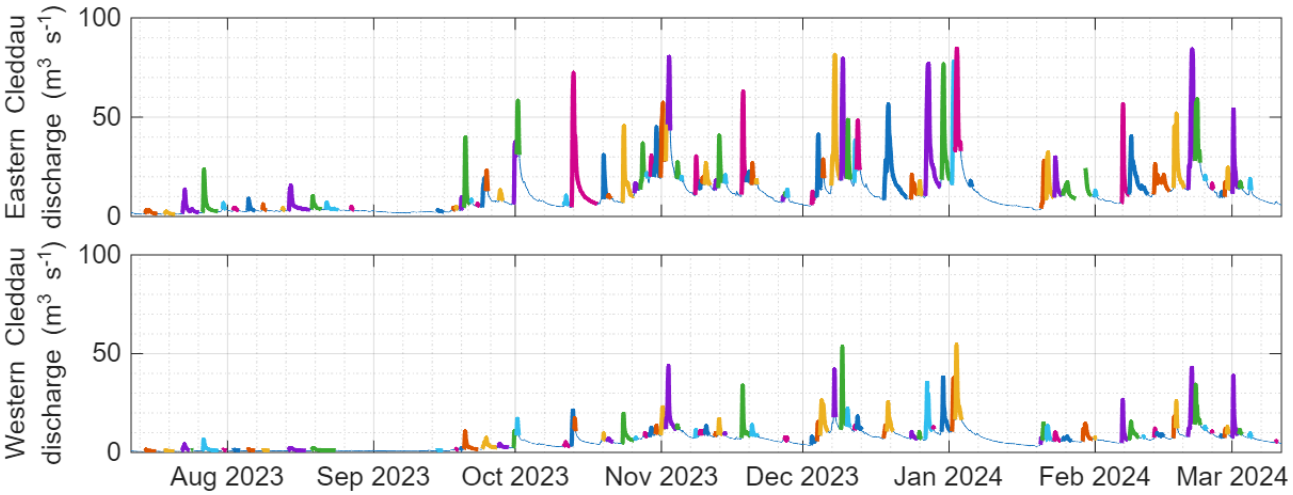


Figure 3.1.12. *River discharge time series for the Eastern Cleddau (top panel) and Western Cleddau (bottom panel), with individual discharge peaks identified and highlighted using different colours.*

River turbidity increased with river discharge in both catchments, although the relationship was clearly nonlinear and exhibited substantial scatter (Figs. 3.1.13–3.1.14). In both the Eastern and Western Cleddau rivers, turbidity increased rapidly at low to moderate discharge before tending to plateau at higher discharge values, as reflected by the fitted curves. The Eastern River showed a broader discharge range and greater variability in turbidity, whereas the Western River displayed a more constrained distribution, with turbidity values clustering more closely around the fitted relationship.

For discharge events that occurred following previous high-magnitude peaks, turbidity during the declining phase of the discharge peak generally remained lower than predicted by the fitted river discharge-river turbidity relationship (Fig. 3.1.13). This suggests that sediment

mobilisation in the river may become limited following large flow events, potentially due to temporary depletion of readily available sediment sources. In contrast, lower antecedent peak discharges were associated with comparatively higher turbidity. Similarly, discharge peaks occurring several days after the previous event were generally associated with low to moderate river discharge but produced relatively large increases in river turbidity (Fig. 3.1.14). By contrast, events occurring shortly after a previous discharge peak tended to generate weaker turbidity responses, suggesting a reduced capacity to mobilise additional sediment. Together, these results indicate that river turbidity was controlled not only by instantaneous discharge magnitude but also by antecedent hydrological conditions and sediment supply in the catchments, highlighting potential memory effects in catchment sediment transport dynamics.

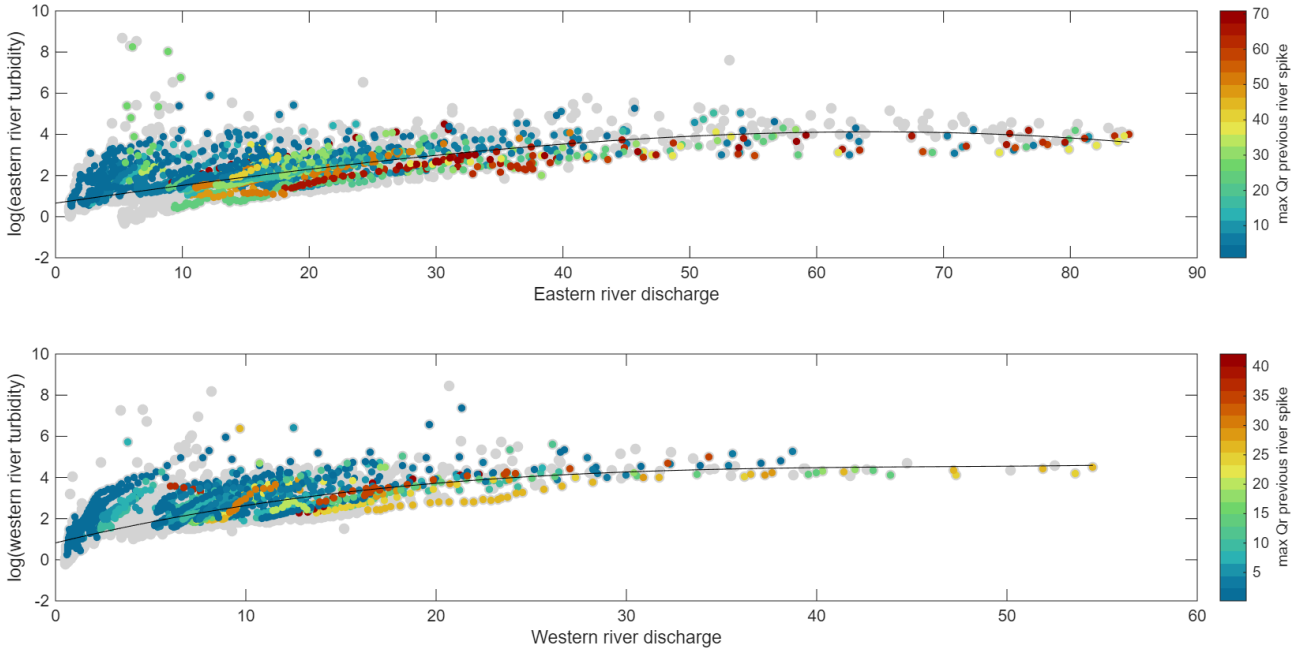


Figure 3.1.13. *Scatter plots of log-transformed river turbidity versus river discharge. The upper panel shows the Eastern River, and the lower panel shows the Western River. Grey markers represent hourly observations. Points corresponding to the recession (declining) phase of discharge events are coloured according to the maximum discharge reached during the preceding event, as indicated by the colour scale.*

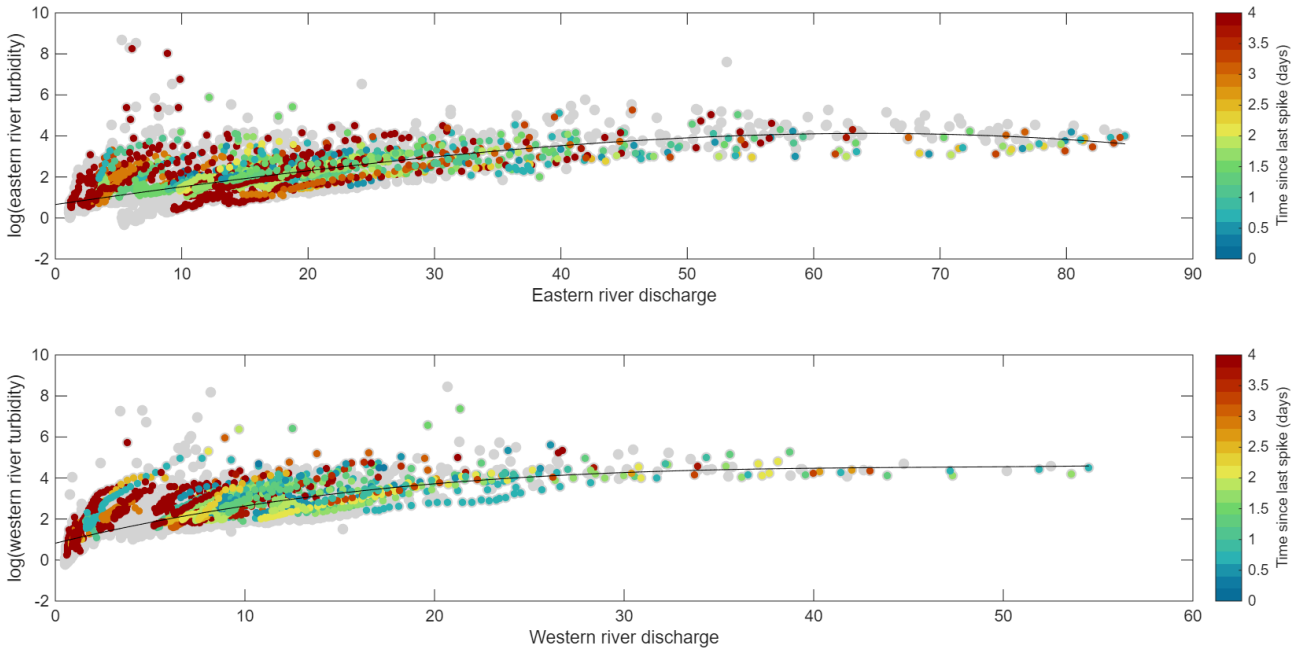


Figure 3.1.14. *Scatter plots of log-transformed river turbidity versus river discharge. The upper panel shows the Eastern River, and the lower panel shows the Western River. Grey markers represent hourly observations. Points corresponding to the recession (declining) phase of discharge events are coloured according to the time elapsed since the last river spike, as indicated by the colour scale.*

Cross-correlation analysis between the river turbidity and de-tided maerl bed turbidity data indicates that riverine suspended sediment inputs exerted a strong and persistent influence on turbidity conditions at the maerl bed (Fig. 3.1.15). Significant positive correlations were observed for both the Eastern and Western Cleddau rivers across both monitoring campaigns, with correlation coefficients generally exceeding r = 0.4. This demonstrates a clear coupling between sediment mobilisation within the catchments and turbidity dynamics at the estuarine maerl bed.

For both deployments, correlations remained consistently high during the first three days following river turbidity events, suggesting that river-derived suspended sediments influence maerl bed turbidity over multi-day timescales. In both datasets, correlations were slightly higher during the first few hours following turbidity peaks, followed by a decline and a secondary increased correlation with lags of approximately 3 days. After this period, correlations decreased. This pattern suggests a delayed response between river sediment mobilisation and maximum turbidity impacts at the maerl bed. This pattern suggests both an

immediate response to river sediment inputs and a delayed response associated with the transport, and potential depletion of riverine sediments before they reached the maerl bed.

The two sensors deployed during the 2025–2026 campaign also revealed vertical differences in the river–turbidity relationship. Correlations were consistently stronger for OSB1, located higher in the water column (34.5 cm above the seabed), than for OSB2, positioned closer to the seabed (20 cm above the seabed). This suggests that turbidity higher in the water column is more directly influenced by river-derived suspended sediments, whereas near-bed turbidity is additionally affected by local bed processes such as tidal resuspension and bed friction, which may partially obscure the river signal.

Although these results demonstrate that river-derived sediments influence maerl bed turbidity over timescales of several days, the response is likely modulated by the magnitude and timing of individual river discharge events. To investigate this further, and given that both the Eastern and Western Cleddau rivers are expected to exert a combined influence on maerl bed turbidity downstream of their confluence, a total river discharge time series was generated by summing discharge from both rivers (Fig. 3.1.16). Individual discharge peaks were then identified within this combined record. Each event was subsequently characterised according to three attributes: (i) peak prominence, (ii) the time elapsed since the previous discharge peak maximum, and (iii) the prominence of the preceding discharge peak.

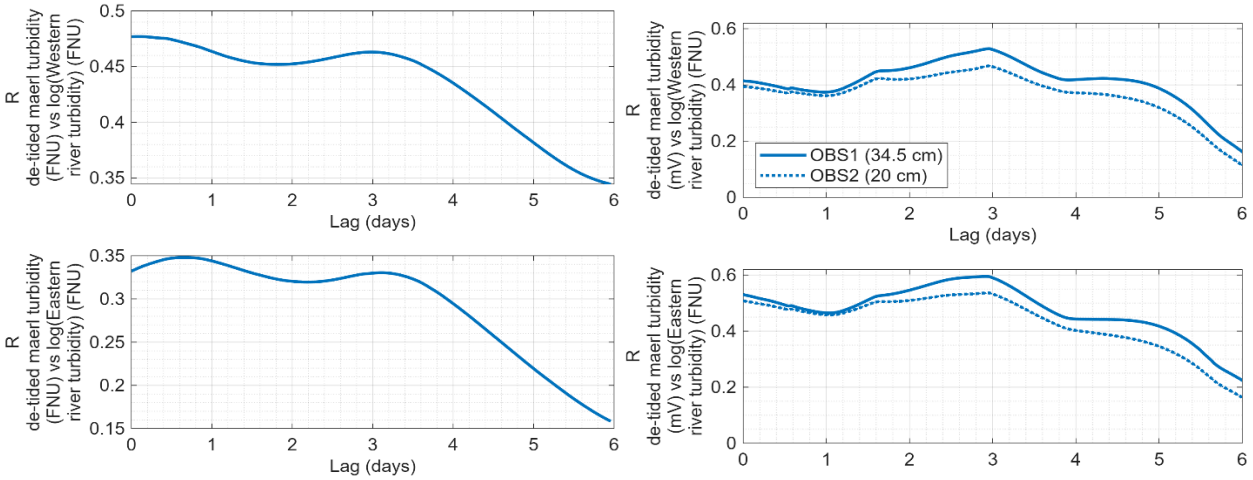


Figure 3.1.15. *Cross-correlation between log-transformed river turbidity and de-tided maerl bed turbidity for hourly lags up to 6 days. Upper panels show results for the Western Cleddau, while lower panels for the Eastern Cleddau. Left panels correspond to the 2023–2024 observations, and right panels to the 2025–2026 campaign, including measurements from two sensors above the seabed: OSB1 (34.5 cm; dotted line) and OSB2 (20 cm; solid line).*

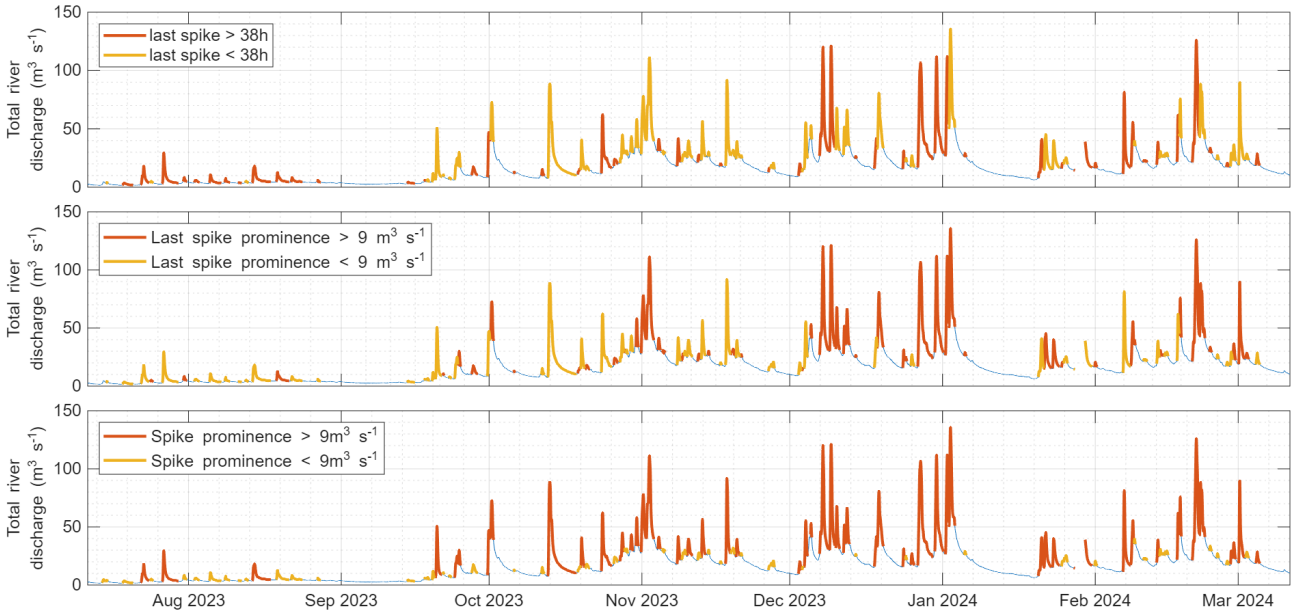


Figure 3.1.16. *Total river discharge (the sum of discharge from the Eastern and Western Cleddau rivers). Individual discharge peaks were identified and classified based on three characteristics: (i) whether the time elapsed since the previous peak exceeded 38 h, (ii) whether the prominence of the previous peak exceeded 9 m³/s, and (iii) whether the prominence of the current peak exceeded 9 m³/s. These threshold values were selected to produce a comparable number of discharge peaks above and below each threshold.*

De-tided turbidity at the maerl bed increased with total (combined) river discharge, although the relationship was nonlinear and characterised by considerable variability (Fig. 3.1.17). Turbidity increased rapidly at low to moderate discharge before approaching a plateau at higher discharge values, as indicated by the logarithmic fitted trend. Most observations clustered within intermediate turbidity values, while extreme discharge events were associated with only modest additional increases in maerl bed turbidity, suggesting a saturation-like response in suspended sediment concentrations at the maerl bed. It should be noted that maerl bed turbidity values were lower than river turbidity values because the maerl bed record was de-tided to isolate the river-driven signal. Compared with the relationship between river discharge and river turbidity, de-tided maerl bed turbidity appeared to reach this plateau more rapidly.

The upper panel of Fig. 3.1.17 shows that antecedent river event magnitude strongly influenced turbidity at the maerl bed during the three days following peak discharge events. Observations collected within three days of peak discharge events preceded by large discharge peak generally exhibited higher turbidity for a given discharge than those following smaller antecedent events. The persistence of elevated turbidity following major discharge events suggests continued resuspension or delayed transport of fine sediment to the maerl bed, particularly during periods of clustered high-discharge events.

The lower panel of Fig. 3.1.17 further indicates that turbidity at the maerl bed declined progressively with increasing time since the previous river discharge peak. Discharge peaks immediately following previous discharge events were characterised by the highest turbidity values but relatively weak turbidity gradients. In contrast, discharge events occurring after longer periods of low flow tended to begin at lower background turbidity levels but were associated with much steeper increases in turbidity. This temporal pattern suggests that the maerl bed responds rapidly to river-driven sediment inputs but gradually recovers as suspended sediments settle, disperse, or are redistributed by tidal processes.

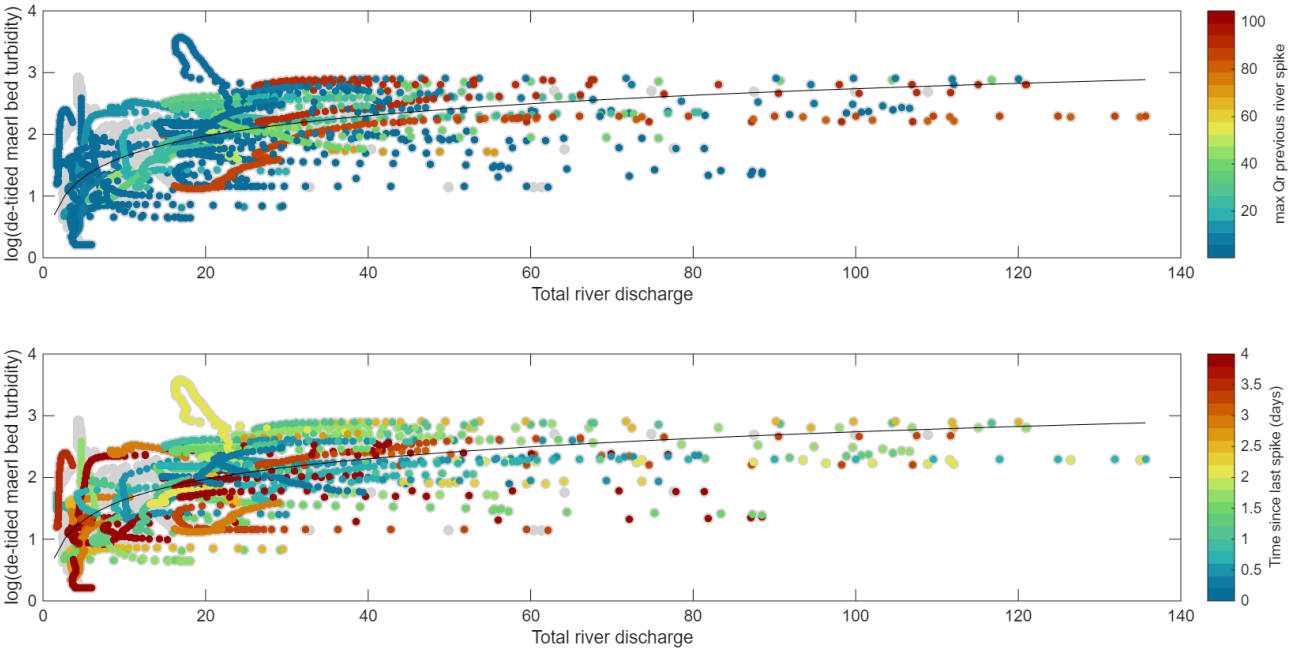


Figure 3.1.17. *Scatter plots of log-transformed, de-tided maerl bed turbidity versus total river discharge (sum of the Eastern and Western Rivers). Grey markers represent hourly observations. Observations within three days following each peak discharge event are coloured according to (upper panel) the maximum discharge reached during the preceding event and (lower panel) the time elapsed since the last river spike.*

To facilitate comparison between river turbidity records and river discharge time series, a variable termed *total river turbidity* was calculated as the sum of turbidity from the Eastern and Western Cleddau rivers. Scatter plots of de-tided maerl bed turbidity against log-transformed total river turbidity reveal a positive relationship, although the strength of this relationship varies substantially between event classes (Fig. 3.1.18a-c). Similarly, de-tided maerl bed turbidity increased with total river discharge (Fig. 3.1.19a-c), although this relationship was less steep than that observed with total river turbidity. This suggests that river turbidity provides a more direct proxy for the supply of suspended particulate material reaching the coastal system than discharge alone.

For discharge events occurring more than 38 h after the previous event, maerl bed turbidity tended to be higher and was associated with higher river turbidity and discharge than events occurring shortly after a previous discharge peak (Fig. 3.1.18a and Fig. 3.1.19a). This suggests that rapid event succession reduces the sensitivity of maerl bed turbidity to variations in river turbidity. Cross-correlation analysis between maerl bed turbidity and river

turbidity showed consistently stronger correlations for events separated by more than 38 h, with the relationship peaking at r=0.5 at lags slightly greater than 3 days (Fig. 3.1.18d). Similarly, cross-correlations between maerl bed turbidity and river discharge were stronger for events separated by more than 38 h (r=0.55) than for events occurring within 38 h of the previous discharge peak (r=0.4). Introducing a lag produced little change in correlation during the first 3 days, after which correlations gradually declined (Fig. 3.1.19d). These results indicate that isolated discharge events are more efficient at mobilising and transferring sediment to the maerl bed than clustered events. This likely reflects partial depletion of available sediment sources and enhanced sediment retention within the estuary during periods of closely spaced river events.

For discharge events following a previous event with prominence greater than 9 m^3/s, similar levels of maerl bed turbidity were associated with a broader range of river discharge values and generally lower river turbidity than events preceded by lower-prominence discharge peaks (Fig. 3.1.18b and Fig. 3.1.19b). Cross-correlation analysis showed that events preceded by high-prominence discharge peaks exhibited two local maxima in the relationship between maerl bed turbidity and river turbidity, with correlations reaching r=0.35 at lags of approximately 0.5 and 3 days, separated by a minimum (r=0.1) near 1.5 days lag. In contrast, when the preceding event had a prominence lower than 9 m^3/s, correlations were generally weaker and increased gradually from approximately r=0.2 to r=0.3 over a 3-day lag period (Fig. 3.1.18e). The relationship between maerl bed turbidity and river discharge displayed a slightly different pattern. Immediately following discharge events, correlations were slightly higher when the preceding event prominence exceeded 9 m^3/s (r=0.4) compared with lower-prominence antecedent events (r=0.3). However, after several days of lag, this pattern reversed, with stronger delayed correlations (r=0.45) observed for events preceded by lower-prominence discharge peaks compared with those preceded by larger antecedent events (r=0.3) (Fig. 3.1.19e). These contrasting patterns suggest that large antecedent discharge events may initially maintain elevated background turbidity within the estuary through the persistence and recirculation of fine suspended sediments. However, over longer timescales, the influence of these events weakens, potentially because sediment sources become progressively depleted or because previously mobilised material settles within low-energy depositional zones.

Finally, high-prominence discharge events generally produced higher river turbidity and higher maerl bed turbidity than lower-prominence events (Fig. 3.1.18c and Fig. 3.1.19c). Cross-correlation analyses between maerl bed turbidity and river turbidity showed that high-prominence events generated stronger correlations at approximately 3 days lag (r=0.4) than weaker events (r=0.3). In contrast, correlations at zero lag were weaker for high-prominence events (r=0.1) than for lower-prominence events (r=0.4) (Fig. 3.1.18f). A similar pattern was observed in the cross-correlations between maerl bed turbidity and river discharge (Fig. 3.1.19e). This delayed response suggests that major discharge events do not instantaneously translate into elevated turbidity at the maerl bed. Instead, large river events likely deliver substantial quantities of fine sediment to the estuary, which are subsequently mixed and redistributed by tidal processes, and can temporarily settle (e.g., during high slack water) and later be resuspended by increased tidal currents.

Overall, these results demonstrate that the influence of river discharge and riverine turbidity on maerl bed turbidity depends not only on the magnitude of individual hydrological events but also on the timing and sequencing of previous discharge events. Correlation maxima generally occurred at lags of approximately 3 days, indicating a delayed response of maerl bed turbidity to river forcing. The delayed correlations and multi-day persistence of turbidity anomalies indicate that sediment dynamics over the maerl bed are strongly influenced by cumulative sediment supply and tidally-driven mixing, advection, settlement and remobilisation, highlighting the importance of hydrological memory and tidal regime in controlling turbidity over the maerl bed.

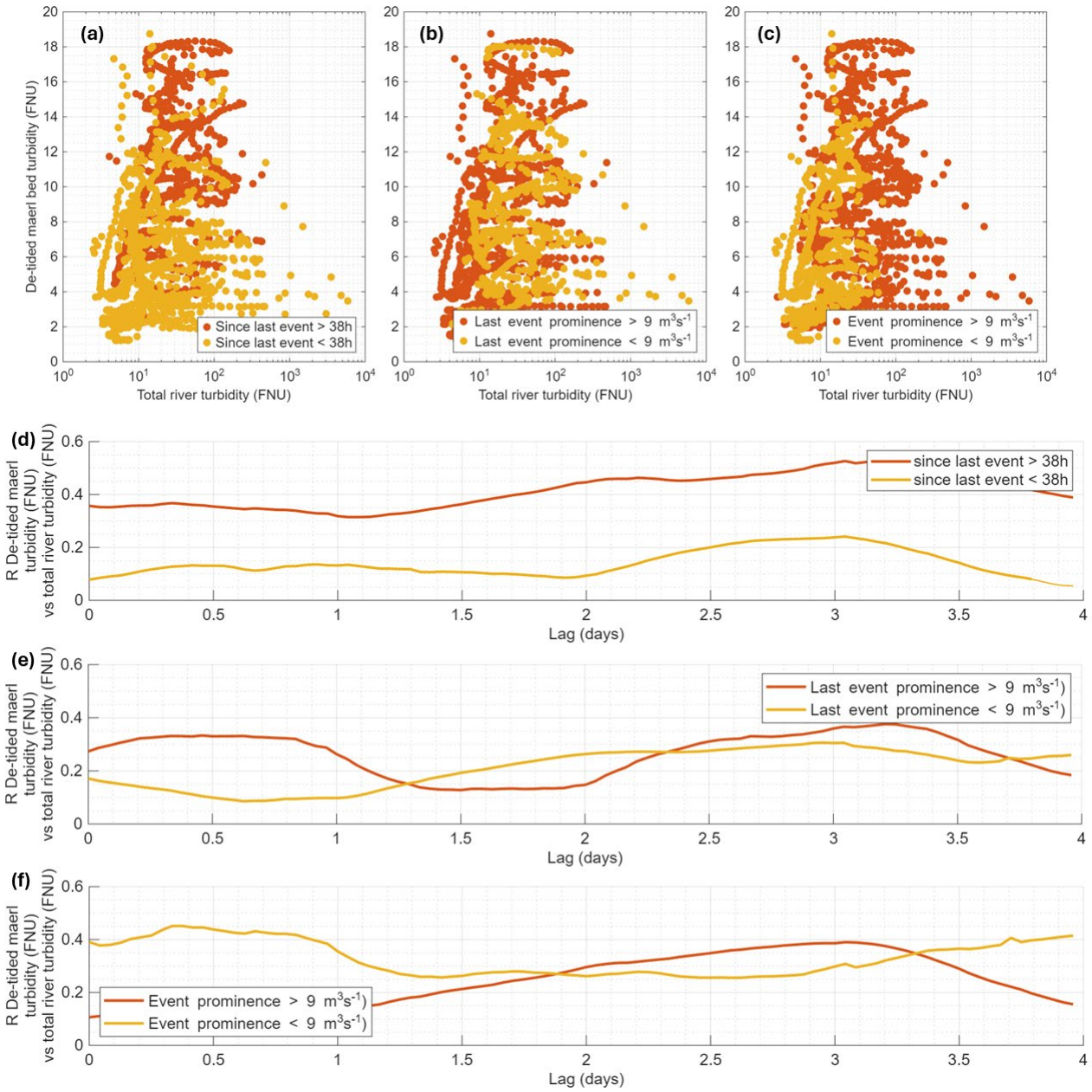


Figure 3.1.18. *Scatter plots and cross-correlations between log-transformed de-tided maerl bed turbidity and river turbidity during the 2023–2024 campaign. The upper panels show scatter plots of the hourly observations for the discharge peak clustered following Fig. 3.1.16 as: (a) river peaks occurring less than or more than 38 h after the previous discharge event, (b) river peaks preceded by discharge events with prominence greater than or less than 9 m³/s, and (c) river peaks with prominence greater than or less than 9 m^3/s. The lower panels (d), (e), and (f) show the corresponding cross-correlation analyses using the same event classifications.*

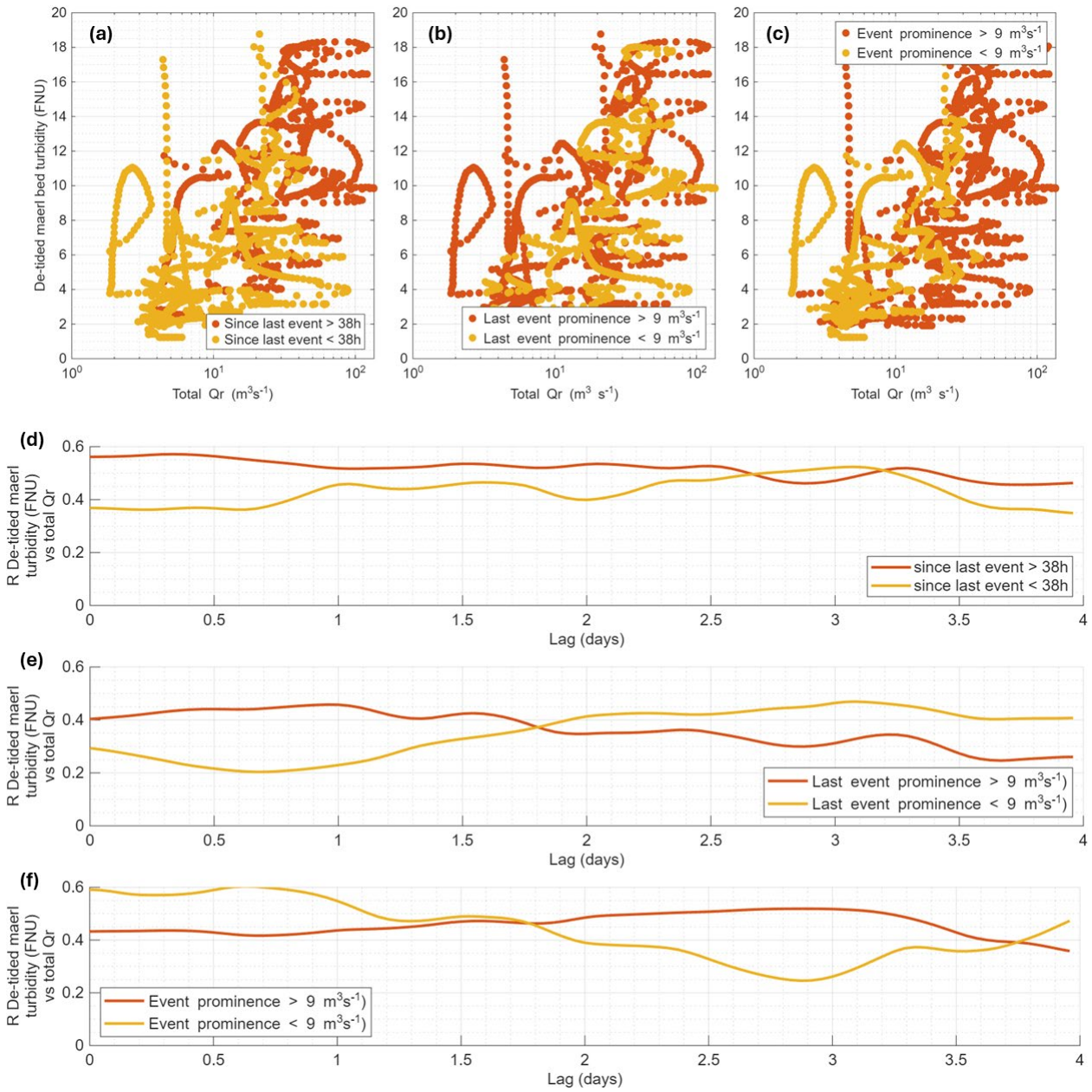


Figure 3.1.19. *Scatter plots and cross-correlations between log-transformed de-tided maerl bed turbidity and river discharge during the 2023–2024 campaign. The upper panels show scatter plots of the hourly observations for the discharge peak clustered following Fig. 3.1.16 as : (a) river peaks occurring less than or more than 38 h after the previous discharge event, (b) river peaks preceded by discharge events with prominence greater than or less than 9 m³/s, and (c) river peaks with prominence greater than or less than 9 m³/s. The lower panels (d), (e), and (f) show the corresponding cross-correlation analyses using the same event classifications.*

3.2 Simulations of turbidity in the Milford Haven

The Delft3D hydrodynamic and sediment transport model simulations are described in this section. The outputs from Scenarios 1-6 (see Table 2.2.2 for a summary of these scenarios) are described in section 3.2.1 – 3.2.7, while the model sensitivity simulations are described in section 3.2.8 (see Table 2.2.3 for a summary of these simulations).

3.2.1 Scenario-1a: December 2023 - January 2024

Under realistic tidal, riverine and suspended sediment conditions in the Milford Haven during Dec 2023 to Jan 2024, coarse silt (83 µm) and fine silt/clay (63 µm) sediment fractions were predicted to reach the maerl bed area and sensitive habitat, i.e., very fine to medium sands (100-500 µm) did not reach the maerl bed and instead settled further upstream (Fig. 3.2.1). Fine silt/clay (63 µm) emerged as the dominant fraction at the maerl bed area, consistent with the preferential advection of finer material.

Over the wider vicinity of the maerl bed (i.e., surrounding but excluding the specific maerl bed location), the simulated turbidity (sourced solely from suspended sediment sources in the Cleddau rivers) remained very low and broadly similar to that predicted at the maerl bed, though with greater spatial variability as indicated by the wider 5^{th}-95^{th} percentile envelopes, and marginally higher peak values in the fine silt/clay fraction reaching 6.21×10^{-8} FNU at the 95^{th} percentile.

The fine silt/clay fraction required approximately 7 days to reach the maerl bed extents (28 km downstream) following the first-flush of the model (start = 04 December 2023 16:30, Fig. 3.2.2) whereas the coarse silt fraction took 7.5 days. Fine silt/clay travelled marginally faster than coarse silt throughout, consistent with its lower settling velocity and greater susceptibility to advective transport under tidal forcing. The dredge disposal site at 12.9 km downstream was reached after approximately 4 days for both fractions, suggesting that sediment mobilised at the disposal site itself would require a further 3-4 days to propagate to the maerl bed.

These travel times fall within the residence time estimates derived from a conservative tracer Delft3D simulation over the same hydrodynamic period, in which a non-decayable tracer initialised at 100% concentration (01 December 2023 00:00:00) across the Water Framework Directive (WFD) Cycle 2 defined estuary boundary area (See Fig 2.2.1) reduced to 37% of its initial concentration (Zimmerman 2018) after 18 days and 18 hours (Appendix A2.1). This indicates that material introduced to the upper estuary during this period would persist within the estuarine system for approximately 3 weeks before being flushed offshore. Spatially, residence times across the estuary were heterogeneous, ranging from less than 1 day in the energetic outer channel to over 31 days in sheltered upper tributary creeks, with the maerl bed exhibiting a mean residence time of 14.4 days (Appendix A2.2).

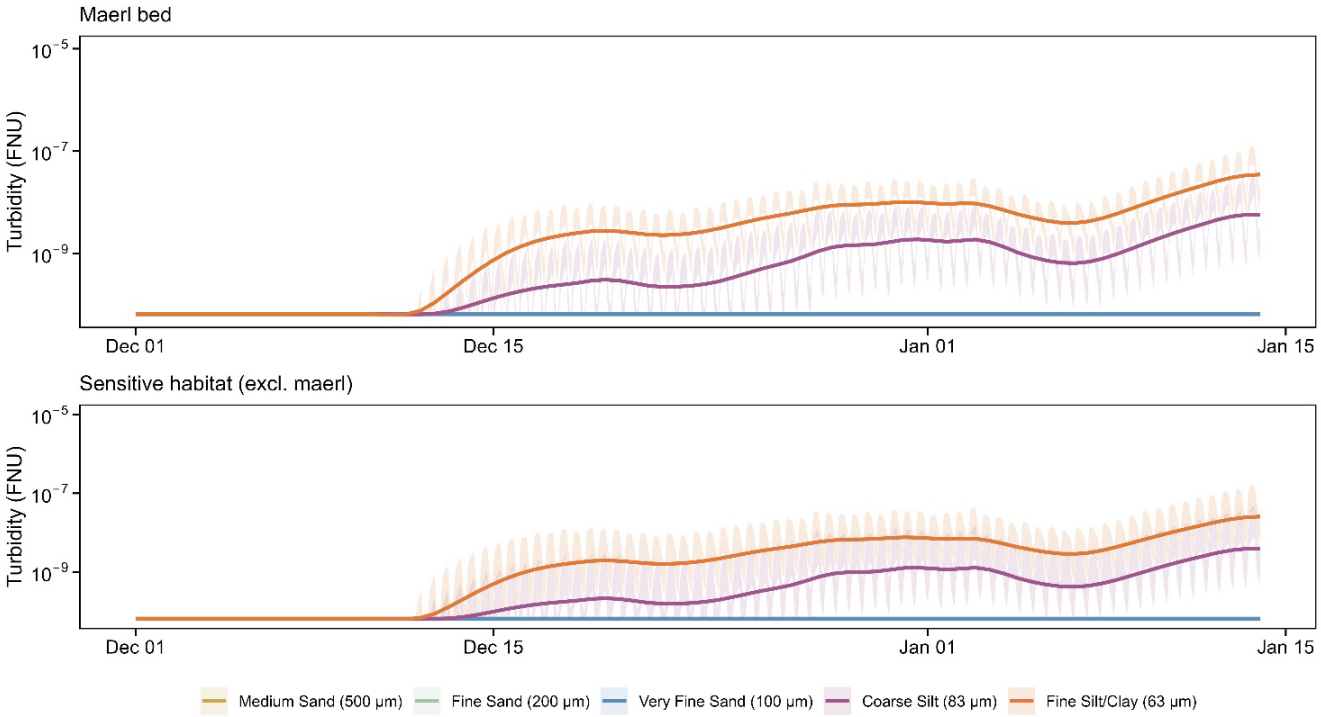


Figure 3.2.1. *Scenario-1a: Median (p50) turbidity time series with 5th–95th percentile envelopes at the maerl bed (upper panel) and sensitive habitat area excluding the maerl bed (lower panel) for all five sediment fractions. Shading represents spatial variability across grid cells within each area. Note the logarithmic y-axis.*

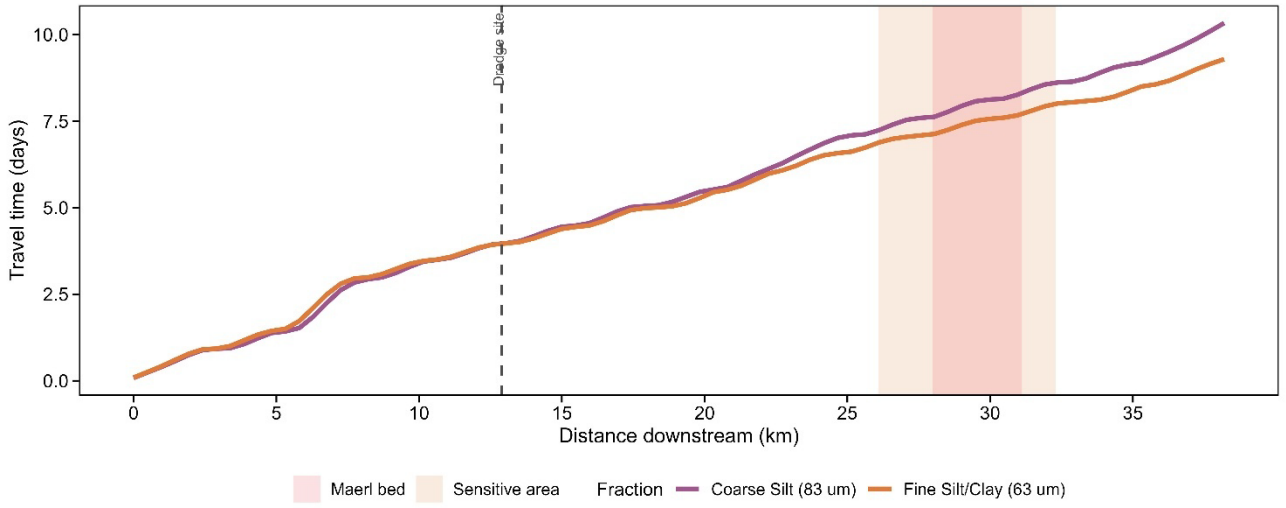


Figure 3.2.2. *Scenario-1a: First-flush sediment travel time from the river input (distance = 0 km) every 100m along the Cleddau thalweg for coarse silt (83 µm) and fine silt/clay (63 µm) fractions, derived from the 2023–2024 real flow model run (December 2023 to January 2024).*

The simulated distribution of maximum turbidity along the central longitudinal transect of the estuary reveals a strong attenuation of riverine suspended sediment with distance downstream from the confluence of the Cleddau rivers (Fig. 3.2.3). Sand fractions (≥100 µm) immediately settled in the rivers near the source. Of the silt fractions, both coarse silt (83 µm) and fine silt/clay (63 µm) reached peak concentrations of approximately 2.0×10^{-2} FNU at the tidal limit, attenuating rapidly to below 10% of their peak values within 1.9 km downstream. By the dredge site (~12.9 km downstream), concentrations had reduced to 7.0×10^{-6} and 1.1×10^{-5} FNU, respectively, and by the maerl bed (~29.6 km downstream) to 2.0×10^{-8} and 7.8×10^{-8} FNU; a reduction of approximately six orders of magnitude from source to maerl bed.

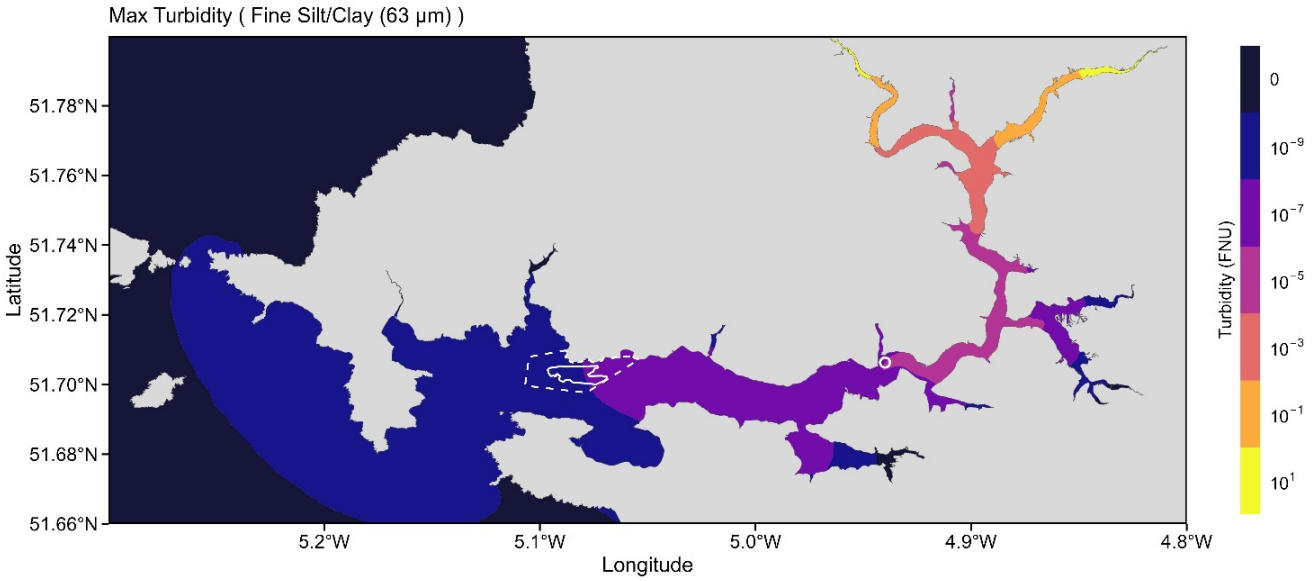


Figure 3.2.3. *Scenario-1a: Spatial distribution of maximum turbidity (FNU) for the fine silt/clay (63 µm) fraction. Note the logarithmic colour scale. The white circle denotes the Neyland Yacht Haven disposal site (LU190); the solid white outline indicates the maerl bed extent and the dashed white outline the sensitive habitat area.*

3.2.1.1 Scenario-2: High river flow

Under the high river flow scenario (constant 95th percentile discharge in both Cleddau rivers, combined with 2023-24 observed suspended sediment loads), the simulated distribution of maximum turbidity shows a markedly more extensive turbidity plume compared to Scenario-1a (observed 2023-24 forcing) (Fig. 3.2.4). Elevated fine silt/clay and coarse silt concentrations extended considerably further downstream in the estuary, reaching 2.29×10^{-6} to 4.78×10^{-6} FNU at the maerl bed (28-31 km downstream). Sand fractions again settled in the immediate vicinity of the tidal limits.

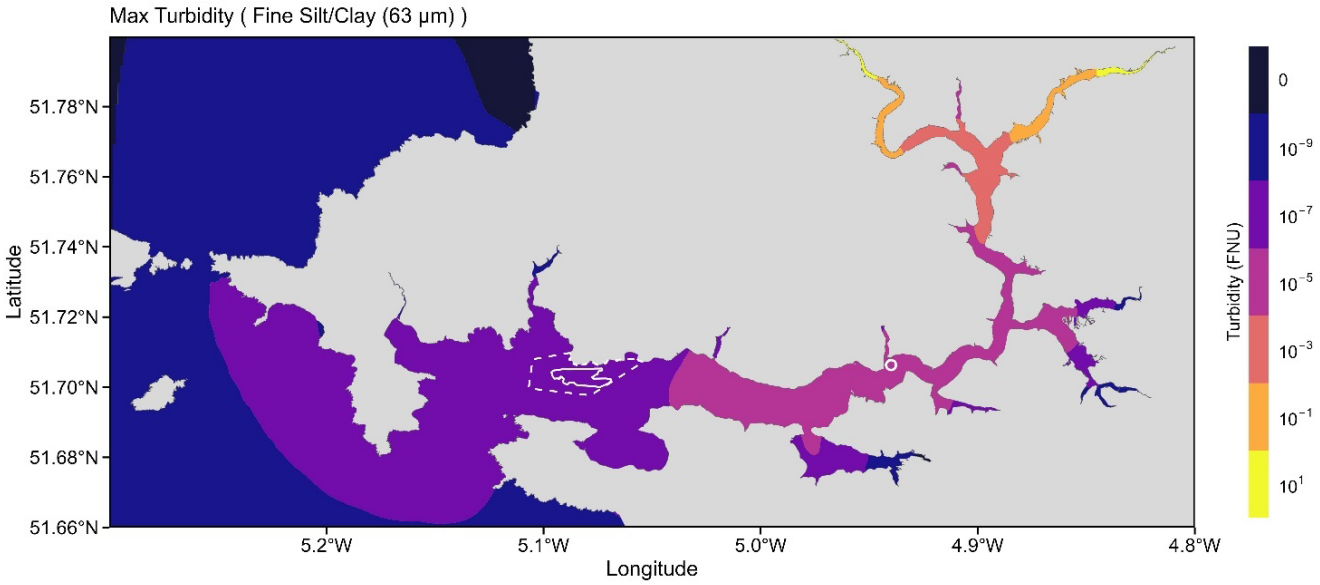


Figure 3.2.4. *Scenario-2: Spatial distribution of maximum turbidity (FNU) for the fine silt/clay (63 µm) fraction. Note the logarithmic colour scale. The white circle denotes the Neyland Yacht Haven disposal site (LU190); the solid white outline indicates the maerl bed extent and the dashed white outline the sensitive habitat area.*

Maximum simulated turbidity along the longitudinal transect of the estuary, from Scenario-2, is presented in Fig. 3.2.5. Both coarse silt and fine silt/clay peaked at approximately 1.29×10^{-2} FNU at the tidal limit, attenuating to below 10% of peak values within 2.5 km downstream. Concentrations at the dredge site (~12.9 km downstream) reached 8.39×10^{-5} and 1.04×10^{-4} FNU for coarse silt and fine silt/clay respectively; approximately an order of magnitude greater than under real-world 2023 forcing. At the maerl bed (~29.6 km downstream), fine silt/clay concentrations reached 3.22×10^{-6} FNU, around 40 times greater than the equivalent real-world value of 7.82×10^{-8} FNU, with the elevated fine silt plume extending to 24.7 km downstream.

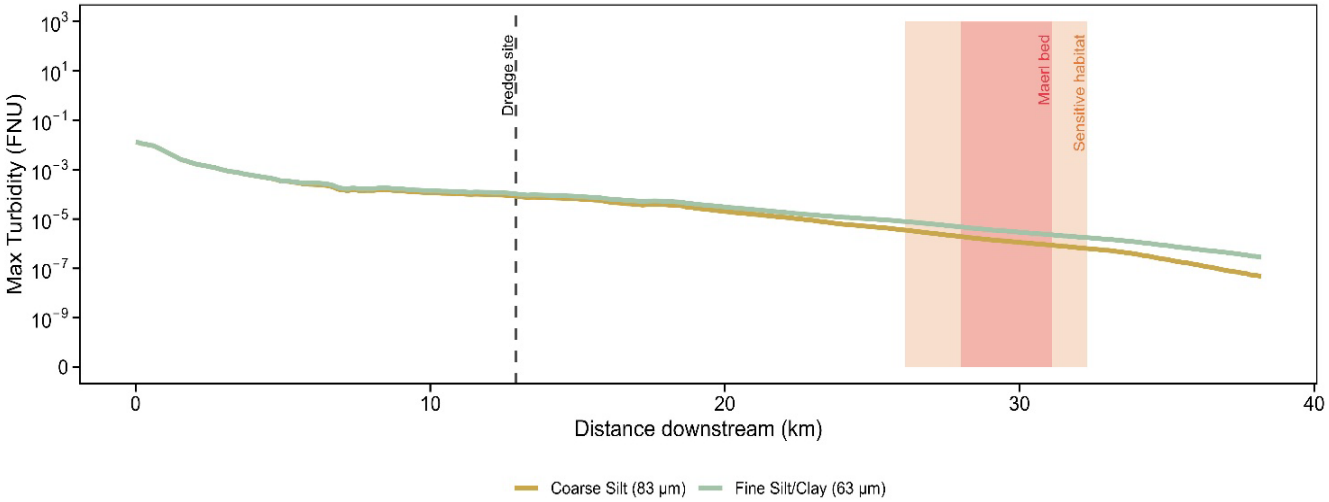


Figure 3.2.5. *Scenario-2: Maximum turbidity (FNU) along the longitudinal estuary transect for coarse silt (83 µm) and fine silt/clay (63 µm) fractions. Note the logarithmic y-axis. The dashed vertical line indicates the Neyland Yacht Haven disposal site (LU190) at 12.9 km downstream. Shaded regions denote the spatial extent of the maerl bed (red) and sensitive habitat area (orange).*

3.2.2 Scenario-1b: November 2025 - January 2026

The spatial distribution of maximum turbidity over the Nov 2025 – Jan 2026 simulation period (Fig. 3.2.6) shows a similar pattern to Scenario-1a (Dec 2023 – Jan 2024). The highest simulated turbidity concentrations were confined to the upper estuary near the tidal limits, reaching 4.35 FNU at the river inputs and attenuating to below 10% of peak values within 2.1 km downstream. Elevated concentrations extended further into the estuary compared to the 2023-24 simulation, reaching 1.85×10^{-3} FNU at the dredge site (~12.9 km) and 3.43×10^{-6} to 8.35×10^{-6} FNU across the maerl bed (28-31 km), compared to negligible values under the 2023-24 forcing. The sensitive habitat area showed slightly higher maximum concentrations than the maerl bed along the transect (mean 8.52×10^{-6} vs 5.40×10^{-6} FNU), consistent with its broader spatial extent encompassing areas closer to the sediment source.

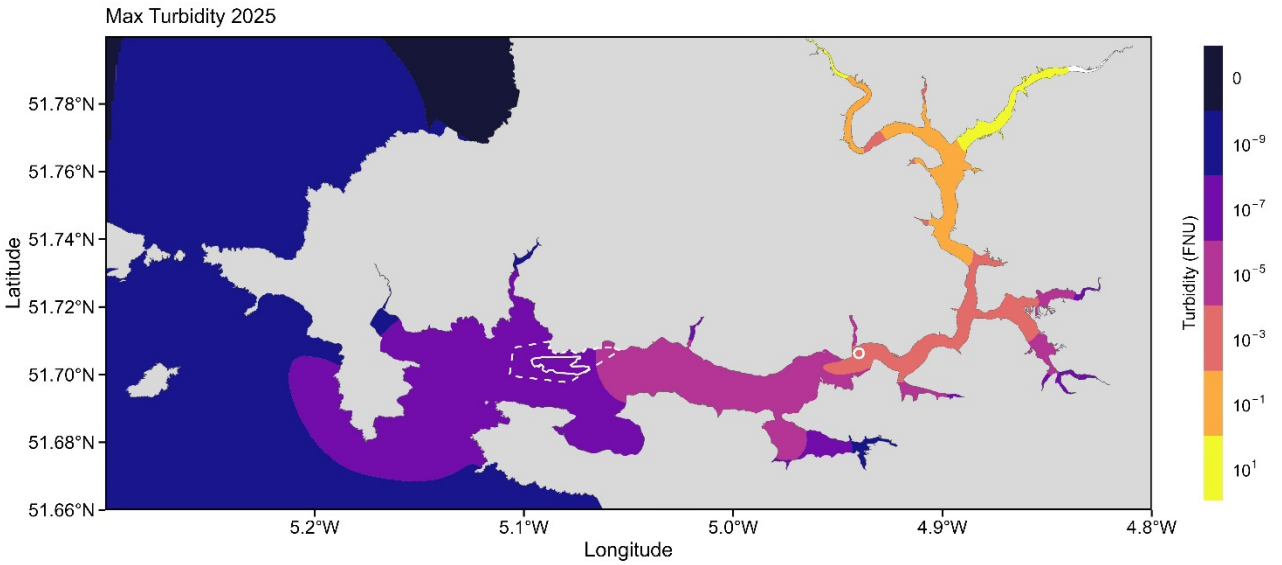


Figure 3.2.6. *Scenario-1b: Spatial distribution of maximum turbidity (FNU) for the fine silt/clay (63 µm) fraction. Note the logarithmic colour scale. The white circle denotes the Neyland Yacht Haven disposal site (LU190); the solid white outline indicates the maerl bed extent and the dashed white outline the sensitive habitat area.*

Fig. 3.2.7 illustrates the simulated temporal evolution of fine silt (63 µm) turbidity at the maerl bed over the Scenario-1b simulation period. Turbidity was low during November 2025, with 94 discrete events identified above the background threshold of 2.85×10^{-7} FNU, averaging 9.0 hours in duration. A sustained period of elevated turbidity developed from early December 2025, with event durations progressively lengthening through the month, peaking in a continuous event from 04 January 2026 lasting 122.5 hours and reaching a median peak of 5.81×10^{-6} FNU (95th percentile 8.02×10^{-6} FNU) on 05 January. The sensitive habitat area followed a similar temporal pattern, with a median peak of 4.07×10^{-6} FNU, though the 95th percentile reached 1.13×10^{-5} FNU in early December 2025, reflecting greater spatial variability within that polygon. Time-averaged concentrations were higher at the maerl bed than the sensitive area (mean p50 ratio 0.68), consistent with the 2023-24 results.

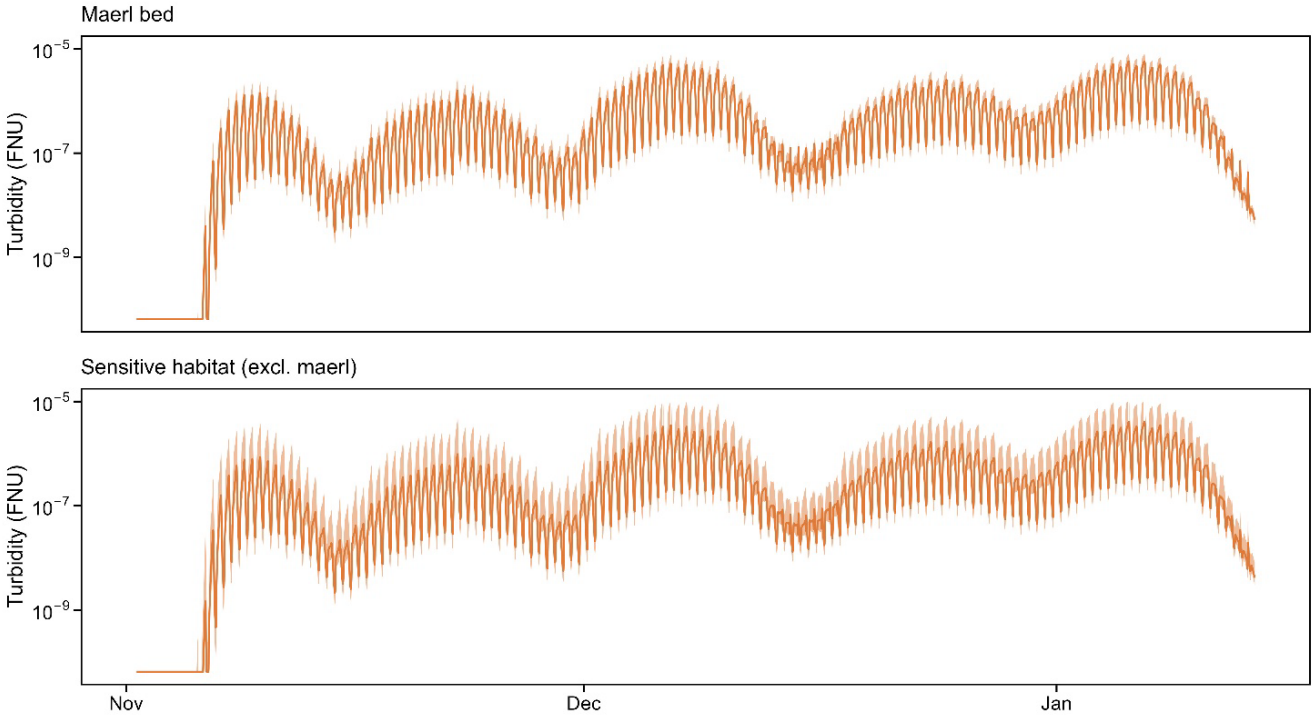


Figure 3.2.7. *Scenario-1b: Median (p50) turbidity time series with 5th–95th percentile envelopes for the fine silt/clay (63 µm) fraction at the maerl bed (upper panel) and sensitive habitat area excluding the maerl bed (lower panel). Note the logarithmic y-axis. Shading represents spatial variability across grid cells within each area.*

The spatial distribution of fine silt/clay (63 µm) bed mass accumulation by the end of the simulation period is shown in Fig. 3.2.8. The figure shows concentrated bed mass accumulation in the upper reaches of the estuary and river channels. Accumulation exceeded 310 kg/m^2 at the tidal limit of the East Cleddau, with domain-wide mean accumulation of 0.82 kg/m^2, though the large disparity between mean and median values (2.90 × 10^{-5} kg/m^2) reflects the strongly skewed spatial distribution, with the majority of the model domain receiving negligible deposition. All areas registered some accumulation over the simulation period, consistent with fine sediment being advected throughout the estuary under tidal forcing, though at very low concentrations in the lower estuary.

At the maerl bed, median bed mass accumulation was 5.45×10^{-7} kg/m^2 (mean 6.52×10^{-7} kg/m^2, maximum 1.70×10^{-6} kg/m^2), with the sensitive habitat area showing slightly higher values (median 5.65×10^{-7} kg/m^2, mean 9.73×10^{-7} kg/m^2, maximum 4.40×10^{-6} kg/m^2). These values are several orders of magnitude lower than accumulation in the upper estuary,

indicating that fluvially-derived fine silt (from the two Cleddau rivers) settling at the maerl bed under the observed 2025 forcing conditions was negligible.

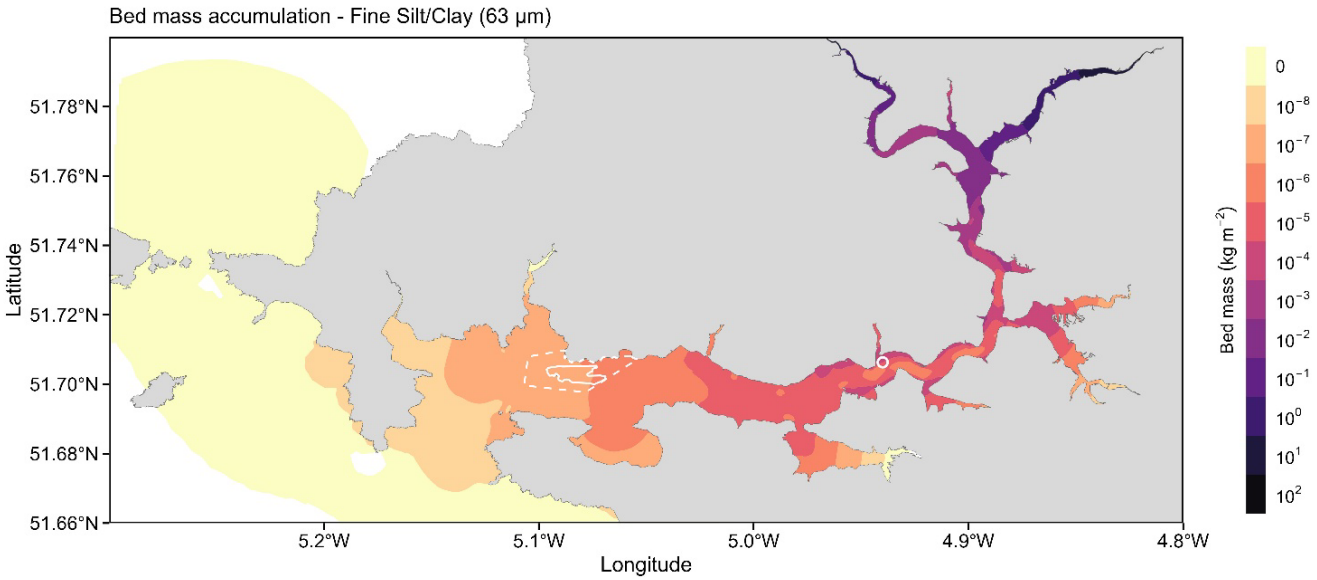


Figure 3.2.8. *Scenario-1b: Spatial distribution of maximum fine silt/clay (63 µm) bed mass accumulation (kg m^{-2}). Note the logarithmic colour scale. The white circle denotes the Neyland Yacht Haven disposal site (LU190); the solid white outline indicates the maerl bed extent and the dashed white outline the sensitive habitat area.*

At the maerl bed, depth-time (tidally-averaged) plots reveal clear vertical structure in turbidity, salinity, and velocity (Fig. 3.2.9). Simulated SSC was consistently higher in the bottom layer than the surface, with bottom concentrations peaking at 6.63×10^{-10} FNU on 06 January 2026, coinciding with the peak surface value of 4.06×10^{-10} FNU. The maximum vertical gradient occurred on 06 December 2025, suggesting enhanced near-bed sediment loading during the earlier high-flow period.

Some weak salinity stratification was simulated, for example on 19 December 2025 bottom salinity was 31.55 psu and surface salinity 31.34 psu. The variability in surface salinity (1.44 psu) was notably larger than at the bed (0.93 psu), reflecting greater tidal flushing influence at the surface. Velocity shear was pronounced, with mean surface velocities (0.31 m/s) approximately twice those at the bed (0.16 m/s).

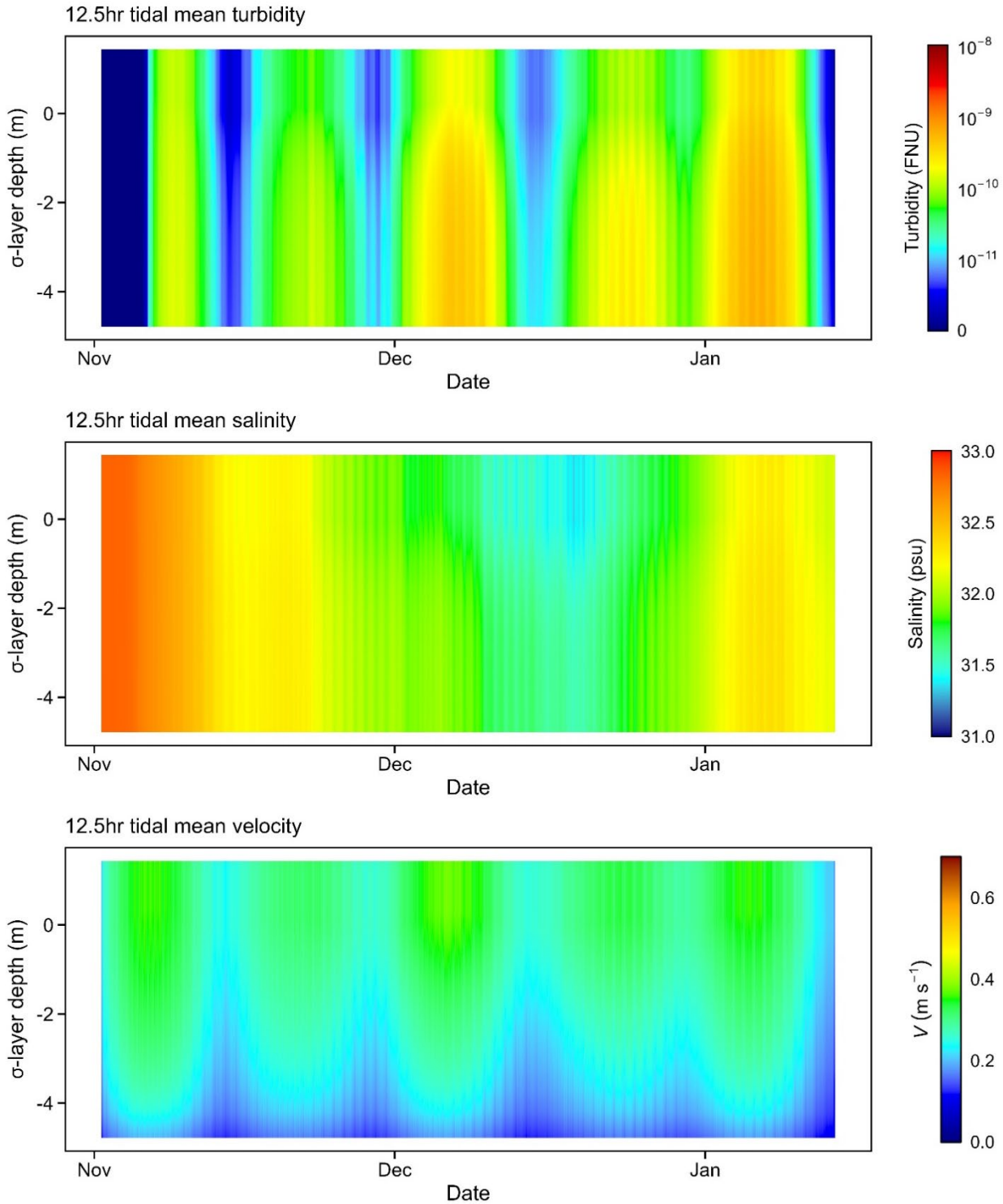


Figure 3.2.9. *Scenario-1b: Depth–time plots of 12.5-hour tidally-averaged turbidity (upper panel), salinity (middle panel) and velocity magnitude (lower panel) at the maerl bed location. The σ-layer depth axis represents the water column from surface (0 m) to bed (approximately −5 m) interpolated from 10 equally spaced depth layers. Note the logarithmic colour scale for turbidity.*

The tidal composite analysis at the maerl bed (Fig. 3.2.10) illustrates the phase relationships between turbidity, salinity, velocity, and bed shear stress over the mean 12.5-hour tidal cycle. The tidal hour refers to the elapsed time within the tidal cycle, with hour 0 corresponding to the start of the flood tidal phase and mean high water occurring at approximately hour 5. Turbidity peaked progressively earlier with depth (at tidal hour 12.0 at the bed, 11.0 at mid-depth, and 9.0 at the surface) indicating upward diffusion of near-bed sediment lagging the tidal cycle, with resuspension initiated near low water and sediment reaching the surface approximately three hours earlier. Ebb turbidity exceeded flood concentrations at all depths, suggesting ebb-dominant suspended sediment transport.

Velocity peaked early in the tidal cycle at both surface (0.59 m/s at tidal hour 1.5) and bed (0.33 m/s at tidal hour 2.0), corresponding to the post-low-water flood jet, with mean flood velocities exceeding ebb at both surface (0.40 vs 0.26 m/s) and bed (0.23 vs 0.12 m/s). Bed shear stress exceeded the critical erosion threshold for fine silt ($\tau_crit = 0.17$ N/m^2) for about half the time (for ~80% of the flood phase and ~30% of the ebb phase). The composite mean τ peaked at 0.95 N/m^2 during tidal hour 1.5, consistent with the velocity maximum, and dropped to 0.03 N/m^2 during high slack water and 0.07 N/m^2 at low slack water; well below τ_crit at both slack water phases. The temporal offset between peak bed shear stress and peak turbidity (e.g., shear stress maxima during the flood phase and turbidity peaking on the ebb) suggests that whilst local resuspension does occur, advection of suspended sediment from upstream sources during the ebb makes a significant contribution to the turbidity signal observed at the maerl bed, with material (i.e., the turbidity plume) subsequently exported seaward and offshore during the ebb.

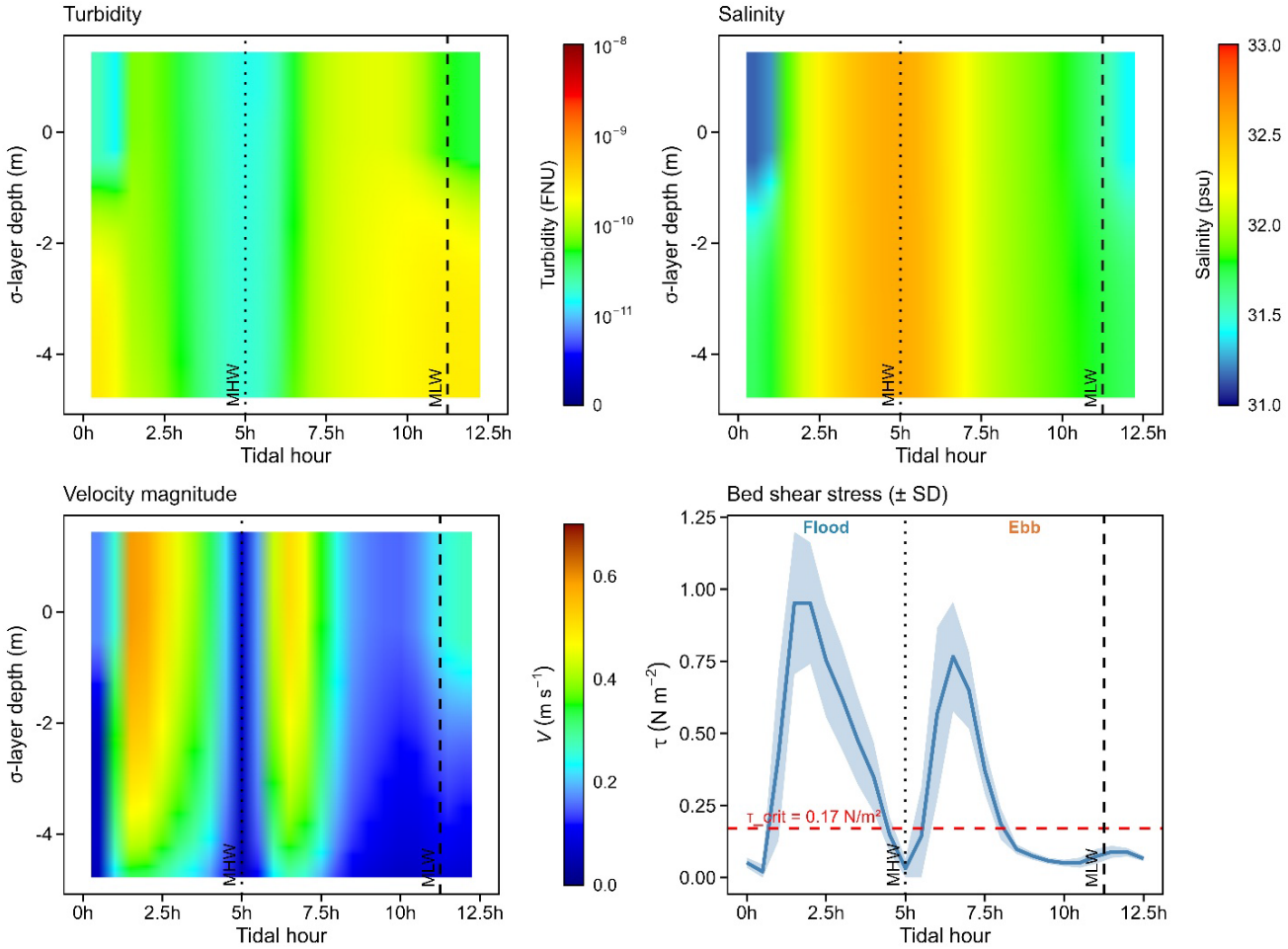


Figure 3.2.10. *Scenario-1b: Tidal composite depth-time plots of turbidity (upper left), salinity (upper right) and velocity magnitude (lower left) over the mean 12.5-hour tidal cycle at the maerl bed location, together with mean bed shear stress (± 1 SD) as a function of tidal hour (lower right). The dotted and dashed vertical lines indicate mean high water (MHW) and mean low water (MLW) respectively. The red dashed horizontal line in the bed shear stress panel denotes the critical erosion threshold for fine silt (τ_crit = 0.17 N/m²). Note the logarithmic colour scale for turbidity.*

3.2.3 Scenario-3: Maintenance dredging

Simulated turbidity at the maerl bed under all three Neyland dredging scenarios was low across all sediment fractions. Fine silt/clay showed the greatest response to increasing dredge concentration, with turbidity at the maerl bed increasing from 4.77×10^{-4} FNU under the low scenario to 1.44×10^{-3} FNU under the high scenario (Fig. 3.2.11). Coarse silt showed a smaller response, with maerl bed values ranging from 1.71×10^{-4} (low) to 5.13×10^{-4} FNU

(high). Sand produced no discernible signal above zero at the maerl bed under any scenario (6.52×10^{-11}).

The relatively rapid settling velocities of both silt fractions (2.47 mm/s for fine silt/clay (63 µm) and 2.94 mm/s for coarse silt (83 µm)) indicate that dredge-derived material has limited capacity to remain in suspension over the ~17 km distance between the licensed disposal site and the maerl bed. Even under the high dredging concentration scenario, modelled turbidity at the maerl bed remained below 1.5×10^{-3} FNU across all fractions, indicating a negligible impact on the maerl bed.

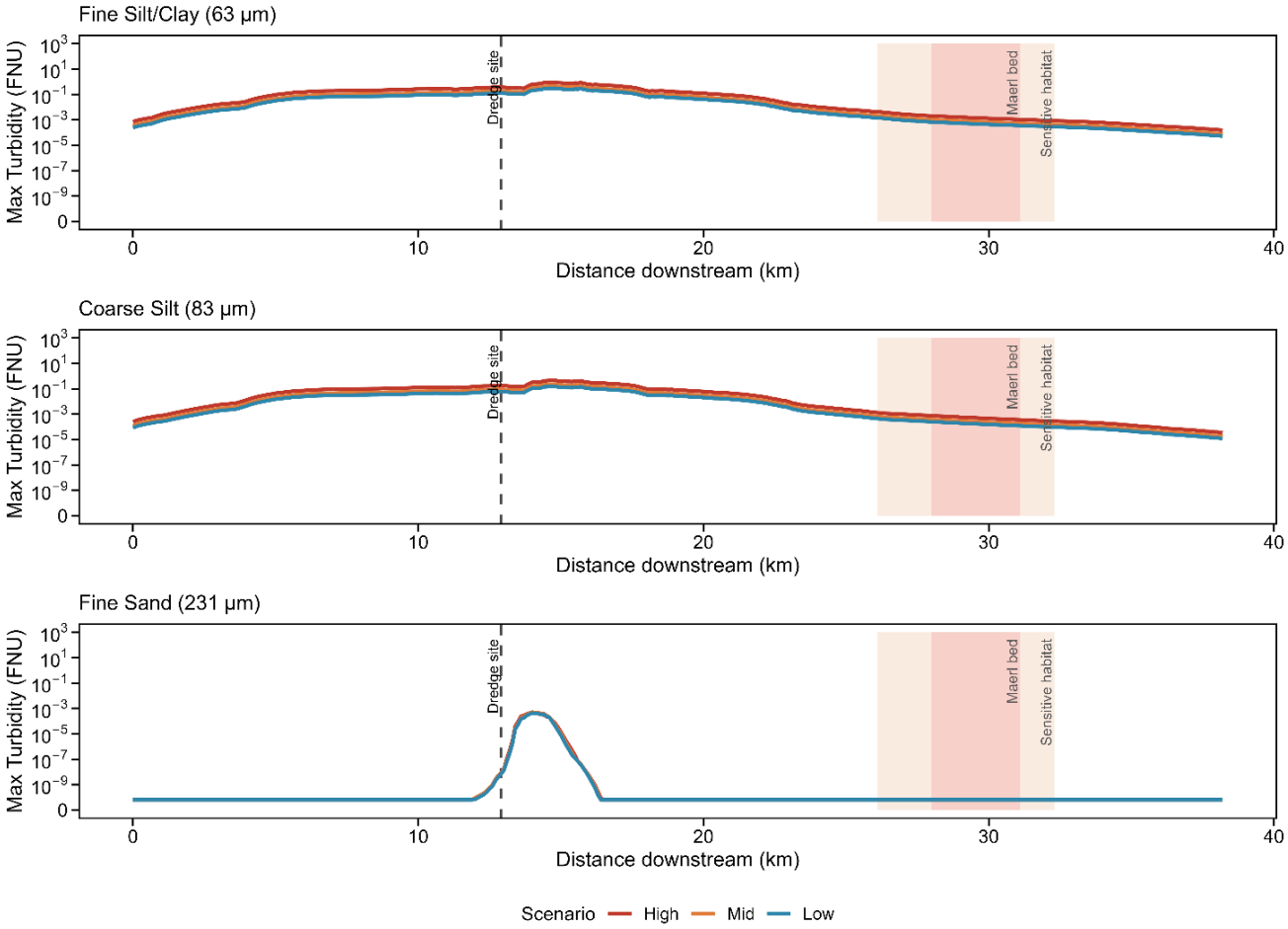


Figure 3.2.11. *Scenario-3: Maximum turbidity (FNU) along the longitudinal estuary transect for fine silt/clay (63 µm, upper panel), coarse silt (83 µm, middle panel) and fine sand (231 µm, lower panel) under low, mid and high dredge discharge concentration scenarios at the Neyland Yacht Haven disposal site (LU190). Note the logarithmic y-axis. The dashed vertical line indicates the disposal site at 12.9 km downstream. Shaded regions denote the spatial extent of the maerl bed (red) and sensitive habitat area (orange).*

3.2.4 Scenario-4: Sediment mobilisation at South Hook jetty

It is known that historical refurbishment of the South Hook jetty mobilised sediment at the jetty location, which was tested in the model (see Section 2.2.3). A total of 150 kg/m^3 was mobilised over 12.5 hours (90kg fine silt, 45kg coarse silt and 15kg sand). From this scenario, the longitudinal transect of simulated maximum turbidity (Fig. 3.2.12) illustrates the substantially elevated near-field suspended sediment signal associated with the resuspension of sediments at the jetty location, which lies within the sensitive habitat area at 28.8 km downstream. Fine silt/clay reached a peak of 0.61 FNU at 28.4 km, with concentrations of 0.59 FNU directly at the jetty and 0.36 FNU at the maerl bed centre (29.6 km), maintaining a mean of 0.38 FNU across the maerl bed extent. Coarse silt reached a peak of 0.31 FNU, with 0.18 FNU at the maerl bed. Both silt fractions showed minimal attenuation with distance, with concentrations remaining above 10% of peak values as far as 35.1-35.2 km downstream, well beyond the sensitive habitat boundary. Fine sand was largely confined to the immediate vicinity of the discharge point, attenuating to below 10% of its peak by 29.5 km.

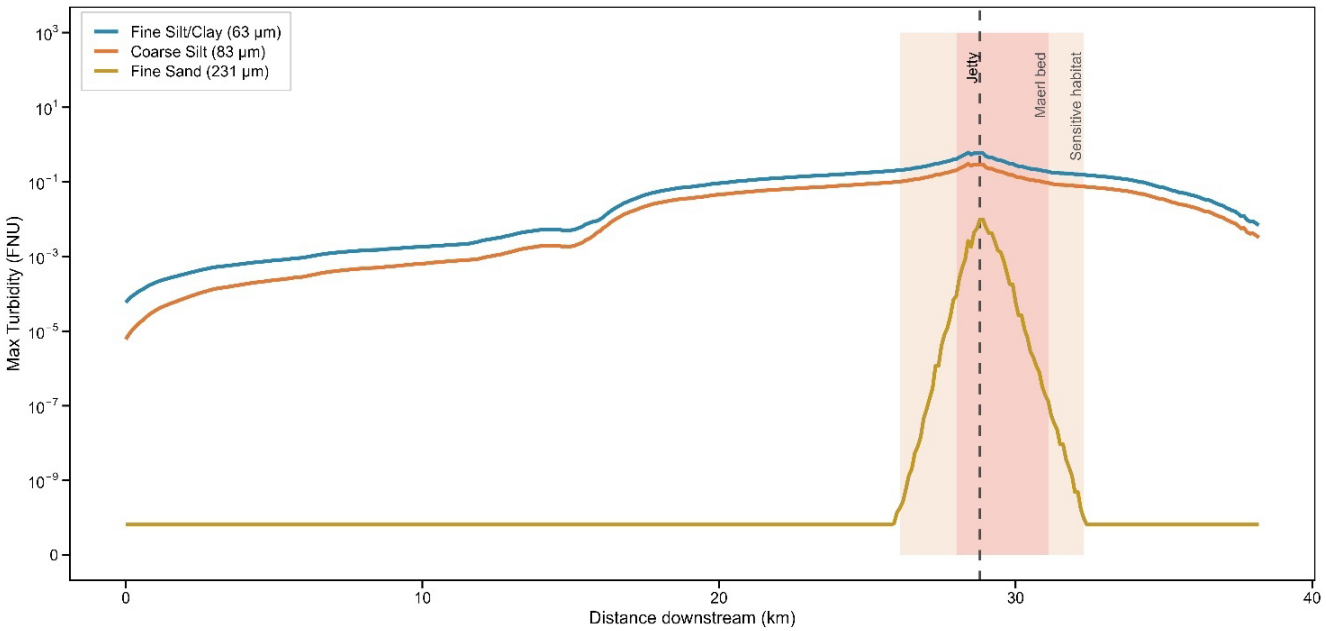


Figure 3.2.12. *Scenario-4: Maximum turbidity (FNU) along the longitudinal estuary transect for all three sediment fractions. Note the logarithmic y-axis. The dashed vertical line indicates the jetty discharge point at 28.8 km downstream, located within the sensitive habitat area.*

Shaded regions denote the spatial extent of the maerl bed (red) and sensitive habitat area (orange).

The spatial evolution of sediment thickness over the six weeks following discharge (Fig. 3.2.13) reveals a progressive expansion of the depositional footprint alongside a gradual decline in peak accumulation. As the sediment disposal effort ceases (Week 0; 06 December 2025 23:30), maximum domain thickness reached 0.49 mm, with 643 model faces exceeding 0.005 mm. By Week 5, the peak had declined to 0.30 mm whilst the spatial extent had increased to 2,136 faces above threshold indicating ongoing redistribution of deposited material by tidal forcing. At the maerl bed, mean thickness declined from 7.12×10^{-3} mm at Week 0 to 1.57×10^{-3} mm by Week 5, whilst the sensitive habitat area showed a similar declining trend from 6.16×10^{-3} to 3.06×10^{-3} mm. Maximum thickness at the maerl bed remained relatively stable throughout (3.11×10^{-2} mm at Week 0 declining to 2.28×10^{-2} mm at Week 5), suggesting persistent localised deposition at specific bed features within the maerl extent throughout the simulation period.

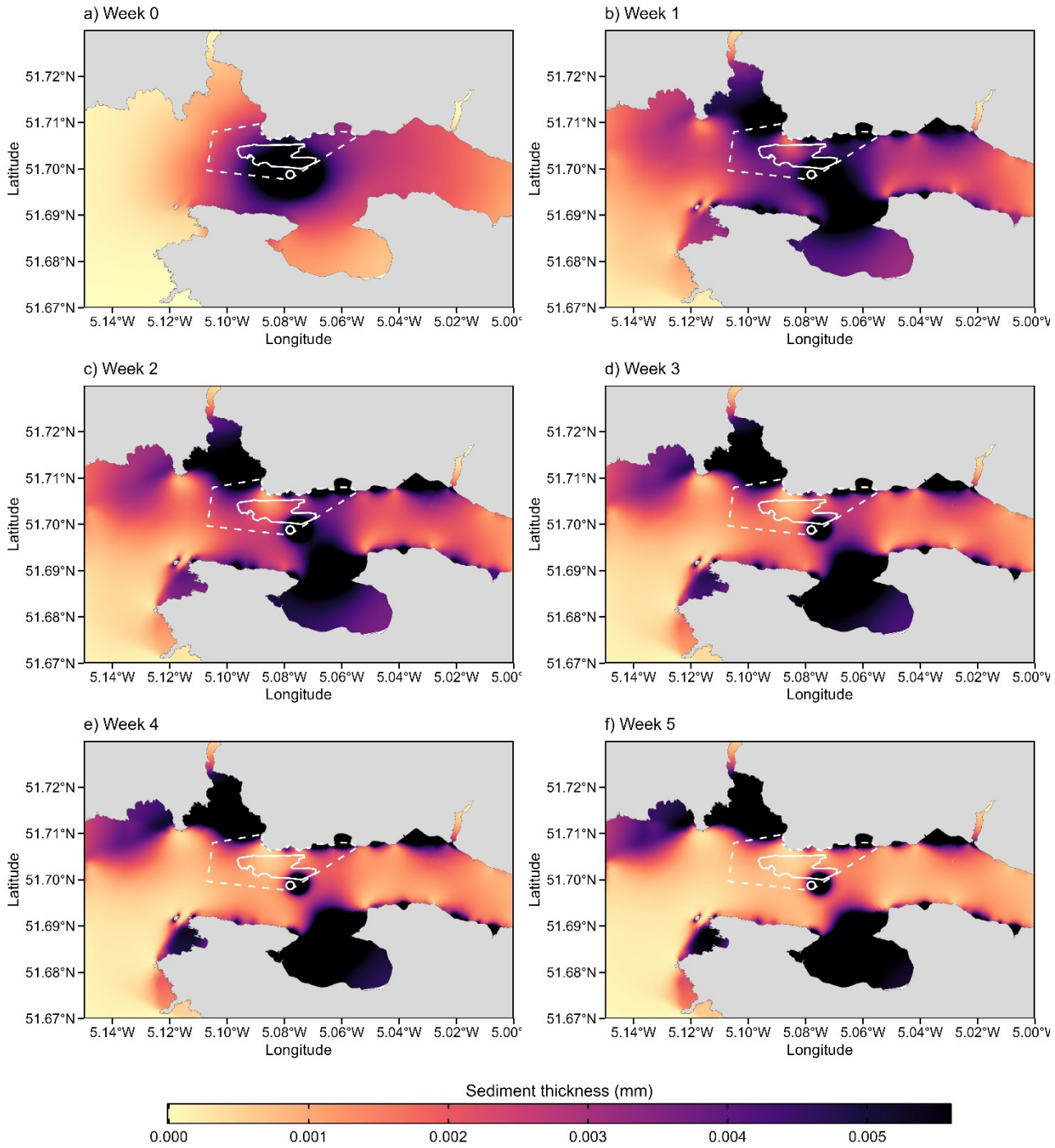


Figure 3.2.13. *Scenario-4: Spatial distribution of total sediment thickness (mm) at weekly intervals following the cessation of jetty sediment mobilisation (Week 0 = 06 December 2025 23:30). The white circle denotes the jetty mobilisation point; the solid white outline indicates the maerl bed extent and the dashed white outline the sensitive habitat area.*

To identify the relative contributions of each sediment fraction to bed accumulation, separate simulations were conducted for fine silt/clay (63 µm), coarse silt (83 µm) and fine sand (231 µm) independently, with spatial evolution figures provided in Appendix A3.1 - A3.3.

Fine silt produced the greatest and most spatially extensive depositional signal. The plume footprint above 0.005 mm expanded from 198 faces at Week 0 to 1,267 by Week 5, with mean maerl bed thickness declining from 4.16×10^{-3} to 2.03×10^{-4} mm as material was redistributed. Coarse silt showed a similar but lower magnitude pattern, with 28 faces above threshold at Week 0 and a maerl bed mean declining from 2.08×10^{-3} to 1.01×10^{-4} mm. In both silt fractions, tidal redistribution progressively transported deposited material towards the channel margins and intertidal banks over the simulation period. Fine sand domain peak thickness was highest of all three fractions (0.43 mm) due to rapid near-field settling, but deposition remained concentrated in the mid-channel area immediately adjacent to the disposal site throughout all six weeks, with the footprint consistently confined to 9-12 faces, negligible tidal redistribution, and maerl bed thickness effectively constant at ~1.2×10^{-4} mm.

3.2.5 Scenario-5: Maerl bed erosion

Under the scenario of bed erosion at the maerl bed, the spatially-averaged time series of resuspension and bed mass change demonstrates sustained erosion and resuspension of the fine silt layer throughout the simulation period (Fig. 3.2.14). Mean suspended silt turbidity reached 28.3 FNU, peaking at 118.2 FNU on 07 November 2025, before declining to 2.55 FNU by the end of the simulation. Bed mass decreased from an initial 662.5 kg/m^2 to a minimum of 3.49 kg/m^2, representing a loss of 99.47% of the initial bed material. The sand fraction exhibited a more limited response, with a spatial median turbidity of 0.11 FNU and a peak of 5.93 FNU (95th percentile 12.2 FNU), alongside a modest net erosion of 2.59%, reducing median bed mass from 662.5 to 645.4 kg/m^2.

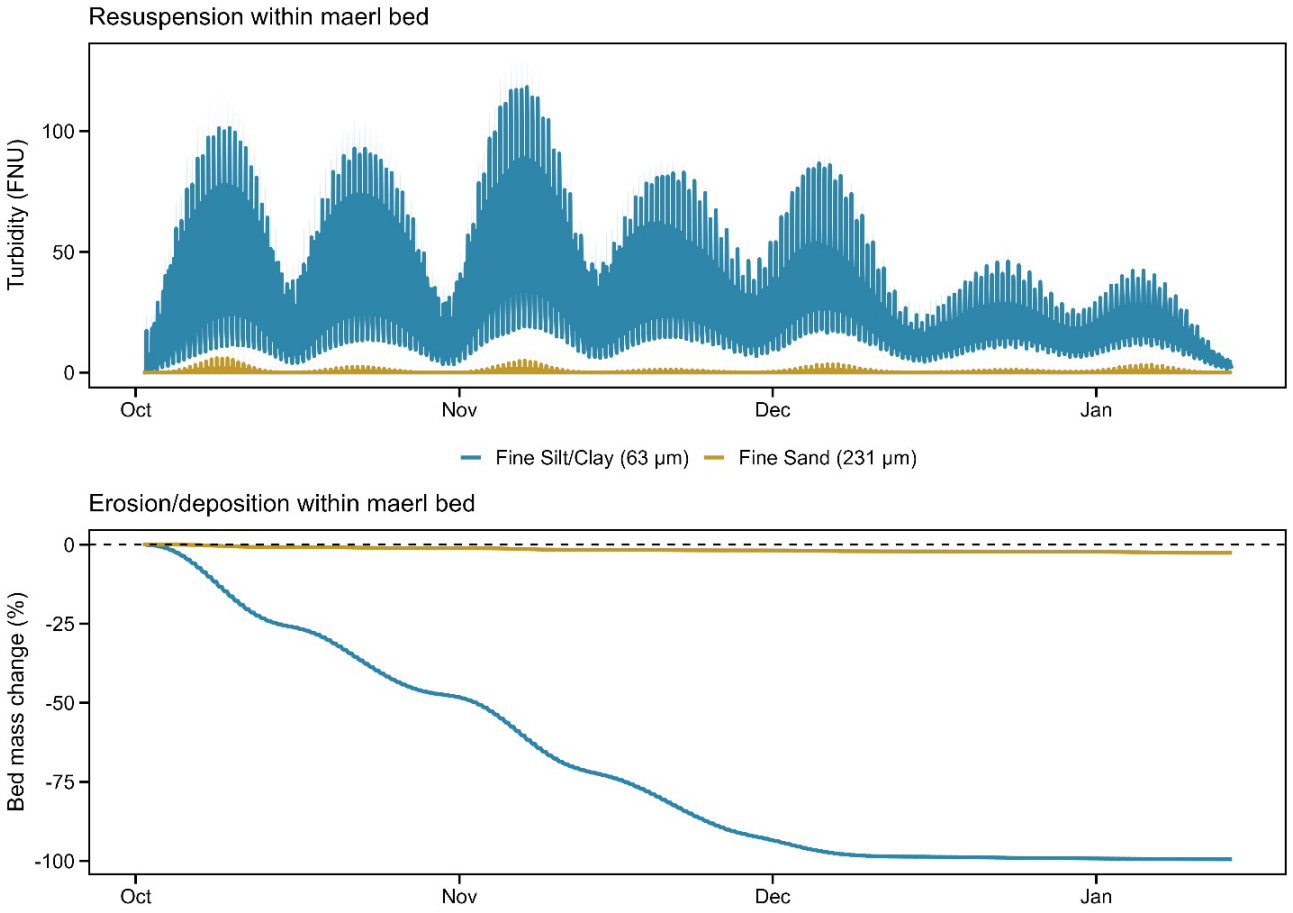


Figure 3.2.14. *Scenario-5: Spatially-averaged turbidity (FNU) within the maerl bed extent (upper panel) and cumulative bed mass change (% of initial mass) for fine silt/clay and fine sand fractions under the maerl bed erosion scenario (lower panel). The dashed horizontal line in the lower panel denotes zero bed mass change.*

The spatial distribution of maximum turbidity (Fig. 3.2.15) reflects these contrasting sediment fraction behaviours. Fine silt/clay (63 µm) produced an extensive turbidity signal, with maximum values reaching 131.7 FNU at the source location and between 1.06 and 101.9 FNU across the maerl bed extent (mean 35.2 FNU). Fine sand (231 µm) produced a considerably weaker signal at the maerl bed, with maximum values of 0.27 FNU (approximately three orders of magnitude lower than the silt fraction) indicating that sand-sized material mobilised at the maerl bed settles rapidly and does not contribute meaningfully to suspended sediment concentrations in the overlying water column.

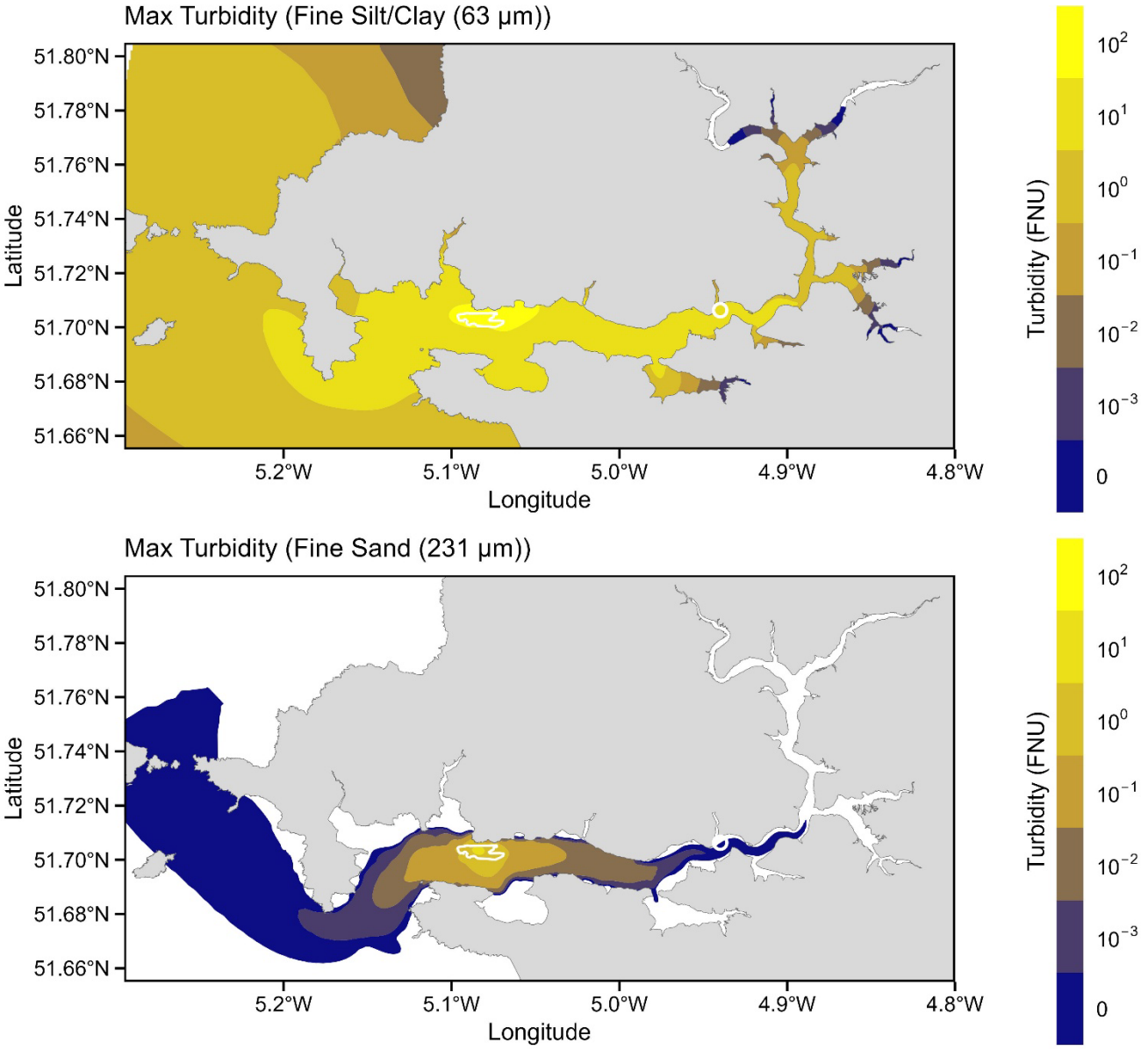


Figure 3.2.15. *Scenario-5: Spatial distribution of maximum turbidity (FNU) for fine silt/clay (63 µm, upper panel) and fine sand (231 µm, lower panel) under the maerl bed erosion scenario. Note the logarithmic colour scale. The white circle denotes the maerl bed erosion source location; the solid white outline indicates the maerl bed extent.*

3.2.6 Scenario-6: Sea-level rise dredging

Under the sea-level rise dredging scenarios, the longitudinal estuary transect of simulated maximum turbidity illustrates how projected sea-level rise modifies the dispersal of dredge-derived sediment from the Neyland Yacht Haven disposal site (Fig. 3.2.16). For the silt fractions, a progressive increase in turbidity at the maerl bed is projected with increasing

sea levels. Fine silt/clay (63 μm) turbidity increased from 1.44×10^{-3} FNU in 2025 to 2.14×10^{-3} in 2050 and 3.62×10^{-3} in 2100, demonstrating a ~2.5-fold increase. Coarse silt (83 μm) demonstrated a similar trend, increasing from 5.13×10^{-4} FNU in 2025 to 1.14×10^{-3} in 2100, representing a 2.2-fold increase. Peak turbidity near the disposal site decreased slightly between scenarios for both silt fractions (fine silt (0.92 FNU 2025, 0.82 FNU 2100), coarse silt (0.42 FNU 2025, 0.41 FNU 2100)), whilst the distance at which turbidity attenuated below 10% of their peak extended from 20.8 km in 2025 to 21.2 km in 2100 for both silt fractions.

The fine sand fraction exhibited a distinctly different response to sea-level rise. Under the 2025 scenario, the sand plume was confined to a narrow zone of 12.9 to 15.9 km downstream, with a peak of 5.18×10^{-4} FNU and a plume centroid of 14.1 km. By 2050 the plume had expanded and migrated upstream, with the signal extending from 11.4 to 16.9 km and peak turbidity increasing by an order of magnitude to 5.91×10^{-3} FNU. Under the 2100 sea-level rise scenario, the upstream migration was more pronounced, with the signal extending from 7.7 to 17.7 km, with peak turbidity values of 1.03×10^{-2} FNU.

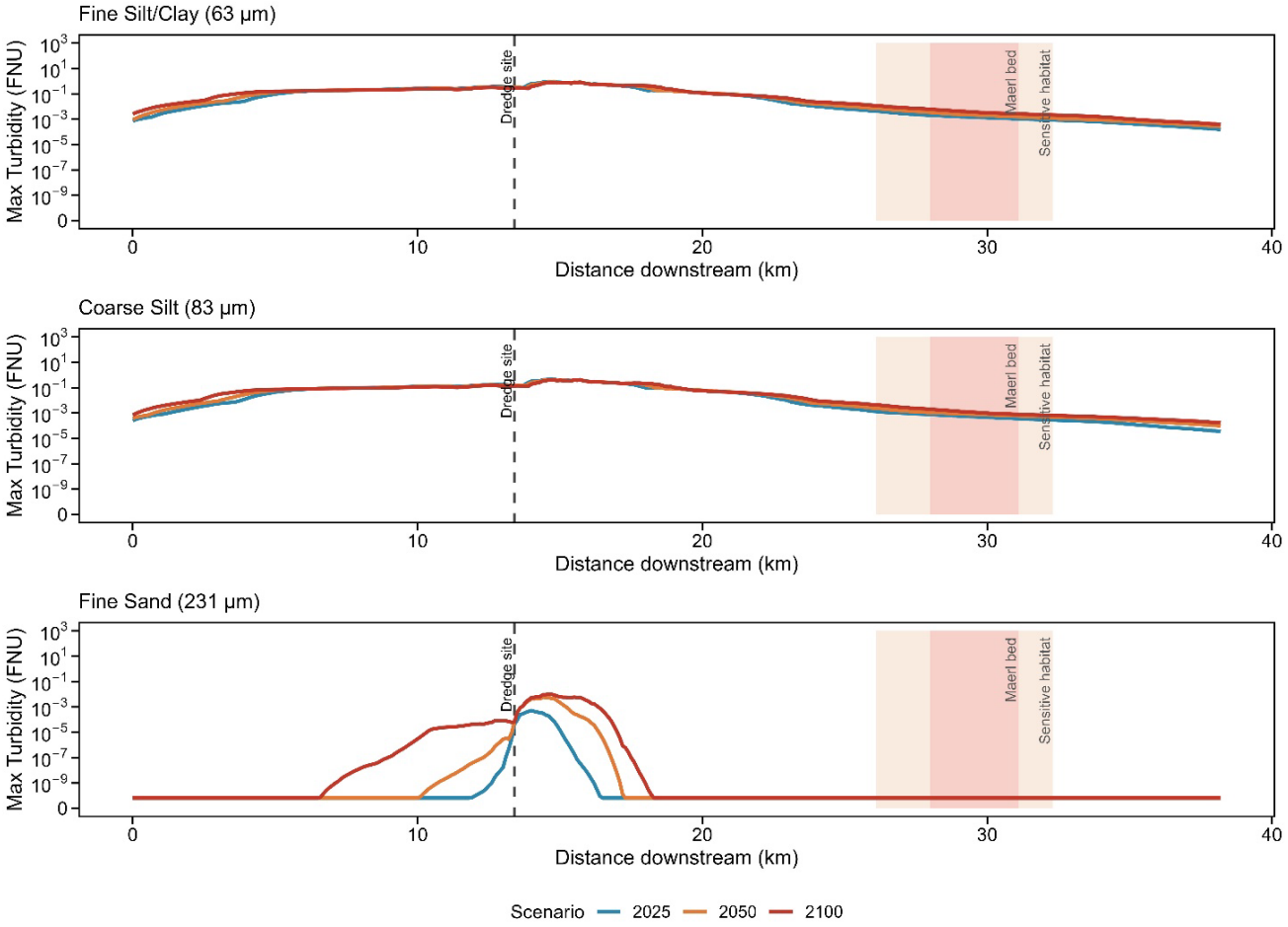


Figure 3.2.16. *Scenario-6: Maximum turbidity (FNU) along the longitudinal estuary transect for fine silt/clay (63 µm, upper panel), coarse silt (83 µm, middle panel) and fine sand (231 µm, lower panel) under 2025 (blue), 2050 (orange) and 2100 (red) UKCP18 RCP8.5 sea-level rise scenarios discharged at the Neyland Yacht Haven disposal site (LU190). Note the logarithmic y-axis. The dashed vertical line indicates the disposal site at 12.9 km downstream. Shaded regions denote the current (2025) spatial extent of the maerl bed (red) and sensitive habitat area (orange).*

The maximum turbidity plume greater than 10^{-4} FNU for fine silt/clay covered approximately 16.23 km^2 under the 2025 baseline, expanding to 18.06 km^2 by 2050 and 19.70 km^2 by 2100 (Fig. 3.2.17). Peak domain turbidity remained comparable across scenarios (29.9, 29.7 and 30.1 FNU for 2025, 2050 and 2100 respectively), indicating that projected sea-level rise extends the spatial footprint of the turbidity plume without substantially altering near-field suspended sediment concentrations. Coarse silt exhibited a comparable response, with estimated plume area increasing from 12.73 km² in 2025 to 16.97 km² by 2100, a 33% increase (Appendix A4.1).

The fine sand fraction demonstrated a substantially stronger sensitivity to projected sea-level rise (Appendix A4.2). Estimated plume area expanded from 0.17 km² under 2025 conditions to 0.37 km² by 2050 and 0.59 km² by 2100, representing a 3.4-fold increase between 2025 and 2100. This response is consistent with the upstream migration of the fine sand plume identified in the transect analysis (Fig. 3.2.16), reflecting the heightened sensitivity of sand-sized particle transport pathways to modifications in tidal prism and residual circulation under elevated mean sea levels.

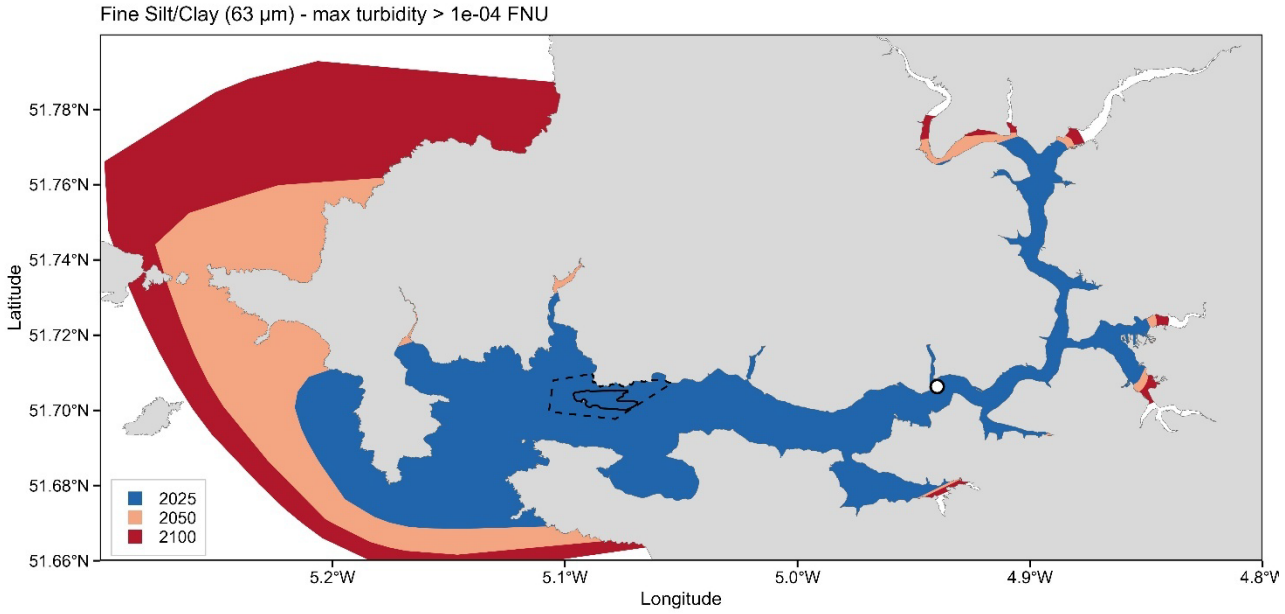


Figure 3.2.17. *Scenario-6: Spatial extent of maximum turbidity exceeding 10^{-4} FNU for fine silt/clay (63 µm) under the 2025, 2050 and 2100 sea-level rise dredging scenarios. The white circle denotes the Neyland Yacht Haven disposal site (LU190); the solid black outline indicates the maerl bed extent and the dashed black outline the sensitive habitat area.*

The spatial extent of maximum sediment thickness under the sea-level rise dredging scenarios expanded progressively with projected increased sea levels (Fig. 3.2.18). Under the 2025 baseline, the depositional footprint above the 0.001 mm threshold covered approximately 6.71 km^2, increasing to 7.68 km^2 by 2050 and 8.43 km^2 by 2100. Despite this spatial expansion, peak domain thickness remained relatively stable across scenarios (3.70, 3.54 and 3.60 mm for 2025, 2050 and 2100 respectively), and mean thickness across affected faces declined slightly from 6.51×10^{-3} to 5.27×10^{-3} mm, consistent with the same

sediment mass being redistributed over a progressively larger area under elevated water levels rather than increasing accumulation at any single location.

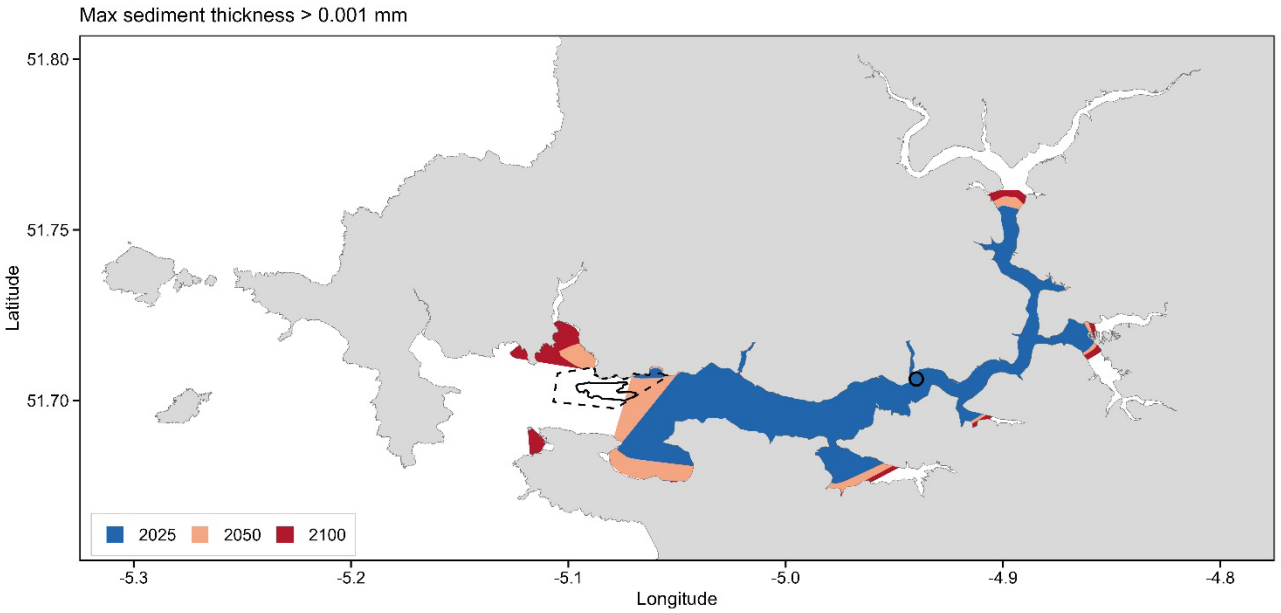


Figure 3.2.18. *Scenario-6: Spatial extent of maximum sediment thickness exceeding 0.001 mm (all fractions) under the 2025, 2050 and 2100 climate change dredging scenarios. The white circle denotes the Neyland Yacht Haven disposal site (LU190); the solid black outline indicates the maerl bed extent and the dashed black outline the sensitive habitat area.*

Hydrodynamic changes

Projected sea-level rise under the UKCP18 RCP8.5 scenario produced statistically significant changes across all hydrodynamic metrics at Milford Haven (Kruskal-Wallis, $p < 2.2 \times 10^{-16}$ for tidal range and ebb discharge; $p = 5.9 \times 10^{-9}$ for flushing time). Estuary volume was calculated assuming a hold-the-line coastal defence strategy, increasing from 504.4×10^6 m^3 in 2025 to 549.1×10^6 m^3 by 2100 (+8.9%), at a broadly consistent rate of ~57×10^6 m^3 per metre of sea-level rise.

At the estuary mouth cross-section, mean tidal range increased from 1.04 m in 2025 to 1.46 m by 2100, with maximum spring tidal ranges increasing from 1.55 to 2.27 m (Fig. 3.2.19a). The tidal prism increased by 34% from 1.98×10^6 to 2.66×10^6 m^3, accompanied by a ~10% increase in cross-sectional area at the mouth (Fig. 3.2.19b). The relationship between tidal prism and cross-sectional area followed the expected O'Brien power law across all scenarios

(r2 = 0.39-0.42), though the weakening exponent (-4.17 in 2025 to -3.04 in 2100) suggests the estuary becomes slightly less efficient at exchanging water per unit area as sea levels rise. Notably, the prism-CSA plot (Fig. 3.2.19b) shows a divided pattern across all scenarios; two distinct clusters reflecting the asymmetric behaviour of flood and ebb tides driven by M4 overtide forcing. This tidal asymmetry (Fig. 3.2.19d), whereby spring ebb-dominated cycles exchange substantially more water per unit cross-section than neap or flood-dominated cycles, persists under all projected sea-level rise scenarios, indicating that the fundamental tidal character of the estuary is preserved under future conditions. Median ebb discharge at the mouth increased from 27.8 to 34.4 $m^3 s^{-1}$ by 2100 (+24%; Fig. 3.2.19c), reflecting the greater tidal volumes driving more water seaward with each ebb cycle.

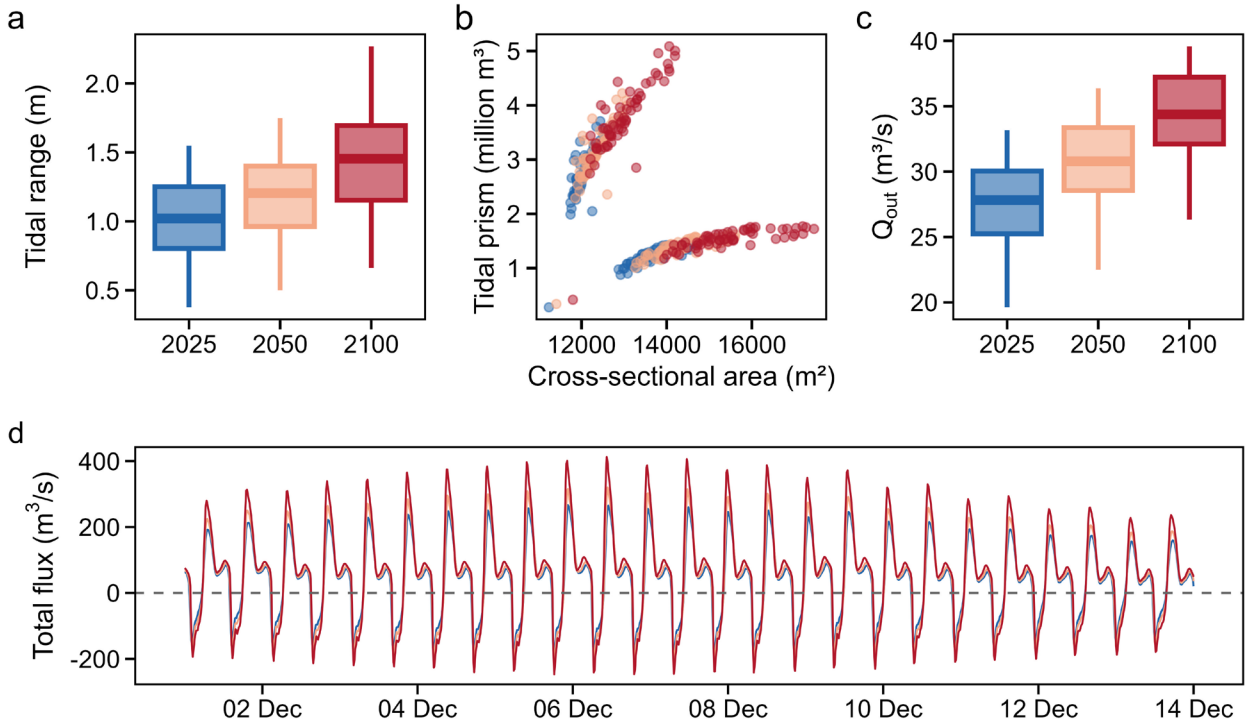


Figure 3.2.19. *Scenario-6: Modelled hydrodynamic response to projected sea-level rise at Milford Haven under the UKCP18 RCP8.5 scenario. (a) Tidal range distribution at the estuary mouth cross-section; (b) relationship between tidal prism and cross-sectional area; (c) ebb discharge distribution; (d) total volumetric flux at the estuary mouth transect during December 2025. Colours denote the 2025 baseline (blue), 2050 mid-century (orange) and 2100 end-century (dark red) scenarios. Boxes show the interquartile range, with median lines and whiskers extending to 1.5x IQR.*

3.2.7 Sensitivity tests: Sediment density

The sensitivity of modelled suspended sediment concentrations to variations in key transport parameters is illustrated for the fine silt/clay fraction in Fig. 3.2.20, with equivalent figures for coarse silt and fine sand fractions provided in Appendix A5.1 and A5.2, respectively. Across all fractions, the pattern of sensitivity was broadly consistent, with the magnitude of response varying according to grain size.

For the fine silt/clay fraction, Run S1 (baseline sediment density configuration based on Lepesqueur et al. 2019) produced the lowest turbidity signal across the domain, with a longitudinal transect maximum turbidity of 0.021 FNU and a median concentration of 8.25×10^{-8} FNU at the maerl bed. Run S2 (corrected (reduced) critical shear stress for deposition) resulted in a 31.5-fold increase in peak maerl bed turbidity (2.76×10^{-6} FNU), with Runs S3 (increased specific density of sediments) increased peak maerl bed turbidity to 4.67×10^{-6} FNU, representing a 53-fold increase relative to Run S1 but similar results to Run S2, suggesting that the differences in sediment density between Runs S2 and S3 did not substantially alter transport behaviour.

The most substantial sensitivity was observed in Runs S5 and S6. Run S5, representing organic-rich or flocculated material with lower specific densities and reduced settling velocities, produced peak maerl bed turbidity of 8.47×10^{-3} FNU. Run S6, representing minimum plausible densities with maximum transport potential, produced similar results (peak maerl bed 6.71×10^{-3} FNU). The near order of magnitude difference between Runs S5/S6 and Run S3 highlights the critical role of settling velocity parameterisation in controlling far-field dispersal of fine suspended sediments. The tidal accumulation pattern visible in Figs. 3.2.20b and c was consistent across all runs, with only the magnitude differing between parameter sets.

Notably, even the maximum suspended sediment transport scenarios (Runs S5/S6) produced maerl bed turbidity values several orders of magnitude below the measured in-situ values recorded by the NRW sondes at the maerl bed, across all sediment fractions and parameter combinations tested. This suggests that the turbidity signal observed at the maerl

bed is not solely attributable to direct sediment inputs from the Eastern and Western Cleddau river catchments, but that other sources of suspended sediments drive local turbidity dynamics, such as tidal resuspension and advection of bed material from elsewhere within the estuary (which could have originated from previous riverine inputs which settled), from other riverine inputs to the Haven (including direct inputs via runoff), and from additional remobilisation activities close to the maerl bed.

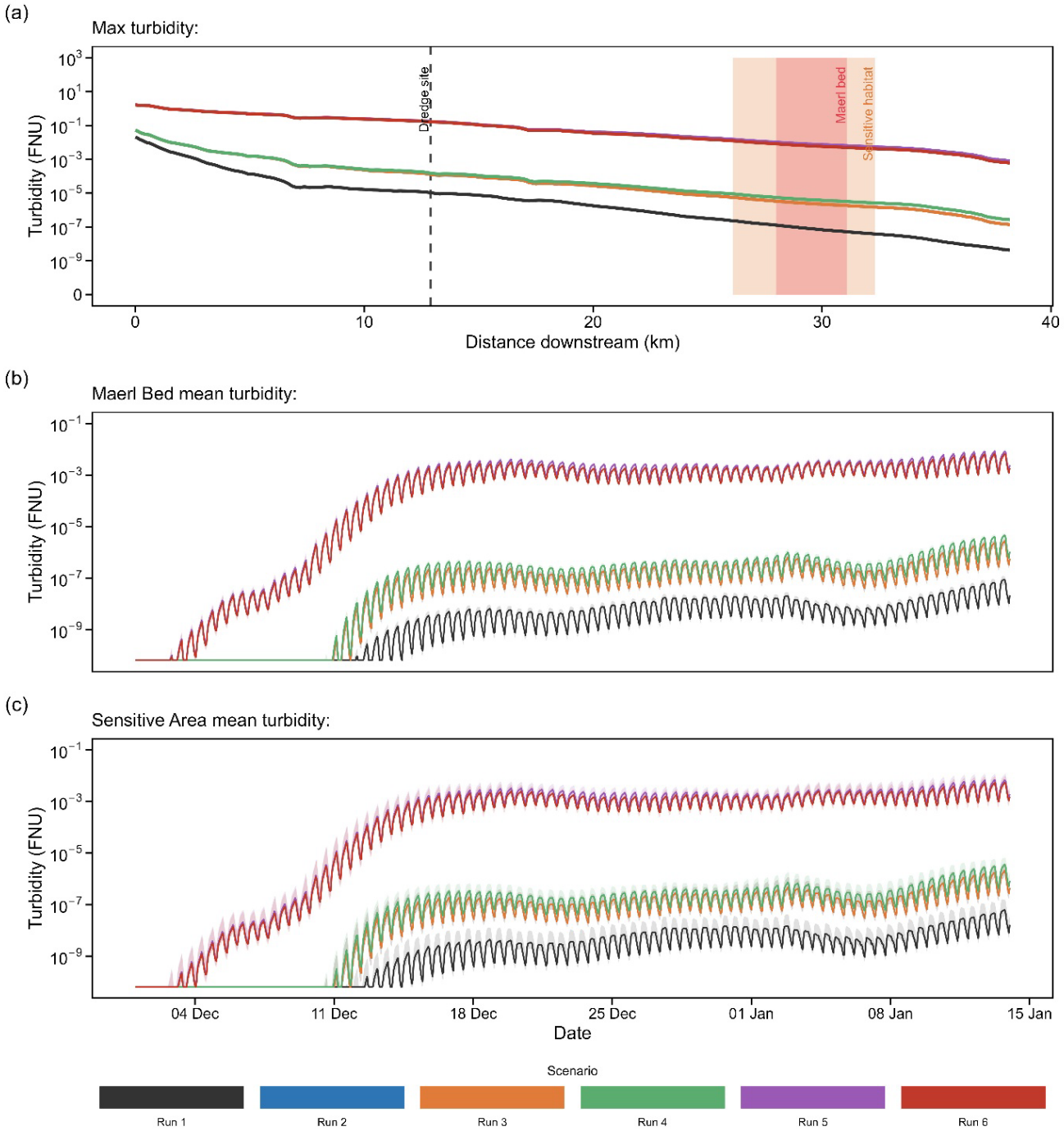


Figure 3.2.20. *Sensitivity of modelled turbidity to sediment transport parameterisation for the fine silt/clay (63 µm) fraction. (a) Maximum turbidity along the Cleddau thalweg transect for all six model runs; (b) median (p50) turbidity at the maerl bed from 1 December 2025 to 14 January 2026; (c) as (b) for the sensitive habitat area. The dashed vertical line in (a) denotes the Neyland Yacht Haven disposal site at 12.9 km downstream; shaded regions indicate the maerl bed (red) and sensitive habitat area (orange). Runs S1-S4 represent progressively refined baseline parameterisations; Runs S5 and S6 represent organic-rich/flocculated and maximum transport scenarios respectively.*

4 Discussion and conclusion

4.1 Summary

Through analyses of observations and model simulation in the Milford Haven, this study has investigated aspects of the turbidity dynamics within the estuary. In this section the main questions (Q1-Q4) of the study have been discussed. We have then discussed the potential management implications of this work, and highlighted areas for improvement and further monitoring and research.

***Q1**) What are the hydrological and riverine turbidity dynamics of the Milford Haven catchment? I.e., How do suspended sediment loads from the Eastern and Western Cleddau rivers vary under different antecedent hydrological conditions?*

Observed turbidity within the Eastern and Western Cleddau rivers (just upstream of the tidal limit) were generally 1–10 FNU during low river flow conditions (i.e., following low rainfall) but increased to 10^4–10^5 FNU during episodic events. Turbidity in the Eastern Cleddau was slightly higher than in the Western Cleddau. Turbidity in the rivers broadly correlated with river flow but tended to plateau during higher discharge values (e.g., above 75th percentile flows), although the relationship was complex and likely also contingent on antecedent rainfall/river flow over the past several days and the availability of erodible sediments within the catchments, i.e., riverine turbidity was higher for 'first flush' river events than after several clustered river events. The specific suspended sediment size fractions and densities of the turbidity measurements were not measured.

The model simulations of the fate of suspended sediments from the Cleddau rivers (reproducing the observed 2023-24 and 2025-26 surveys) predicted that riverine suspended sediments attenuated rapidly with distance downstream, especially sand fractions. Only small proportions of fine silts and clays were simulated to remain in suspension and disperse downstream throughout the estuary.

***Q2**) Focussing on the maerl bed in the lower Milford Haven estuary, how do river flows and associated suspended sediments influence the maerl bed? How do tidal and estuarine hydrodynamics affect riverine suspended sediments? What is the sedimentation and resuspension behaviour of riverine suspended sediments at the maerl bed?*

The observations and the modelling suggest that the tidal regime is a primary driver of turbidity at the maerl bed. Although this study was not able to consider all possible sources of suspended sediment to and within the estuary, nor all biogeochemical processes acting on the suspended sediments, we propose the following likely description of the turbidity dynamics during a typical tidal cycle. Fine sediment fractions (silts and clays), from several sources including river inputs and resuspended estuarine deposits, are mixed by tidal processes and remain in suspension for several days – forming a turbidity plume that is advected back and forth through the estuary with the flooding and ebbing tidal currents. The flooding tide brings the turbidity plume into the estuary from offshore (which was advected there during the previous ebbing tide) and over the maerl bed. Increased bed shear stress locally during the peak flood currents may also resuspend fine sediments. Turbidity at the maerl bed remains high for most of the flood tidal phase before reducing towards high slack water, presumably because the plume has passed through the site and bed shear stress has reduced. The turbidity plume advances upstream to the upper estuary, carrying with it the resuspended sediment from intertidal flats as it advances, and concentrates in the narrowing and shoaling channel where the plume interacts with the opposing river flow (which is typical in UK estuaries, e.g., Jago et al. (2024) but was not investigated further here). The following ebbing tide then transports the turbidity plume seawards and back over the maerl bed (and resuspends settled fine sediments) producing a peak turbidity signal during the late ebb tide. The plume continues offshore and spreads out in the coastal waters, where a proportion of sediments will be mixed with offshore waters. Coarser sediments will also settle during slack water. The cycle then repeats over the next tide.. For sediments that remain in suspension, the estuary residence time (simulated here as ~18 days but will vary by several days depending on tidal state and river flow (Robins and Lyddon 2026)) gives an indication of the time the sediment will remain within the turbidity plume before being exported from the estuary and mixed with offshore waters.

Notably, the fortnightly spring-neap tidal cycle strongly modulated turbidity at the maerl bed, with the stronger spring tidal currents causing higher turbidity (e.g., ~10 FNU) than during neap tides (e.g., ~2 FNU). Additionally, the higher water level during spring tides increases the estuarine subtidal area and so increases the footprint from which sediment resuspension could occur (although this was not investigated in this study).

The analysis of observations revealed a statistically significant relationship between riverine turbidity and turbidity at the maerl bed, which suggests that riverine suspended sediments also contribute to turbidity at the maerl bed. To investigate this further, we applied the model to simulate the observation campaigns but with only riverine suspended sediment inputted to the model. The simulated riverine suspended sediments (silts and clay fractions only) did indeed reach the maerl bed but remained several orders of magnitude below observed turbidity measurements, since the turbidity plume likely comprises suspended sediments from multiple riverine/catchment sources and cumulative riverine events, as well as from resuspension of sediments from throughout the estuary. These sediments can mix and remain in suspension for several days. Additional model scenarios suggested that resuspension and remobilisation of fine sediments from within the estuary contribute to turbidity over the maerl bed. These sediments can remain in suspension and be advected over the maerl bed by tidal currents. Further observations of turbidity and suspended sediment concentrations within the estuary and its tributaries would help improve understanding of the turbidity source apportionment of the system.

The simulated riverine suspended sediments from the Cleddau catchments attenuated rapidly with distance downstream – suspended sediment concentrations reduced substantially between the tidal limits and the maerl bed. Even under simulated high (95^{th} percentile) river flow conditions, the model predicted very low turbidity concentrations at the maerl bed. The sensitivity simulations (Runs S1-S6), varying sediment densities and settling velocities, showed considerable variability in simulated turbidity at the maerl bed (although always lower than observed turbidity values), suggesting that further fieldwork and model parameterisation should consider carefully the riverine suspended sediment classifications.

The maerl bed erosion simulation (Scenario-5) suggests that tidal bed shear stresses at the maerl bed exceeded the critical erosion threshold for fine silt during nearly half of the simulations (and for almost 80% of the flood tidal phase). The fine silt bed layer (prescribed as 0.5 m thick) was almost entirely mobilised within the simulation period, generating peak turbidity of 118 FNU, comparable to observed sonde records. This identifies local tidal resuspension of fine sediment at, or transported to, the maerl bed as the dominant turbidity source. The analysis of the simulated hydrodynamics at the maerl bed further corroborated this, identifying bottom-intensified turbidity and upward sediment diffusion through the water column lagging the tidal cycle.

***Q3**) How does permitted dredging and sediment remobilisation in the Milford Haven affect the suspended sediment dynamics of the estuary, and specifically at the maerl bed?*

The simulations that reproduced licensed maintenance dredging at the Neyland Yacht Haven disposal site (Scenario-3) predicted negligible turbidity at the maerl bed. The 17 km separation between the Neyland site and the maerl bed, combined with the settling characteristics of the sediment fractions, was sufficient to limit the dredge-derived sediment signal reaching the maerl bed. However, the jetty sediment mobilisation scenario (Scenario-4) revealed that this site, being near to the maerl bed, is potentially a critical source of sediment influencing turbidity at the maerl bed – simulating turbidity of nearly 1 FNU over the maerl bed. Fine sands eroded from the jetty settled in the vicinity of the maerl bed. This highlights the importance of maintaining adequate spatial separation between sediment remobilisation activities and sensitive habitats in future licensing decisions.

***Q4**) How might projected 21st century sea-level rise influence the riverine suspended sediment dynamics within the Milford Haven?*

Under projected 21st century sea-level rise (Scenario-6), the estuary tidal prism is expected to increase by ~34% (in response to a +0.78 m sea-level rise), in turn increasing the volume flux through the estuary mouth (from maximum values of ~250 m^3/s presently to ~400 m^3/s by 2100). This change was predicted to increase peak tidal velocities throughout the estuary

and lengthen the tidal excursion. As an example consequence, the spatial footprint of remobilised sediments from the Neyland dredging activity was predicted to expand, with the plume area increasing by 21% for fine silt fractions and by 3.4-fold for fine sands – lengthening the plume by several kilometres both seawards and upstream. However, near-field peak concentrations remained stable, indicating that sea-level rise redistributes rather than intensifies turbidity levels. The increased tidal prism in response to sea-level rise will reduce estuarine sediment flushing/residence times. These findings emphasise the need to consider climate change projections in the long-term management of dredging licences within estuaries containing sensitive benthic habitats.

4.2 Synopsis of likely factors affecting sedimentation at the maerl bed

The observations show that turbidity at the maerl bed can be linked to both tidal effects (spring-neap and semi-diurnal cycles) and fluvial inputs. However, the model suggests that fluvial sediment loads from the two Cleddau rivers (where the sondes and gauging stations were situated) are unlikely to reach the maerl bed before depositing further up-estuary. Therefore, it is believed that the good correlation with the Cleddau data should be considered as a proxy for a good correlation with other fluvial or pluvial sources of sediment within Milford Haven. This means that while land management to reduce fluvial sediment loads could be beneficial, activity should focus on rivers and streams closer to the maerl bed.

Tidal forcing is also likely to play an important role in driving turbidity and sedimentation at the maerl bed. The asymmetric tidal cycle, characterised by a short energetic flood phase and longer, weaker ebb, creates conditions conducive to net landward sediment transport and preferential deposition during slack water. Spring-neap variability further influences this, with elevated bed shear stresses during spring tides capable of resuspending fine sediment locally. The relatively long residence time at the maerl bed (~14 days) provides repeated opportunity for deposition during successive tidal cycles. These tidal dynamics suggest that even modest inputs of fine sediment to the mid estuary, whether from fluvial, resuspension,

or remobilisation sources, may be concentrated at the maerl bed through tidally driven residual transport, irrespective of the source location.

The project used the Neyland marina trickle dredge site as an example to understand the fate of dredged sediments from a permitted activity. This modelling shows that sediment from this activity would not reach the maerl bed in significant quantities and so is unlikely to be a cause of the decline in the maerl bed. The projected sea-level rise scenarios showed that, in the future, the deposited sediment could be advected further downstream and so may have a greater influence.

A postulated cause of decline at the maerl bed is sediment disturbance related to historical jetty refurbishment. Use of jack-up barges and vessel movement is known to have mobilised significant quantities of sediment. Poate et al. (2026) calculated combined wave-current bed shear stress from measurements and identified that there would be limited mobility for the local sediment (sands). Therefore, the model was used to assess whether it was likely that sediment mobilised at the jetty would deposit on the maerl bed and how long it would take to be re-mobilised. The model showed deposition over and in the vicinity of the maerl bed was likely.

4.3 Comparative studies

An ephemeral estuarine turbidity maximum (ETM) has been observed in the macrotidal Taf estuary in South Wales (Jago et al. 2006). The ETM forms due to resuspension and advection of estuarine material by tidal currents. The flood tide advances across intertidal sand flats, progressively entraining material to create a turbid front that constitutes the ETM as it reached the tidal limit. Deposition occurs at high slack water but the ETM retains high suspended sediment concentrations. The ETM retreats down the estuary during the ebb; some material is deposited thinly across emergent intertidal flats and some is flushed out of the estuary. A new ETM is generated by the next flood tide. The ETM intensified during spring tides coinciding with low river discharge but was poorly developed during neap tides

and did not form during high river discharge. High chlorophyll concentrations in the ETM suggest that flocs probably originate from biological production within the estuary.

Lunt and Smee (2020) analysed an 18-year fisheries dataset from four estuaries (Gulf of Mexico) and compared biological communities under low turbidity (<30 FNU) and high turbidity (>30 FNU) conditions. They found that elevated turbidity significantly reduced fish species richness and Shannon diversity, while increasing the abundance of benthic organisms such as crabs and shrimp. High turbidity over oyster reefs supported significantly fewer juvenile oysters and porcelain crabs. Community composition differed significantly between low- and high-turbidity reefs, indicating that turbidity altered estuarine food-web structure and predator–prey interactions. The study suggested that increased turbidity can shift estuarine ecosystems away from visually oriented fish communities toward benthic, chemosensory-dominated communities, with implications for biodiversity, habitat functioning, and ecosystem stability.

4.4 Management implications

The findings from the project will help NRW and other stakeholders to ensure that activities, advice and management of the Milford Haven are supported by robust evidence of the natural physical behaviour of the estuary. By providing a foundation to understanding suspended sediment dynamics in the estuary, NRW will be in a better position to bring the estuary into a favourable condition in terms of the habitats and ecosystems it sustains. This is in line with the Sustainable Management of Natural Resources (SMNR) ethos that underpins NRW's activities. Specifically, the analyses of observations and findings from the hydrodynamic/ sediment transport modelling will be used for:

Casework: To provide sound evidence for advising on the impacts of activities such as dredging and installation of marine renewables. The project has considered the influence of the suspended sediments from the Cleddau rivers as well as modelled the sediment movements from two types of activities, Neyland trickle dredging and South Hook jetty sediment release. Future development and casework advice will be in a better place to tease

out the influence of background river sedimentation against impacts of a proposed activity. Using the modelled examples, there will also be better information available on the fate of different types of sediment released at different locations in the Haven, which can act as a proxy to wider dredging activities.

Restoration projects: NRW, other eNGOs, and community groups have a better understanding of the conditions in the Haven to promote restoration projects such as native oyster regeneration and seagrass planting. The project has demonstrated the likely fate of sediments originating from the Cleddau Rivers and where in the Milford Haven they are likely to be deposited. This can help to support the location search of a restoration project, particularly if the target species is sensitive to sedimentation.

Management: There is more knowledge on how sensitive species and habitats such as maerl and herring spawning grounds are being impacted and how they will be impacted in the future. This is particularly important for climate change related extreme events such as increased storm rainfall which will likely increase turbidity in the Haven. Simulations of the combinations of events that cause high turbidity in different regions allow NRW to better prepare for future impacts and help to make informed decisions to bring the designated species and habitats into favourable condition. The project has indicated that the Cleddau Rivers are not a significant contributor to sedimentation in the Haven and that suspended sediments from these main rivers are deposited in the upper reaches of the estuary. Although further work is needed to understand, e.g.: (1) the subsequent long-term bedload transport and resuspension and fate of deposited riverine sediments; and (2) the impact of suspended sediment loads from smaller rivers inputting into the Haven. The modelled outputs demonstrate that it is possible that other factors other than sedimentation are impacting the SAC species and habitats.

Monitoring and reporting: NRW's duties around monitoring and reporting on the status of marine species and habitats will be strengthened with by this project. The modelling can be used to target monitoring of specific locations to ground truth and understand how predicted sediment impacts are affecting the marine environment.

Policy: There is currently a UK Government policy gap in how to effectively manage the ~162 UK estuaries into the future. This project, building on several UK estuary climate impact studies by the investigators at Bangor, will contribute towards the scientific evidence needed to future proof UK estuaries over the coming century.

All data, models, and learned outcomes form the project will be shared publicly so that other coastal researchers and regulators can benefit from the work.

4.5 Limitations and future recommendations

This work has identified several data gaps and knowledge gaps that we discuss here. The study's findings also identify several priorities for future monitoring and modelling work that would strengthen the evidence base for managing turbidity and dredging impacts within Milford Haven and guide transferable projects in other estuarine regions.

Several limitations should be considered when interpreting the 2023–2024 and 2025–2026 datasets:

The two monitoring campaigns differed substantially in duration: the 2023–2024 deployment spanned approximately eight months and captured multiple extreme discharge events, whereas the 2025–2026 deployment lasted only six weeks and included only two complete spring–neap cycles. Consequently, the shorter deployment may not fully represent the range of estuarine hydrodynamic and sediment transport conditions.

Turbidity was measured using different sensor configurations and units (FNU in 2023–2024 and mV in 2025–2026). Although percentile-based conversions enabled approximate comparison between datasets, the calibration remains a first-order approximation, particularly at high turbidity values where the relationship becomes nonlinear.

The precise elevation of the 2023–2024 turbidity sensor above the seabed is unknown. Near-bed suspended sediment concentrations can vary substantially over vertical distances

of only a few centimetres, as shown with the 2025-2026 campaign. Differences in sensor height may therefore have contributed to some of the observed differences between deployments.

Turbidity was used as a proxy for suspended sediment concentration, although the relationship between turbidity and sediment concentration depends on particle size, composition, and flocculation processes.

After the de-tiding procedure used to isolate river-driven turbidity variability, the spring-neap cycle still remained within the de-tided signal.

Several periods of the observational record were affected by sensor malfunction and deployment issues, introducing additional uncertainty despite quality-control and reconstruction procedures.

Correlation and cross-correlation analyses also identify statistical relationships rather than direct causal mechanisms, and the observed lagged responses likely reflect a combination of advection, sediment storage, deposition, and tidal resuspension processes that cannot be fully resolved using the present observational dataset alone.

The model simulations covering the observational campaigns were parameterised with a non-erodible bed. This was primarily a pragmatic choice due to the difficulty in separating sediment sources if an erodible bed was included. In reality, the estuarine bed comprises a heterogeneous mixture of sand, mud, and organic material that will differ substantially in its erodibility, settling velocity, and cohesive behaviour from the parameterisations applied here.

The modelled sensitivity analysis demonstrates that bed composition assumptions exert a very strong control on turbidity, with maerl bed turbidity concentrations varying by nearly five orders of magnitude across the parameter space tested. Therefore, the absolute magnitude of modelled turbidity should be treated with caution, though the relative comparisons between scenarios remain valid. Further sampling is recommended to substantiate sediment density classifications for the range of sediment types.

A notable data gap identified is the composition and thickness of erodible bed and composition of suspended sediment concentrations present at the river sampling locations, at the maerl bed, and elsewhere within the estuary. This data gap prevents accurate model parameterisation, calibration, and validation considering all sediment sources. Future work should prioritise spatially distributed sediment sampling across the estuary, with particular focus on the maerl bed and sensitive habitat extents, to characterise grain size distribution, organic content, bulk density, and critical erosion thresholds. These data would directly reduce uncertainty in bed/SSC parameterisation and enable a more physically defensible representation of local resuspension dynamics. Particle size distribution measurements of suspended sediment using laser diffraction or acoustic backscatter alongside optical turbidity sensors (Matos et al., 2024), would substantially improve the FNU-SSC conversion and the apportionment of turbidity between grain size fractions.

The aggregation behaviour of cohesive sediments is also a key knowledge and data gap. The Partheniades-Krone framework used here applies erosion/deposition thresholds but does not directly model cohesion dynamics. Run S5/S6 of the sensitivity testing to some extent proxy this via reduced settling velocities. Further monitoring and research should aim to better understand these complex processes, which could improve the parameterisation of cohesive sediment dynamic within sediment transport models.

Whilst the Cleddau rivers are the dominant riverine sediment sources to the Haven, there are likely additional contributions to estuarine turbidity from other rivers, direct runoff, and from the estuary seabed. Episodic sediment delivery from these other riverine/runoff sources during storm events may contribute meaningfully to turbidity at the maerl bed, particularly from within the outer- and mid-estuary. The degree to which this contributes to observed turbidity at the maerl bed is currently unknown. However, the Cleddau river sondes could be considered as a proxy for other fluvial inputs to Milford Haven. Further modelling in the Haven should include minor tributary inputs along the estuary margins (i.e., Rivers Pembroke, Cresswell, and Castlemartin Corse), particularly those draining agricultural catchments (e.g., into Sandy Haven Bay) where episodic fine sediment delivery during storm events may be significant. Coupling the hydrodynamic model to a catchment-scale sediment

delivery model would enable dynamic representation of fluvial sediment supply under varying discharge conditions (Huang et al. 2022) and would be particularly valuable for assessing the combined effects of multiple simultaneous high-discharge events.

The December 2025 – January 2026 measurements (Poate et al. 2026), indicated that waves play a role in turbidity at the Maerl bed. Therefore, inclusion of waves in the simulation would provide additional realism which is likely to be important, especially if an erodible bed with variable sediment was included.

The observed turbidity data used for model forcing and validation were collected as FNU units using optical backscatter sensors, without concurrent grain size or particle size distribution measurements. The conversion from FNU to suspended sediment concentration necessarily assumes a fixed particle size and density relationship, whereas in practice the optical response of natural suspended sediment varies with grain size, shape, organic content, and flocculation state. The absence of disaggregated grain size data for the suspended load means that the apportionment of turbidity between sediment fractions within the model is an approximation, and the FNU-SSC calibration may not hold consistently across the range of hydrodynamic and biological conditions present throughout the simulation period.

Extending the simulation framework to cover multiple years incorporating inter-annual variability in river discharge, tidal conditions, and storm frequency would improve understanding of the cumulative sediment budget at the maerl bed and the long-term trajectory of bed composition change. This is particularly relevant given the potential for progressive fine sediment accumulation at the maerl bed under repeated high-discharge winters, which the current single-season simulations cannot resolve.

The sea-level rise scenarios adopted a hold-the-line coastal defence assumption, whereby estuary geometry, bathymetry, and intertidal extent were held constant at present-day locations under all future scenarios. In reality, managed realignment, defence failure, saltmarsh migration, and intertidal morphological adjustment are all likely in response to sea-level rise. These changes would alter estuarine volume, tidal prism, tidal velocities, bed

shear stress, turbulence, residence times, and sediment transport pathways in ways that are not captured by the current approach. Further morphodynamic modelling should consider the long-term redistribution of bed sediment, infilling of channels, or accretion of intertidal areas that would occur over decadal timescales and alter the bathymetry. This would require either long-term continuous simulation (Hoagland et al. 2023) or a schematised tidal forcing approach (Elmilady et al. 2022) and would provide a more realistic representation of the future estuarine state against which dredging impacts should be assessed.

Further climate impact modelling should also consider projected changing hydrology, riverine sediment loads, morphology, and sea level variability (Lyddon et al. 2025), as well as projected changes in other water quality indicators, e.g., temperature, salinity, and nutrient and pollution inputs (Robins and Lyddon 2026).

Alternative coastal adaptation strategies including managed realignment and regulated tidal exchange should be explored alongside the hold-the-line assumption, as these may produce substantially different hydrodynamic and sediment transport outcomes for the sensitive habitat (e.g., Barada et al. 2026a). However, such adaptations are less likely to make a significant difference to results of this case study because Milford Haven is a ria-type estuary with limited accommodation space for realignment due to the topography and geology.

References

Barada, M., Skov, M., Lewis, M. and Robins, P., 2026a. Combining moored observations and SAR images in validating compound flood models. *Geomatics, Natural Hazards and Risk*, *17*(1), p.2608912.

Barada M., Lyddon C., Clough T., et al., Robins P. 2026b. Integrated high-resolution nationwide bathymetry of English estuaries. *Earth System Data Science* (*in review*).

Biguino, B., Haigh, I.D., Dias, J.M. and Brito, A.C., 2023. Climate change in estuarine systems: Patterns and gaps using a meta-analysis approach. *Science of the Total Environment*, *858*, p.159742.

BODC (2025). Search the data. Available at: https://www.bodc.ac.uk/data/hosted_data_systems/sea_level/uk_tide_gauge_network/processed/ [Accessed 15 September 2025].

Bohn, K. 2014. The distribution and potential northwards spread of the invasive slipper limpet Crepidula fornicata in Wales, UK. NRW Evidence Report No: 40, 43pp, Natural Resources Wales, Bangor.

Bunker, F. StP. D, Ratcliffe, F.C., *in press*. Maerl Bed monitoring in Milford Haven, Wales using diving between 2005 and 2023. (NRW Evidence Report No 882). A report to Natural Resources Wales by Aquatic Survey and Monitoring Ltd.

Clermont, M., Kinnard, C., Dubé-Richard, D., Campeau, S., Bordeleau, P.A., de Grandpre, A., Ziyad, J. and Roy, A., 2023. Using remote sensing to assess how intensive agriculture impacts the turbidity of a fluvial lake floodplain. *Journal of Great Lakes Research*, *49*(6), p.102240.

CMEMS (2026). Atlantic-European North West Shelf Ocean Physics Reanalysis. Copernicus Marine Environment Monitoring Service. Available at: https://data.marine.copernicus.eu/product/NWSHELF_MULTIYEAR_PHY_004_009/description [Accessed 08 January 2026].

Deltares (2025). *Delft3D FM Suite 2D3D*. Available at: https://www.deltares.nl/en/software-and-data/products/delft3d-flexible-mesh-suite [Accessed 02/09/2025].

Elmilady, H.M.S.M.A., Van Der Wegen, M., Roelvink, D. and Van Der Spek, A., 2022. Modelling the morphodynamic response of estuarine intertidal shoals to sea-level rise. *Journal of Geophysical Research: Earth Surface*, *127*(1), p.e2021JF006152.

EMODnet Bathymetry Consortium (2022). EMODnet Digital Bathymetry (DTM 2022). Distribution through windPRO and EMD. This dataset is released following the Creative Commons Attribution 4.0 International license.

Friedrichs, C.T. and Aubrey, D.G., 1988. Non-linear tidal distortion in shallow well-mixed estuaries: a synthesis. *Estuarine, Coastal and Shelf Science*, 27(5), pp.521-545.

Gameiro, C., Zwolinski, J. and Brotas, V., 2011. Light control on phytoplankton production in a shallow and turbid estuarine system. *Hydrobiologia*, *669*(1), pp.249-263.

Hoagland, S.W., Jeffries, C.R., Irish, J.L., Weiss, R., Mandli, K., Vitousek, S., Johnson, C.M. and Cialone, M.A., 2023. Advances in morphodynamic modelling of coastal barriers: A review. *Journal of Waterway, Port, Coastal, and Ocean Engineering*, *149*(5), p.03123001.

Holt, J., Katavouta, A., Hopkins, J., Amoudry, L.O., Appendini, C.M., Arneborg, L., Arnold, A., Artioli, Y., Aucan, J., Berx, B. and Cagigal, L., 2025. Future climate projections in the global coastal ocean. Progress in Oceanography, 235, p.103497.

Huang, R., Ni, Y. and Cao, Z., 2022. Coupled modelling of rainfall-induced floods and sediment transport at the catchment scale. *International Journal of Sediment Research*, *37*(6), pp.715-728.

Jackson-Bué, M., Wynter, E., Cuthbertson, S. and Hatton-Ellis., M. 2025. Condition Assessments for the Designated Features of Ardal Cadwraeth Arbennig Sir Benfro Forol / Pembrokeshire Marine Special Area of Conservation. NRW Evidence Report No. 909, 359pp, Natural Resources Wales, Cardiff.

Jago, C.F., Ishak, A.K., Jones, S.E. and Goff, M.R.G., 2006. An ephemeral turbidity maximum generated by resuspension of organic-rich matter in a macrotidal estuary, SW Wales. *Estuaries and Coasts*, *29*(2), pp.197-208.

Jago, C., Robins, P., Howlett, E., Hassard, F., Rajko-Nenow, P., Jackson, S., Chien, N. and Malham, S., 2024. Trapping and bypassing of suspended particulate matter, particulate nutrients and faecal indicator organisms in the river-estuary transition zone of a shallow macrotidal estuary. *Science of the Total Environment*, *917*, p.170343.

Lepesqueur, J., Hostache, R., Martínez-Carreras, N., Montargès-Pelletier, E. and Hissler, C., 2019. Sediment transport modelling in riverine environments: on the importance of grain-size distribution, sediment density, and suspended sediment concentrations at the upstream boundary. *Hydrology and Earth System Sciences*, *23*(9), pp.3901-3915.

Lowe, M.L., Morrison, M.A. and Taylor, R.B., 2015. Harmful effects of sediment-induced turbidity on juvenile fish in estuaries. *Marine Ecology Progress Series*, *539*, pp.241-254.

Lunt, J. and Smee, D.L., 2020. Turbidity alters estuarine biodiversity and species composition. *ICES Journal of Marine Science*, *77*(1), pp.379-387.

Lyddon, C., Robins, P., Lewis, M., Barkwith, A., Vasilopoulos, G., Haigh, I. and Coulthard, T., 2023. Historic spatial patterns of storm-driven compound events in UK estuaries. *Estuaries and Coasts*, *46*(1), pp.30-56.

Lyddon, C., Devitt, L., Barada, M., Coxon, G., Tinker, J., Coulthard, T., Barkwith, A. and Robins, P., 2025. Climate change likely to intensify storm-driven compound flooding in an exemplar UK estuary. *Earth's Future*, *13*(12), p.e2024EF005822.

Malham, S.K., Rajko-Nenow, P., Howlett, E., Tuson, K.E., Perkins, T.L., Pallett, D.W., Wang, H., Jago, C.F., Jones, D.L. and McDonald, J.E., 2014. The interaction of human microbial pathogens, particulate material and nutrients in estuarine environments and their impacts on recreational and shellfish waters. *Environmental Science: Processes & Impacts*, *16*(9), pp.2145-2155.

Matos, T., Martins, M.S., Henriques, R. and Goncalves, L.M., 2024. A review of methods and instruments to monitor turbidity and suspended sediment concentration. *Journal of Water Process Engineering*, *64*, p.105624.

Met Office (2018). *UKCP18 sea level anomalies for marine projections around UK coastline (2007–2100)* [dataset]. Available at: https://ukclimateprojections-ui.metoffice.gov.uk/products/MS4_Anomalies_Subset_01 [Accessed 07/07/2025].

Neill, S.P., Fairley, I.A., Rowlands, S., Young, S., Hill, T., Unsworth, C.A., King, N., Roberts, M.J., Austin, M.J., Hughes, P. and Masters, I., 2023. Characterizing the marine energy test area (meta) in Wales, UK. *Renewable Energy*, *205*, pp.447-460.

Natural Resources Wales (2025) *LIDAR terrain and surfaces models Wales* [Dataset]. data.gov.uk. Last updated 14 October 2025. https://www.data.gov.uk/dataset/afbb6701-533e-40cd-a35f-5319664fd91c/lidar-terrain-and-surfaces-models-wales2

NRFA (2025a) *61005 - Western Cleddau at Treffgarne.* Available at: https://nrfa.ceh.ac.uk/data/station/info/61005 [Accessed 18/11/2025].

NRFA (2025b) *61001 - Eastern Cleddau at Canaston Bridge.* Available at: https://nrfa.ceh.ac.uk/data/station/info/61002 [Accessed 18/11/2025].

NTSLF (2025) *Tides.* Available at: https://ntslf.org/tides [Accessed 18/11/2025].

Partheniades, E., 1965. Erosion and deposition of cohesive soils. *Journal of the Hydraulics Division*, *91*(1), pp.105-139.

Poate, T., Masselink, G., Fairley, I. 2026. Measurements of near-bed current, suspended sediment concentration and waves at the Milford Haven Maerl bed. NRW evidence report 962, in prep

Ratcliffe, F.C., 2026 (*in press*). Investigation into the decline of the Maerl bed in the Pembrokeshire Marine (PM) Special Area of Conservation. NRW Evidence Report Report No: 976, 94pp, Natural Resources Wales, Cardiff.

Robins, P.E., Skov, M.W., Lewis, M.J., Giménez, L., Davies, A.G., Malham, S.K., Neill, S.P., McDonald, J.E., Whitton, T.A., Jackson, S.E. and Jago, C.F., 2016. Impact of climate change on UK estuaries: A review of past trends and potential projections. *Estuarine, Coastal and Shelf Science*, *169*, pp.119-135.

Robins, P. and Lyddon, C., 2026. INVEST: Investigating the vulnerability of estuarine water quality to climate change.

Schmidt, S., Diallo, I.I., Derriennic, H., Fallou, H. and Lepage, M., 2019. Exploring the susceptibility of turbid estuaries to hypoxia as a prerequisite to designing a pertinent monitoring strategy of dissolved oxygen. *Frontiers in Marine Science*, *6*, p.352.

Thomson, R.E. and Emery, W.J., 2024. *Data analysis methods in physical oceanography*. Elsevier.

United Kingdom Hydrographic Office (UKHO), (2024). Combined bathymetry at 10 m for estuary's in England. (Personal communication) © British Crown Copyright 2024. All rights reserved.

Van Rijn, L.C., 1993. *Principles of sediment transport in rivers, estuaries and coastal seas*.

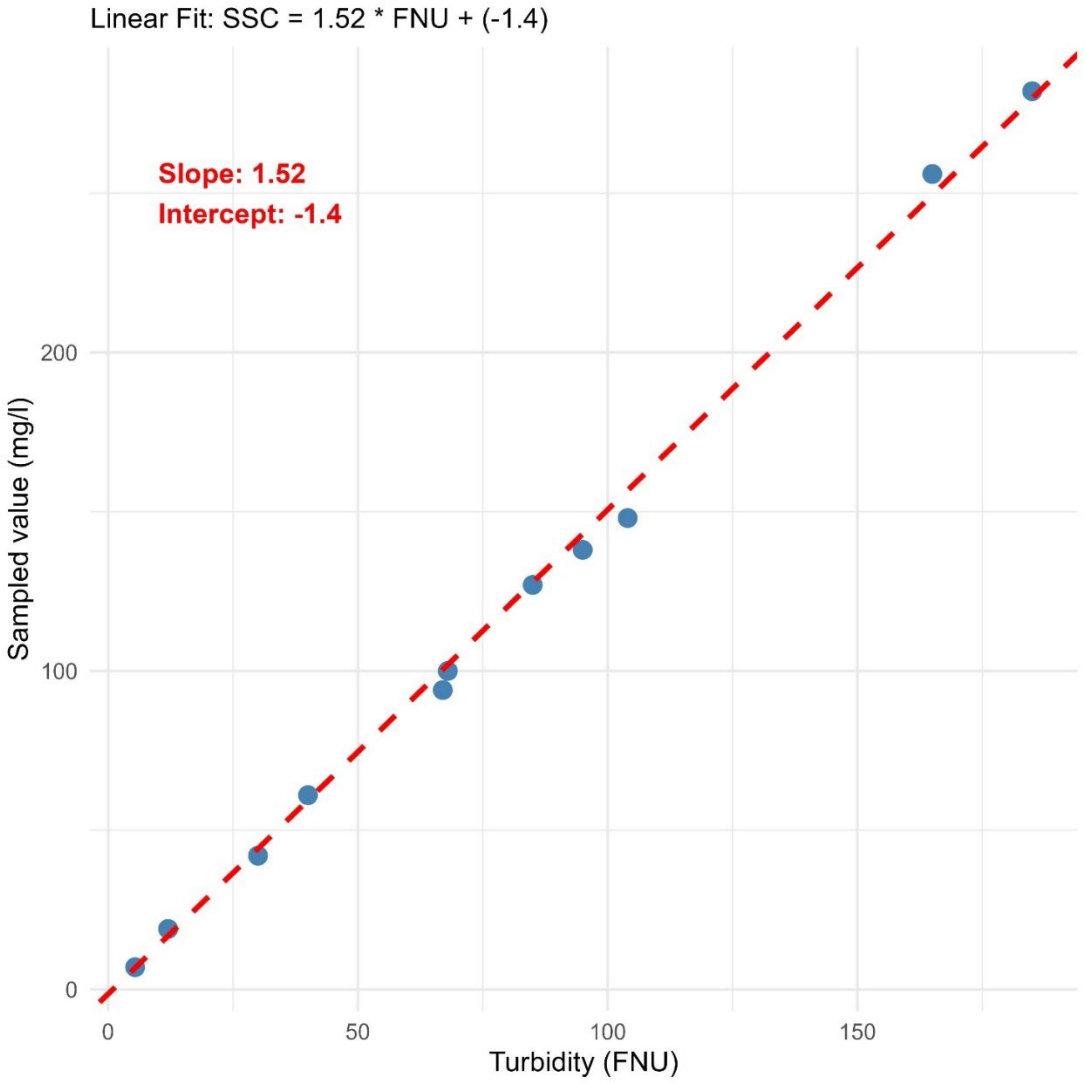
Wolanski, E. and Elliott, M., 2024. The physics-biology links in suspended and settled estuarine mud dynamics: A review. *Sediment Transport Research-Further Recent Advances*.

Wurtsbaugh, W.A., Paerl, H.W. and Dodds, W.K., 2019. Nutrients, eutrophication and harmful algal blooms along the freshwater to marine continuum. *Wiley Interdisciplinary Reviews: Water*, *6*(5), p.e1373.

Zimmerman, J.T.F., 2018. Estuarine residence times. In *Hydrodynamics of Estuaries* (pp. 75-84). CRC Press.

5 Appendices

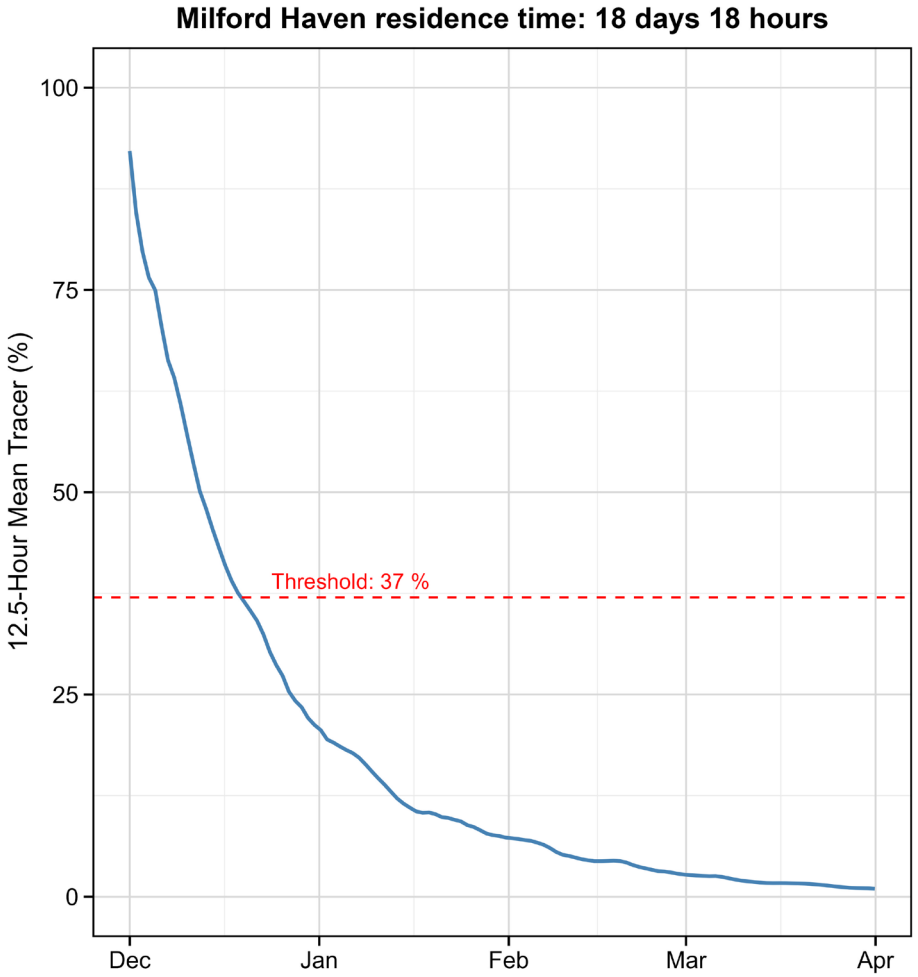
5.1 Appendix A1 - Turbidity calibration



Appendix A1.1. *Linear calibration relationship between observed turbidity (FNU) and Suspended Sediment Concentration (SSC, mg/l). The red dashed line represents the site-specific linear fit (SSC = 1.52 x FNU + (- 1.40)) derived from the 2023-2024 NRW field campaign calibration samples. Blue points represent individual water samples used for validation.*

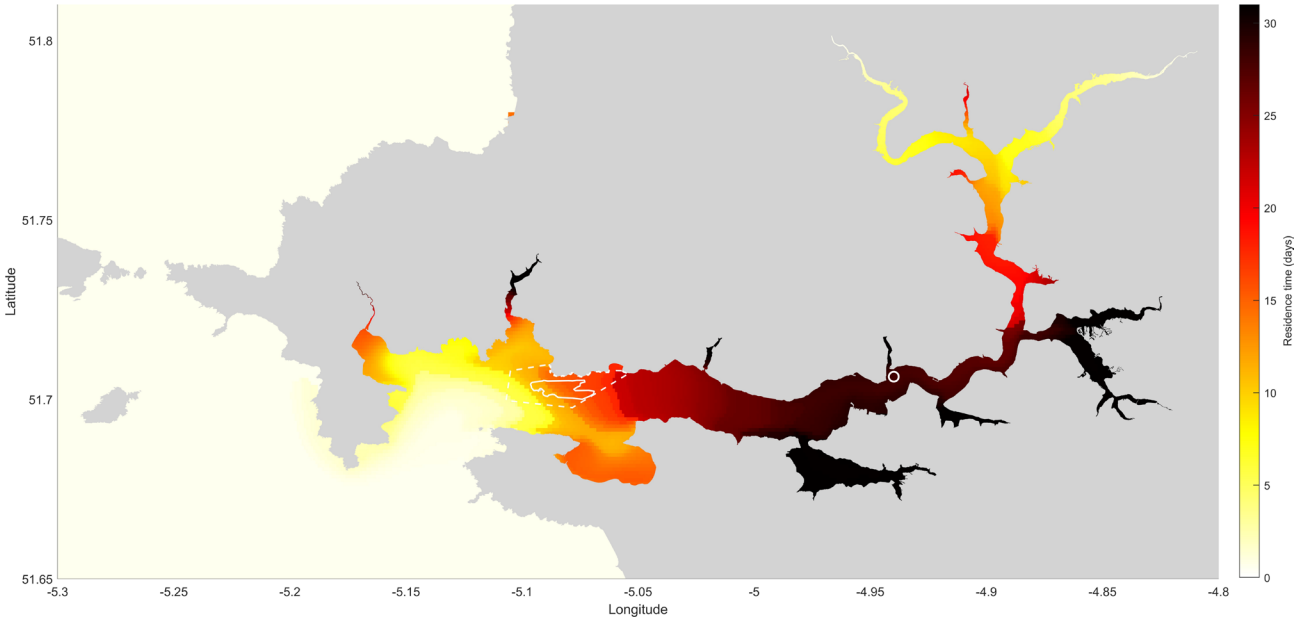
5.2 Appendix A2 – Estuary residence time

Estuarine residence time was estimated using a conservative tracer simulation within the calibrated Delft3D-FM hydrodynamic model for 2023-24. A non-decayable tracer was applied uniformly across the entire estuary area at 100% concentration at midnight on 01 December 2023. The time in which the spatially averaged tracer concentration fell to 37% of its initial value was taken as the e-folding residence time, a standard metric for estuarine flushing (Zimmerman. 2018), which was reached in 18 days and 18 hours.



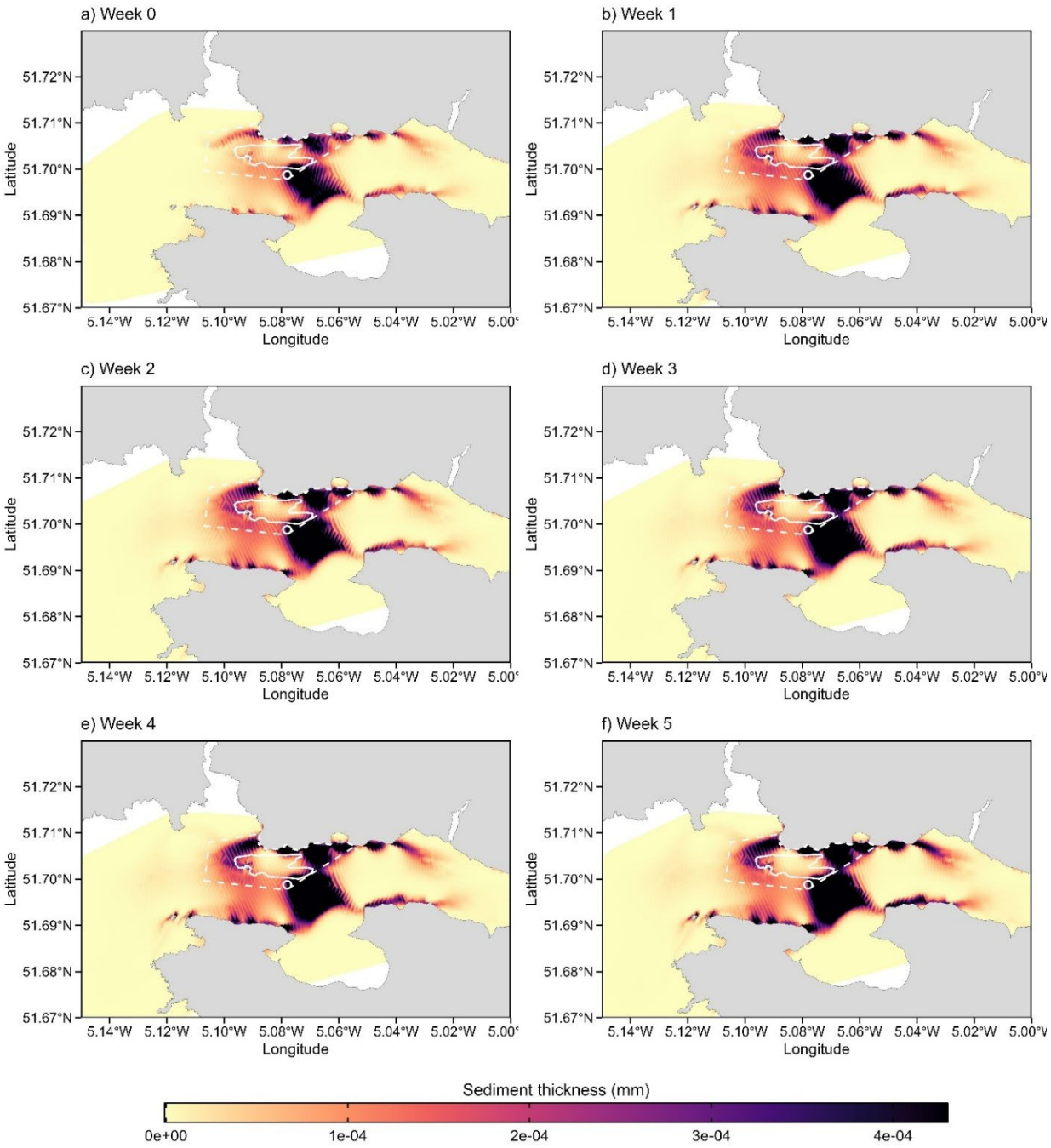
Appendix A2.1. *12.5 hour mean time series of spatially averaged conservative tracer concentration within the Milford Haven estuary (WFD boundary) following initialisation at midnight on 01 December 2023. The dashed horizontal line represents the 37% threshold used to indicate the e-folding residence time.*

The spatial distribution of residence times across Milford Haven shows strong gradients between the outer and upper estuary. The domain-averaged e-folding residence time was 12.5 days (median 6.1 days), with the skewed distribution reflecting rapid flushing of the outer channel relative to sheltered upper tributary creeks. Residence times ranged from 0.5 days in the most energetic outer reaches to a simulation maximum of 31 days in areas where the tracer did not fully resolve within the modelled period. The dredge disposal site exhibited notably elevated residence times of 28.2 to 28.5 days, consistent with its sheltered mid-estuary position. The maerl bed showed residence times of 11.0 to 16.5 days (mean 14.4 days), indicating that material reaching this location would persist for approximately two weeks. The wider sensitive habitat area showed more variable residence times of 3.8 to 22.3 days (mean 13.1 days), reflecting spatial heterogeneity in tidal flushing across the polygon.

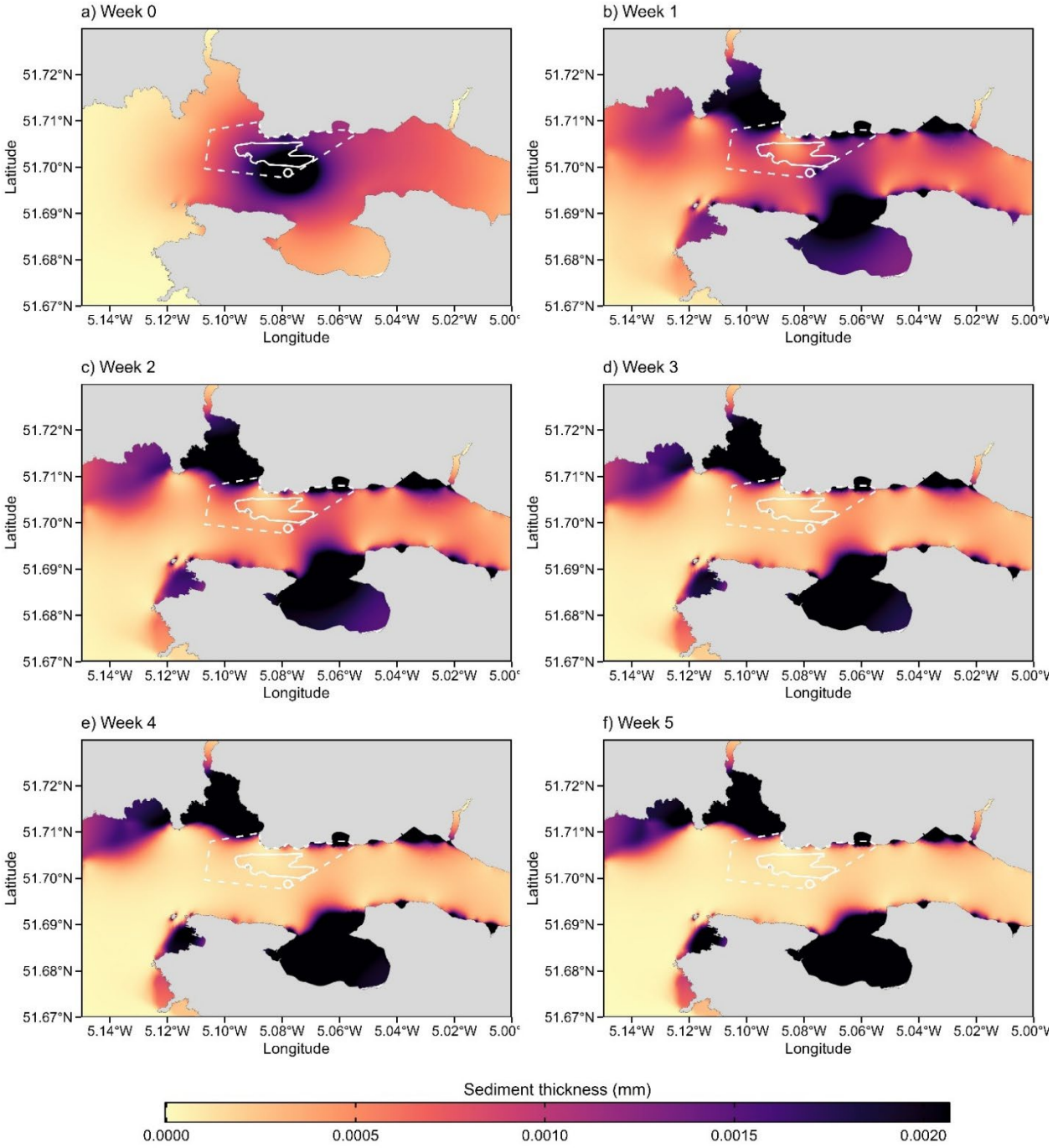


Appendix A2.2. *Spatial distribution of residence time (days) across the Milford Haven estuary, derived from a conservative tracer simulation initialised at midnight on 1 December 2023. Residence time is defined as the time for each grid cell to reach 37% of its initial tracer concentration following a 12.5-hour tidal average. The solid white polygon denotes the maerl bed and the dashed white polygon the wider sensitive habitat area. The open circle marks the capital dredge disposal site. Grid cells where the tracer concentration did not resolve within the simulation period are shown at the maximum value of 31 days.*

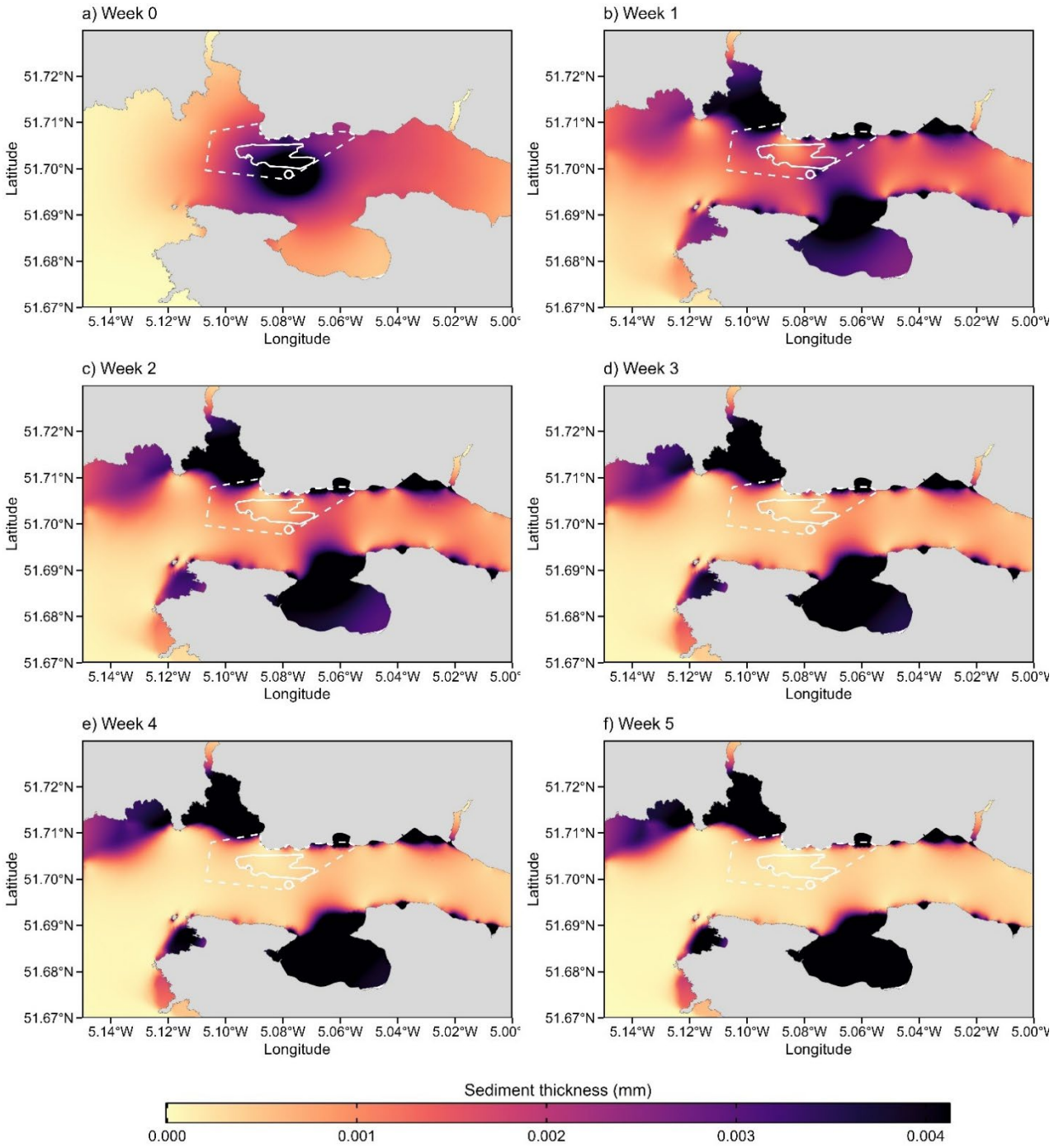
5.3 Appendix A3 – Sediment evolution



Appendix A3.1. *Spatial distribution of sand sediment thickness (mm) at weekly intervals following the cessation of jetty sediment mobilisation (Week 0 = 06 December 2025 23:30). The white circle denotes the jetty discharge point; the solid white outline indicates the maerl bed extent and the dashed white outline the sensitive habitat area.*

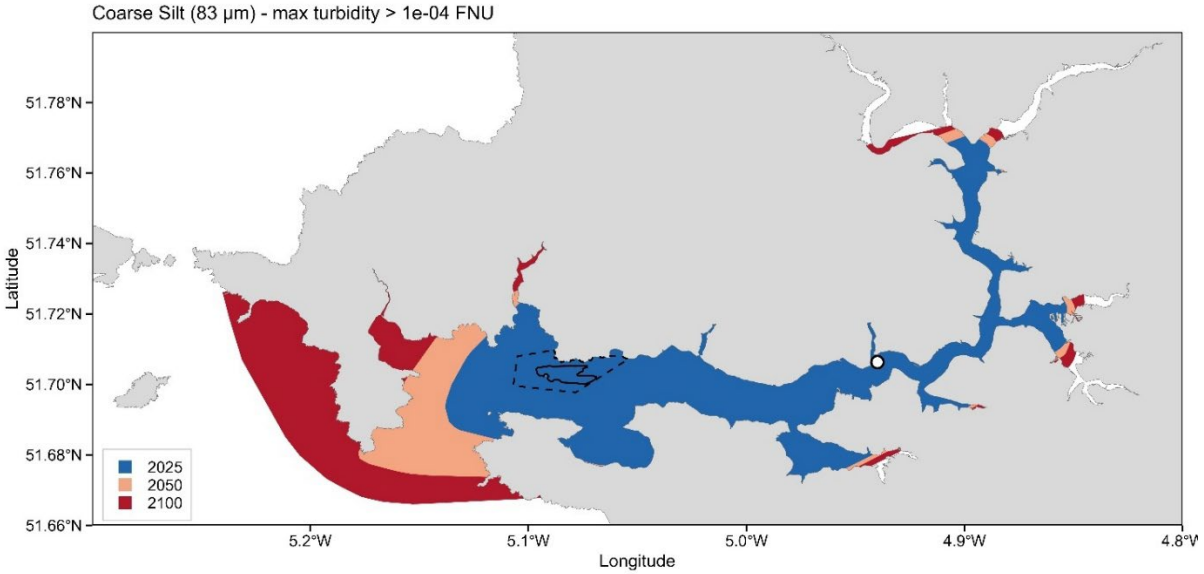


Appendix A3.2. *Spatial distribution of coarse silt sediment thickness (mm) at weekly intervals following the cessation of jetty sediment mobilisation (Week 0 = 06 December 2025 23:30). The white circle denotes the jetty discharge point; the solid white outline indicates the maerl bed extent and the dashed white outline the sensitive habitat area.*

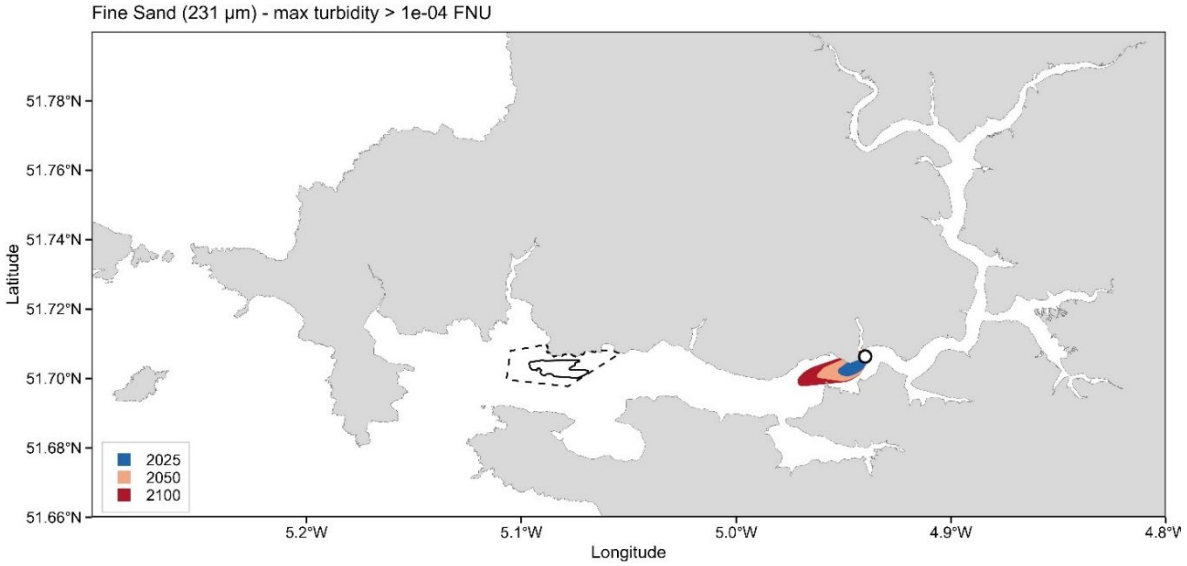


Appendix A3.3. *Spatial distribution of fine silt sediment thickness (mm) at weekly intervals following the cessation of jetty sediment mobilisation (Week 0 = 06 December 2025 23:30). The white circle denotes the jetty discharge point; the solid white outline indicates the maerl bed extent and the dashed white outline the sensitive habitat area.*

5.4 Appendix A4 – Sea-level rise scenarios

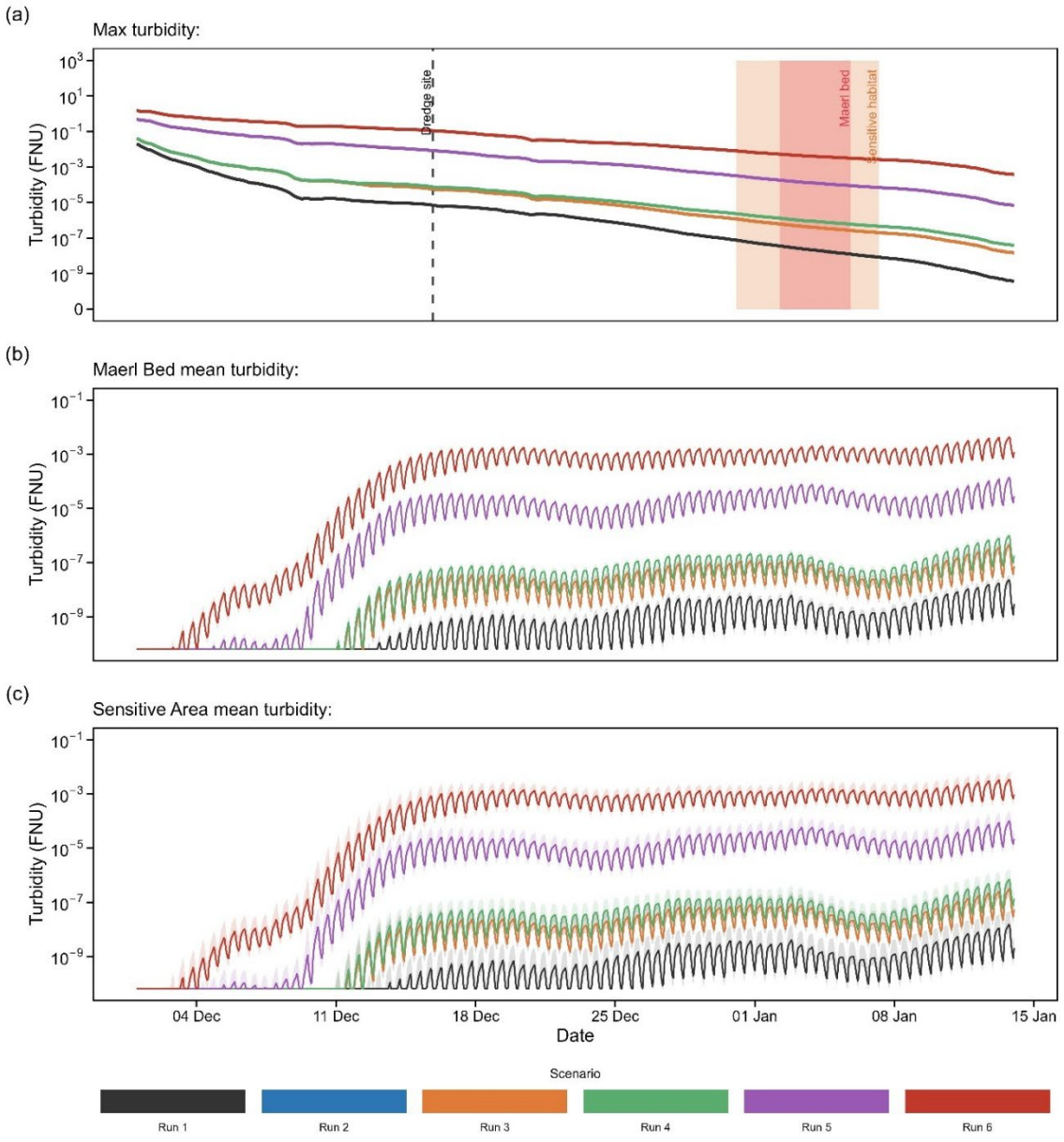


Appendix A4.1. *Spatial extent of maximum turbidity exceeding 10^{-4} FNU for coarse silt (83 µm) under the 2025, 2050 and 2100 sea-level rise dredging scenarios. The white circle denotes the Neyland Yacht Haven disposal site (LU190); the solid black outline indicates the maerl bed extent and the dashed black outline the sensitive habitat area.*

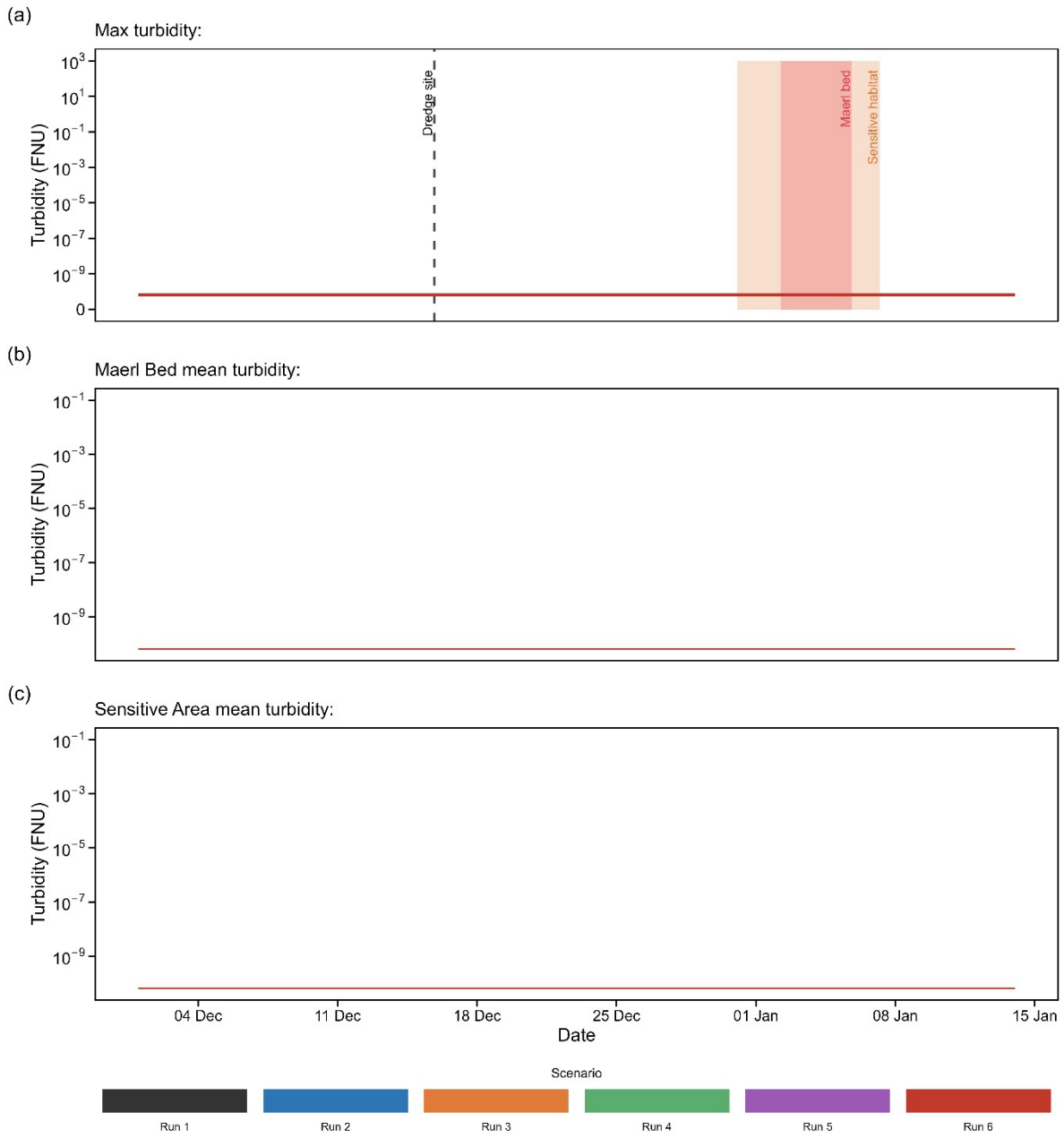


Appendix A4.2. *Spatial extent of maximum turbidity exceeding 10^{-4} FNU for fine sand (231 µm) under the 2025, 2050 and 2100 sea-level rise dredging scenarios. The white circle denotes the Neyland Yacht Haven disposal site (LU190); the solid black outline indicates the maerl bed extent and the dashed black outline the sensitive habitat area.*

5.5 Appendix A5 – Model sensitivity testing



Appendix A5.1. *Sensitivity of modelled turbidity to sediment transport parameterisation for the coarse silt (83 µm) fraction. (a) Maximum turbidity along the Cleddau thalweg transect for all six model runs; (b) median (p50) turbidity at the maerl bed from 1 December 2025 to 14 January 2026; (c) as (b) for the sensitive habitat area. The dashed vertical line in (a) denotes the Neyland Yacht Haven disposal site at 12.9 km downstream; shaded regions indicate the maerl bed (red) and sensitive habitat area (orange). Runs S1-S4 represent progressively refined baseline parameterisations; Runs S5 and S6 represent organic-rich/flocculated and maximum transport scenarios respectively.*



Appendix A5.2. *Sensitivity of modelled turbidity to sediment transport parameterisation for the fine sand (231 µm) fraction. (a) Maximum turbidity along the Cleddau thalweg transect for all six model runs; (b) median (p50) turbidity at the maerl bed from 1 December 2025 to 14 January 2026; (c) as (b) for the sensitive habitat area. The dashed vertical line in (a) denotes the Neyland Yacht Haven disposal site at 12.9 km downstream; shaded regions indicate the maerl bed (red) and sensitive habitat area (orange). Runs S1-S4 represent progressively refined baseline parameterisations; Runs S5 and S6 represent organic-rich/flocculated and maximum transport scenarios respectively.*